SYNTHESIS AND CHARACTERIZATION OF NEW METAL-CARBON CATALYSTS FOR HYDROGENATION OF D-GLUCOSE

LIU JIAJIA

NATIONAL UNIVERSITY OF SINGAPORE

2010

SYNTHESIS AND CHARACTERIZATION OF NEW METAL-CARBON CATALYSTS FOR HYDROGENATION OF D-GLUCOSE

LIU JIAJIA

(M.Eng, Tianjin University)

A THESIS SUBMITTED

FOR THE DEGREE OF DOCTOR OF PHILOSOPHY

DEPARTMENT OF CHEMICAL AND BIOMOLECULAR ENGINEERING

NATIONAL UNIVERSITY OF SINGAPORE

2010

Acknowledgement

I am heartily thankful to my supervisor, Assoc. Prof. Zhao X. S., George, whose constant encouragement, invaluable guidance, patience and support throughout the whole period of my PhD candidature. I would also like to thank Assoc. Prof. Zhao for his guidance on writing scientific papers including this PhD thesis.

In addition, I want to express my sincerest appreciation to the Department of Chemical and Biomolecular Engineering for offering me the chance to study at NUS with a scholarship.

It's my pleasure to work with a group of brilliant, warmhearted and lovely people. Wish all my lab mates go well with their work.

Particular acknowledgement goes to Dr. Liu Tao, Mr. Chia Phai Ann, Mr. Shang Zhenhua, Dr. Yuan Zeliang, Mr. Mao Ning, Mr. Liu Zhicheng, Dr. Rajarathnam D., Madam Chow Pek Jaslyn, Mdm Fam Hwee Koong Samantha, Ms Lee Chai Keng, Ms Tay Choon Yen, Mr. Toh Keng Chee, Mr. Chun See Chong, Ms. Ng Ai Mei, Ms. Lum Mei Peng Sharon, and Ms. How Yoke Leng Doris for their kind supports.

I thank my parents and my husband. It is no exaggeration to say that I could not complete the PhD work without their generous help, boundless love, encouragement and support.

Lastly, I offer my regards and blessing to all of those who supported me in any respect during the completion of the project.

Table of Contents

Summary

Catalytic hydrogenation is a process for the reduction of chemical substances, and has found numerous applications in the chemical and petrochemical industries. The hydrogenation reaction can be carried out heterogeneously or homogeneously. The heterogeneous catalysts are in generally a metal supported on a solid that are prepared by using conventional methods, such as impregnation followed by hydrogen reduction. Such supported catalysts suffer from a number of problems, such as aggregation and leaching of the metal particles. Thus, new methods that afford the preparation of catalytically highly active, chemically and thermally stable, technically reusable, and cost-effective are highly desirable.

In this thesis work, the template strategy was employed to prepare new heterogeneous catalysts. The catalysts were characterized using a number of techniques, such as extended X-ray absorption spectroscopy (XAS) and chemisorption of hydrogen and carbon monoxide. The catalytic properties of the catalysts were evaluated using the hydrogenation of D-glucose in a batch reactor.

First, ruthenium nanoparticles embedded in the pore walls of templated carbon (denoted RuC) were prepared by using H-form zeolite Y and mesoporous silica SBA-15 as templates. Compared with other ruthenium catalysts prepared using conventional methods, the RuC catalysts prepared using the template method exhibited a significantly improved catalytic performance because of the unique structure of the RuC catalysts.

Second, bimetallic ruthenium-copper (Ru-Cu) nanoparticles embedded in the pore walls of mesoporous carbon were prepared. The presence of bimetallic entities was supported by the characterization data of both Ru L_{III}-edge and Cu K-edge X-ray

absorption. It was observed that additional active sites were created because of the spillover of H from Ru to Cu at low Cu contents while three-dimensional islands of segregated metallic Cu phase covering the surface of Ru nanoparticles appeared at high Cu contents.

Third, alumina microfibers were also used as templates to prepare Ru nanoparticles embedded in mesoporous carbon fibers. In comparison with Ru nanoparticles supported on other carbon materials (e.g., multi-walled carbon nanotubes, carbon fibers, alumina microfibers, and the activated charcoals), the Ru catalyst prepared using the template method displayed a remarkably higher catalytic activity and a better stability, again attributed to the features of unblocked mesopores, hydrogen spillover, and unique surface contact between the Ru nanoparticles and the carbon supports. In addition, the incorporation of nitrogen significantly improved the catalytic performance due to the enhanced hydrogen adsorption, improved surface wettability, and modified electronic properties of the Ru nanoparticles.

Fourth, the kinetics of D-glucose hydrogenation over a bimetallic catalyst was studied. In the operation regime studied, the reaction rate showed a first order dependency with respect to hydrogen. The rate dependence on D-glucose was found to be concentration-dependent: at low D-glucose concentrations the reaction rate showed a first order dependency while at higher concentrations a zero order behavior was observed. Experimental data were fitted to the kinetic model using the Matlab software with the fminsearch method. The kinetic model was found to nicely predict the experimental data.

In short, the template method offers opportunities to prepare novel solid catalysts with unique properties, such as controllable catalyst particle size, enhanced catalyst dispersion, improved thermal stability, lowered diffusion resistance of both reagent

and product, and intimate interfacial contact between metal particles and the carbon support. In addition, the template method could be extended to the preparation of bimetallic or tri-metallic carbon nanocomposites. Furthermore the template method allows one to easily control the chemical properties of carbon by changing carbon precursor (incorporation of heteroatom such as nitrogen).

Nomenclature

1D	One-dimensional
3D	Three-dimensional
^{o}C	Degree Centigrade
λ	Wavelength
BET	Brunauer-Emmett-Teller
BJH	Barrett-Joyner-Halenda
CVD	Chemical vapor deposition
d	Diameter
DI	Deionized
EDX	Energy dispersive X-ray spectroscopy
FT-IR	Fourier transform infrared
FESEM	Field emission scanning electron microscopy
h	hour
HK	Horvath-Kawazoe method
HRTEM	High-Resolution Transmission Electron Microscopy
mL	mille liter
nm	nanometer
P123	Poly(ethylene glycol)$_{20}$-block poly(propylene glycol)$_{70}$-block poly(ethyleneglycol)$_{20}$
PSD	Pore size distribution
SBA	Santa Babara
SEM	Scanning electron microscopy
TEM	Transmission electron microscopy
TEOS	Tetraethyl orthosilicate
TGA	Thermogravimetric analysis
XAS	X-ray Absorption Spectroscopy
XPS	X-ray Photoelectron Spectroscopy
XRD	X-ray Diffraction

List of Tables

Chapter 3

Chapter 4

Chapter 5

Chapter 6

Chapter 7

List of Figures

Chapter 1

Chapter 2

Chapter 3

Chapter 4

Chapter 5

Chapter 6

Chapter 7

CHAPTER 1

INTRODUCTION

1.1 Hydrogenation reactions

The catalytic hydrogenation of organic compounds is an important reaction in organic synthesis that can be dated back to 1897 when a French Chemist, Paul Sabatier (Sabatier, 1905), discovered that the introduction of a trace of nickel metal (a catalyst) facilitated the addition of hydrogen to molecules of hydrocarbon compounds. Since then catalytic hydrogenation has been widely used in various fields. Important examples of industrial hydrogenation processes are the synthesis of methanol, liquid fuels, hydrogenated oils, cyclohexanol and cyclohexane.

In the food industry, hydrogenation is applied to process vegetable oils and fats (Patterson, 1983). Triglycerides are the main constituents of vegetable oils and fats, which consist of one molecule of glycerol combined with three molecules of fatty acids (as shown in Figure 1.1). If the result is liquid at ambient temperature, it is commonly known as an oil and if it is solid, as a fat. In nature, fats are physical mixtures of various triglycerides. The proportions of the different triglycerides which go to make the complete fat and the different kinds of fatty acid combined in any one triglyceride will determine the chemical and physical nature of the fat. Unsaturated vegetable fats and oils can be hydrogenated by the catalytic addition of hydrogen at the ethylenic linkages of their acids to produce saturated or partially saturated fats and oils of higher melting point. The most common forms are shortening, margarines, and the partially hydrogenated fats used for frying and in processed food. These fats are desirable for its melting point, allowing for high temperature cooking and frying.

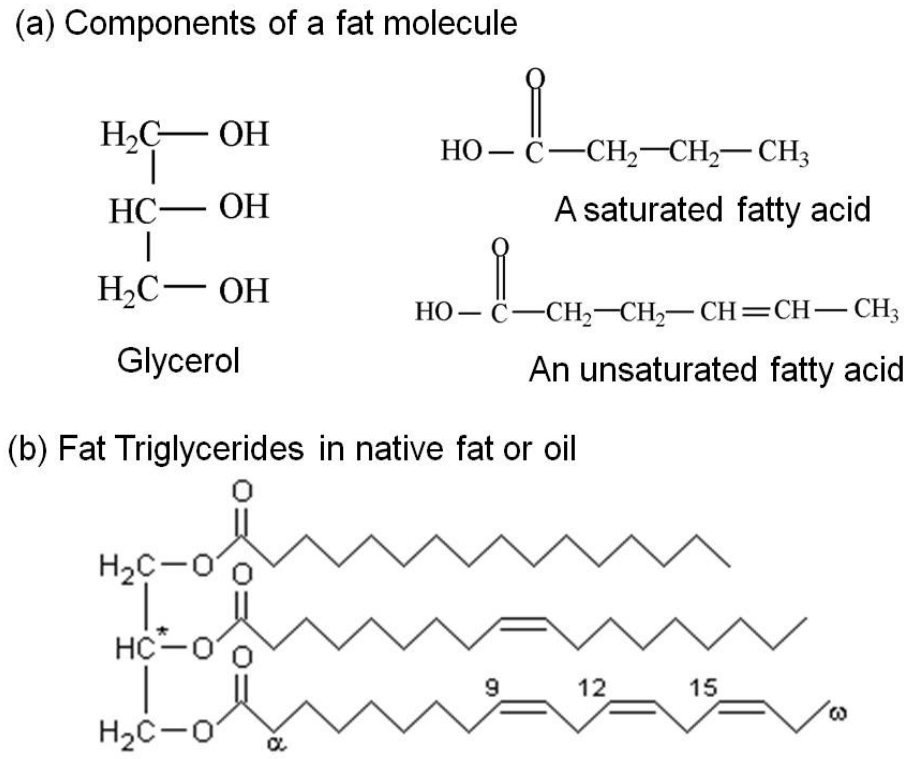

Figure 1.1 (a) Components of a fat molecule, (b) Fat triglyceride shorthand formula.

In the petroleum industry, catalytic hydrogenation has become an important refining technique in upgrading low quality petroleum distillates to premium fuels (Dodgson, 1993). Petroleum (crude oil) comprises not only alkanes, cyclic alkanes and aromatic hydrocarbons of different molecular weight, but also a small amount of sulfides, oxides, and nitrides, as well as some trance amounts of metal compounds of iron, nickel, copper and vanadium, etc. In the crude state, petroleum has little value but, when refined, it provides liquid fuels (gasoline, diesel fuel, aviation fuel), solvents, heating oil, lubricants, and the distillation residuum asphalt. Hydrogenation processes uses the principle that the presence of hydrogen during a thermal reaction of a petroleum feedstock will terminate many of the coke-forming reactions and enhance the yields of the lower-boiling components, such as gasoline, kerosene, and jet fuel. Hydrogenation is also used for improving product quality without appreciable alternation of the boiling range. Nitrogen, sulfur, and oxygen compounds undergo

reaction with the hydrogen, forming ammonia, hydrogen sulfide, and water, respectively.

1.2 Importance of hydrogenation of D-glucose

Sorbitol ($C_6H_{14}O_6$) is a sugar alcohol, found in nature as the sweet constituent of many berries and fruit. It is available in both liquid and crystalline form with a world capacity of more 1 Mt/a (Eisenbeis et al., 2009). It was first isolated in 1873 by the French chemist, Joseph Boussingault (Fedor, 1960). Today, it is commercially produced by the catalytic hydrogenation of D-glucose ($C_6H_{12}O_6$) over nickel and ruthenium catalysts. Because sorbitol is about 60 percent as sweet as sucrose with one-third fewer calories, it is a sugar substitute for diabetics. In addition, sorbitol is used as a humectant in many types of products for protection against loss of moisture content. The moisture-stabilizing and textural properties of sorbitol are used in the production of confectionery, baked goods and chocolate where products tend to become dry or harden. Since sorbitol has no cariogenic activity, most toothpaste contains sorbitol. Moreover, it is also used as a feedstock for L-sorbose – an important intermediate in manufacture of L-ascorbic acid (vitamin C). Furthermore, sorbitol can be efficiently converted into H_2, synthesis gas, alkanes, liquid fuels, and oxygenates (Huber et al., 2003; Davda and Dumesic, 2004; Huber et al., 2004).

1.3 Catalysts for hydrogenation reactions

With rare exception, no reaction below 480 ^oC occurs between H_2 and organic compounds in the absence of metal catalysts (Nishimura, 2001). The catalyst binds both the H_2 and the unsaturated substrate and facilitates their union. There are two types of catalysts, homogeneous catalysts and heterogeneous catalysts. The

homogeneous catalysts are metal complexes that are soluble in the reaction medium. Such metal complexes consist of a central metal ion and organic ligands. The activity and selectivity of homogeneous catalysts are adjusted by changing the ligands. The catalytic cycle starts with oxidative additive of an H_2 molecule to the metal centre to give a metal dihydride species and ends with reductive elimination of the product (Dwars and Oehme, 2002; Blaser et al., 2003). Because these complexes are difficult to remove and reuse, numerous attempts have been made to anchor of homogeneous system on organic or inorganic supports to combine the advantages of homogeneous catalytic systems (high activity, high selectivity, excellent reproducibility) with the advantages of heterogeneous catalytic systems (long life, recycling, continuous application).

Heterogeneous transition metal catalysts for hydrogenation are usually employed in the states of metals, oxides, or sulfides that are either unsupported or supported. The physical form of a catalyst suitable for a particular hydrogenation is determined primarily by the type of reactions, such as fixed-bed, fluidized-bed, or batch reaction. For industrial purposes, unsupported catalysts are seldom employed since supported catalysts have many advantages over unsupported catalysts. One exception to this is Raney-type catalysts, which are effectively employed in industrial hydrogenations in unsupported states. In general, use of support allows the active component to have a large exposed surface area, which is particularly important in those cases where a high temperature is required or where the active component is very expensive. An active component may be incorporated with a carrier in various ways, such as, by deposition, impregnation, precipitation, coprecipitation, adsorption, or ion exchange. For these preparation methods catalyst pretreatment is often necessary, because the solid materials containing metal compounds in non-metallic state can exhibit only low

catalytic activity or be catalytically inactive. Catalyst pretreatment involves the catalyst calcination, catalyst reduction, and the catalyst aging. Unlike homogeneous hydrogenation, which takes place on a well-defined single metal centre, heterogeneous hydrogenation proceeds over a vast surface of a metal cluster. This gives rise to a large number of interaction possibilities and variety of relevant and irrelevant species present on the surface during the reaction. Hydrogenation over heterogeneous catalysts proceeds via several surface reaction steps, like adsorption, reaction and desorption. Additionally, the reaction mechanism is rather complicated including competitive/non-competitive and dissociative/non-dissociative adsorption as well as adsorption of solvents, formation of coke etc. As a result, it is important to understand the catalyst structure and relate performance of the catalyst (e.g. activity) to its structure. Any small improvement of the performance and cost of the catalysts would help to cut the cost of these important processes.

The most common catalyst in D-glucose hydrogenation is nickel promoted by electropositive metals, such as molybdenum and chromium (Gallezot et al., 1994; Li et al., 2000; Hoffer et al., 2003; Schimpf et al., 2007). However, due to the leaching of nickel and catalyst promoters into the product and fast deactivation of the catalyst, new catalysts, such as cobalt, copper, platinum, palladium, rhodium and ruthenium (Wisnlak and Simon, 1979; Makkee et al., 1985; Li et al., 2001) have been studied. Among these catalysts, ruthenium nanoparticles dispersed on solid supports, such as mesoporous silica, activated carbon, titania, and alumina oxides (Gallezot et al., 1998; van Gorp et al., 1999; Hoffer et al., 2003; Kusserow et al., 2003; Besson et al., 2005; Perrard et al., 2007; Yuan et al., 2008), have been found to display the best catalytic performance in D-glucose hydrogenation. However, these supported catalysts have a common issue, namely rapid deactivation (Arena, 1992; Besson and Gallezot, 2003;

Kusserow et al., 2003), partially due to sintering and/or migration of the Ru particles (Maris et al., 2006).

1.4 Carbon-supported catalysts for hydrogenation reactions

Many heterogeneous hydrogenation catalysts consist of metals or metal compounds supported on an appropriate support, the basic role of which is to maintain the catalytically active phase in a highly dispersed state to obtain a large active surface per unit weight used. In addition, a supported catalyst facilitates the flow of gases through the reactor and the diffusion of reactants through the pores to the active phase, improving the dissipation of reaction heat, retarding the sintering of the active phase and increasing the poison resistance. The selection of support is based on a series of desirable characteristics: inertness, stability under reaction, regeneration conditions, adequate mechanical properties, appropriate physical form for the given reactor, high surface area, porosity and chemical nature (Rodriguez-Reinoso, 1998). Carbon has been used as hydrogenation catalyst support for a long time because their specific properties, including (a) resistance to acid/basic media, (b) possibility to control, up to certain limits, the porosity and surface chemistry, and (c) easy recovery of precious metals by burning (Serp et al., 2003). The most common carbon support material is activated carbon, followed by carbon black and graphite or graphitized materials.

However, the properties of these commercial use carbons are difficult to control and their microporosity has often hampered catalyst development. Furthermore, the impact of the chemical and physical properties of the carbon on the catalyst preparation and the catalytic performance are not yet sufficiently understood. New carbon materials, like carbon nanotubes (CNTs), carbon nanofibers (CNFs), graphene, and templated-synthesized porous have been applied in hydrogenations in the scientific community.

1.5 Recent advance on template approach to preparing novel porous carbons and catalysts

The template method has been widely used to prepare novel porous carbon with various structural, morphological, and compositional properties (Zhao et al., 2006a; Lu et al., 2006; Lee et al., 2006). Because of their uniform pore size, high surface area and interconnected pore network, templated carbon is a better catalyst carrier than traditional porous carbon. There are two types of template, namely soft template and hard template (Liang et al., 2008). The former refers to those organic species, which can be subsequently removed by calcination or solvent extraction. The latter refers to porous structures (e.g., zeolites, mesoporous silicas, and colloidal crystals), which guide the formation of the structure of a templated carbon. The hard template method works this way. First, the template pores are filled with a carbon precursor such as sucrose, furfuryl alcohol, ethylene, and propylene et al. After carbonization under proper conditions followed by removal of the template framework, a porous carbon with pores replicated from the template framework is obtained.

On the other hand, this template approach to prepare porous carbon has also opened a new avenue to prepare novel catalysts (Lu et al., 2007). By embedding metal particles in the carbon walls of templated porous carbon, thermally stable and catalytically active catalysts can be obtained. Lu et al. (2007) reported that molecular-level palladium clusters dispersed in the carbon walls can be synthesized by pyrolyzing palladium nitrate and polyacrylonitrile in the pores of SBA-15. The confined palladium clusters did not grow during the pyrolysis because they were stabilized by the carbon framework. Thus-prepared palladium catalysts were found to show a high selectivity of aldehydes in the catalytic oxidation of various alcohols and a high activity was maintained over multiple runs.

In our lab, Su et al. (2007, 2008) reported that porous carbon could act both as the support and the reducing agent for Ru nanoparticles, and the intimate interfacial contact between the Ru nanoparticles and the carbon support was believed to be responsible for the remarkably high catalytic activity and stability in the hydrogenation of benzene and toluene. The above studies suggest that the embedding of active component in carbon walls and the generating of a strong interaction between the active component and the support would help to yield a thermally stable and highly active catalyst. However, there are still a number of remaining challenges: i) for many target compositions, the chemistry of the target material is not compatible with the conditions of the template-removal process; ii) increasing metal loading is also a challenge; iii) it is necessary to ensure a rigid structure, thus avoiding collapse of the pore system after removal of the template.

1.6 Objective of project

The main objective of this project is to use the template method to prepare highly active and stable heterogeneous catalysts, competing with currently used catalyst for hydrogenation reaction (in general) and for hydrogenation of D-glucose (in particular). To accomplish the objective, the following work was carried out:

- The template method was used to prepare Ru nanoparticles embedded in the pore walls of template microporous and mesoporous carbons. The catalysts were characterized using FESEM, TEM, XRD, nitrogen adsorption, and TGA analysis. The catalytic properties of the catalysts were evaluated using the hydrogenation of D-glucose. The effects of the particle size of Ru nanoparticles and pore structure on catalytic activity were investigated.

- The template method was used to prepare bimetallic Ru-Cu particles embedded in the pore walls of mesoporous carbon. The effect of the second metal (Cu) on the physicochemical properties and catalytic performance of the bimetallic Ru-Cu catalysts was studied.
- The template method was used to prepare Ru nanoparticles embedded in mesoporous carbon microfibers by using alumina microfibers as templates. The effect of carbon morphology on the catalytic performance was investigated. The influence of the nitrogen doping in the carbon fibers was examined.
- The kinetics and mechanism of D-glucose hydrogenation over a bimetallic catalyst in aqueous solution were studied in a batch reactor. The experimental data were fitted to a kinetic model and important parameters were derived.

1.7 Structure of thesis

This thesis is organized into eight chapters. With a brief introduction and a summary of the objectives of this project in chapter 1, an extensive literature review on the hydrogenation reactions, catalysts for the hydrogenation reactions, and carbon supports is presented in chapter 2. The details of chemicals, synthesis methods, characterization techniques used, and catalytic evaluation conditions are given in chapter 3. In chapter 4, the syntheses of RuC catalysts by using H-form zeolite HY and ordered mesoporous silica SBA-15 as templates are discussed. The catalytic performances of the RuC catalysts were compared with other Ru-C catalysts prepared by conventional method. Chapter 5 describes the fabrication of bimetallic Ru-Cu nanoparticles embedded in the pore walls of mesoporous carbon. The presence of bimetallic entities was characterized and the bimetallic catalysts were evaluated in D-glucose hydrogenation. Chapter 6 is the details of synthesis of the mesoporous carbon microfiber supported Ru catalysts by

using alumina microfibers as templates. The catalytic performances of the mesoporous carbon microfiber supported Ru catalysts were compared with Ru deposited on multi-walled carbon nanotubes, carbon fibers, alumina microfibers, and the activated charcoals. In addition, the effect of nitrogen incorporation on the catalytic performance was investigated. Kinetics of D-glucose hydrogenation over RuCuC catalyst in aqueous solutions is presented in Chapter 7. The hydrogenation experiments were carried out batchwise, operating at 4.0-10.0 MPa and between 90 and 120 ^{o}C. Finally, in chapter 8 an overall summary and recommendations for further work are given.

CHAPTER 2

LITERATURE REVIEW

2.1 Hydrogenation reactions

Catalytic hydrogenation is one of the most useful and versatile tools available to the synthetic organic chemist. It can be meeting in the large scale chemical and petrochemical industry (removal of benzene from fuels, oils, etc.), the food processing industry (fat hardening), fine chemicals and pharmaceutical industries and in many laboratory-scale operations. Many books and reviews published in this area underscore the synthetic important of these reactions (Augustine, 1997; Singh and Vannice, 2001). The literature review below is organized around the functional group undergoing reduction.

2.1.1 Hydrogenation of carbon-carbon multiple bonds

The hydrogenation of carbon-carbon double and triple bonds is a very common reaction in heterogeneous catalysis. There are four types of hydrogenations (Kralik and Biffis, 2001): (i) total hydrogenation of unsaturated molecule without other hydrogenation moieties; (ii) partial hydrogenation of a molecule with more than one multiple bond, either conjugated or not; (iii) partial hydrogenation of alkynes to alkenes; (iv) selective hydrogenation of an unsaturated molecule bearing other unsaturated moieties, such carbonyl groups or halogen substituent. The hydrogenation of fatty oils is one of the most striking industrial application of hydrogenation of carbon-carbon multiple bonds. The classical heterogeneous catalysts for carbon-carbon multiple bond hydrogenations involve supported precious metals, activated base metal catalysts (such as Raney-Ni) and nickel supported on oxides. For fine chemicals

manufacture activated carbon is the most common support material. Aluminas and silicas as well as $CaCO_3$ or $BaSO_4$ are preferred for special applications (Molnar et al., 2001).

2.1.2 Hydrogenation of C=O bonds

Hydrogenation of carbonyl groups occurs readily over most catalysts. However, hydrogenolysis of the resulting hydroxyl group and further reduced to methylene group must be careful to be prevented. The hydrogenation of carbonyl groups can be summarized to a few reaction types: i) hydrogenation of aliphatic aldehydes and ketones; ii) hydrogenation of unsaturated aldehydes; iii) hydrogenation of aromatic aldehydes and ketones; iv) sugar hydrogenation; v) enantioselective carbonyl hydrogenation; vi) hydrogenation of esters, anhydrides and carboxylic acids. The rates of hydrogenation of carbonyl compounds depend on the nature of catalyst, the structure of compounds, such as aliphatic or aromatic and hindered or unhindered, the reaction medium, as well as the reaction conditions. Carbonyl compounds are readily hydrogenated to alcohols under mild conditions with platinum catalysts preferably in acidic media as well as with rhodium and ruthenium most commonly under neutral or basic circumstances (Nishimura, 2001). Palladium catalysts are not usually used for these reductions however they have found utility in the selective hydrogenation of aromatic carbonyls. Carbonyl groups are also hydrogenated with base metals such as nickel, copper, and cobalt. Although the base metals tend to require higher hydrogen pressures, their cost-to-performance ratios are very good and they provide economically suitable alternatives to the precious metals. The base metals are usually used as either Raney-type or supported (e.g., Al_2O_3 and SiO_2 supported) catalysts. Promoters typically enhance the activity and selectivity of both precious and base

metal catalysts for carbonyl reductions where the types and amounts of promoters need to be optimized for the desired reaction.

2.1.3 Hydrogenation of nitrogen-containing multiple bonds

The metal catalyzed hydrogenation of nitro-, nitroso-, azo-, and nitrile-groups represents a class of reactions widely employed in industrial organic synthesis which are commonly encountered in large-scale chemical production plants (e.g. in the preparation of aniline from nitrobenzene). Hydrogenation of multiple bonds containing nitrogen are relative easily accomplished and have been extensively reviewed (Gomez et al., 2002). These nitrogen compounds are relatively strongly adsorbed on most catalytic surfaces, so they resided on the surface sufficiently long enough to allow side reactions to occur. Catalytic hydrogenation of nitriles may result in several products: primary, secondary, and tertiary amines; imines; hydrocarbons; aldehydes; amides; and alcohols. The main product depends on the nature of catalyst, structure of substrate, basic and acidic additives, the reaction medium and other reaction conditions. Supported and unsupported palladium, platinum, and nickel are excellent catalysts for the hydrogenation of nitro functions. Rhodium is also effective, but a special requirement would be necessary to justify its use. The catalyst of choice for any particular reduction depends largely on other functional groups present and on the product required.

2.2 Catalysts in hydrogenation reactions

Most hydrogenations involve the direct addition of diatomic hydrogen under a high pressure in the presence of a catalyst. Hydrogen is activated by the catalyst to dissociate into two hydrogen atoms. The unsaturated hydrocarbon molecule is either

activated by the catalysts or directly reacts with the hydrogen atom. There are two types of catalysts used in hydrogenation reactions, namely homogeneous catalysts and heterogeneous catalysts. A homogeneous catalyst is a transition metal complex that is soluble in the reaction medium. A metal complex consists of a central metal ion and one or more ligands (Dwars et al., 2002). The natures of the ligand control the catalytic properties of a particular metal for a specific hydrogenation reaction. The detailed mechanism of the reaction is fairly well understood (Blaser et al, 2003). The catalytic cycle starts with oxidative additive of an H_2 molecule to the metal center to give a metal dihydride species and ends with reductive elimination of the product.

A heterogeneous catalyst for hydrogenation reactions contains usually a metal supported on a carrier. The metal is the catalyst component that can activate hydrogen molecules. The metal is made as small particles (in order to increase surface area) dispersed on the carrier. In comparison with the homogeneous catalyst system, the heterogeneous catalyst system has a number of advantages, including 1) the stability of catalyst, 2) ease of separation of product from catalyst, 3) a wide range of applicable reaction conditions, and 4) high catalytic ability for the hydrogenation of hard-to-reduce functional groups such as aromatic nuclei and sterically hindered unsaturations (Nishimura, 2002). Figure 2.1 schematically illustrates the mechanism of alkene hydrogenation over a metal catalyst surface (Blaser et al., 2003). The catalytic addition of hydrogen to an X=Y bond occurs stepwise. The first step is called dissociative adsorption. With the presence of a metal catalyst, the H-H bond in H_2 cleaves, and each hydrogen atom attaches to the metal catalyst surface, forming metal-hydrogen bonds. A second function of the metal is the formation of complexes with the X=Y most probably via a π-bond thereby activating the second reactant and placing it close to the M-H fragments, allowing the addition to take place. The last step is desorption

of the product from the metal surface. Additionally, the reaction mechanism is rather complicated including competitive/non- competitive and dissociative/non-dissociative adsorption as well as adsorption of solvents, formation of coke etc.

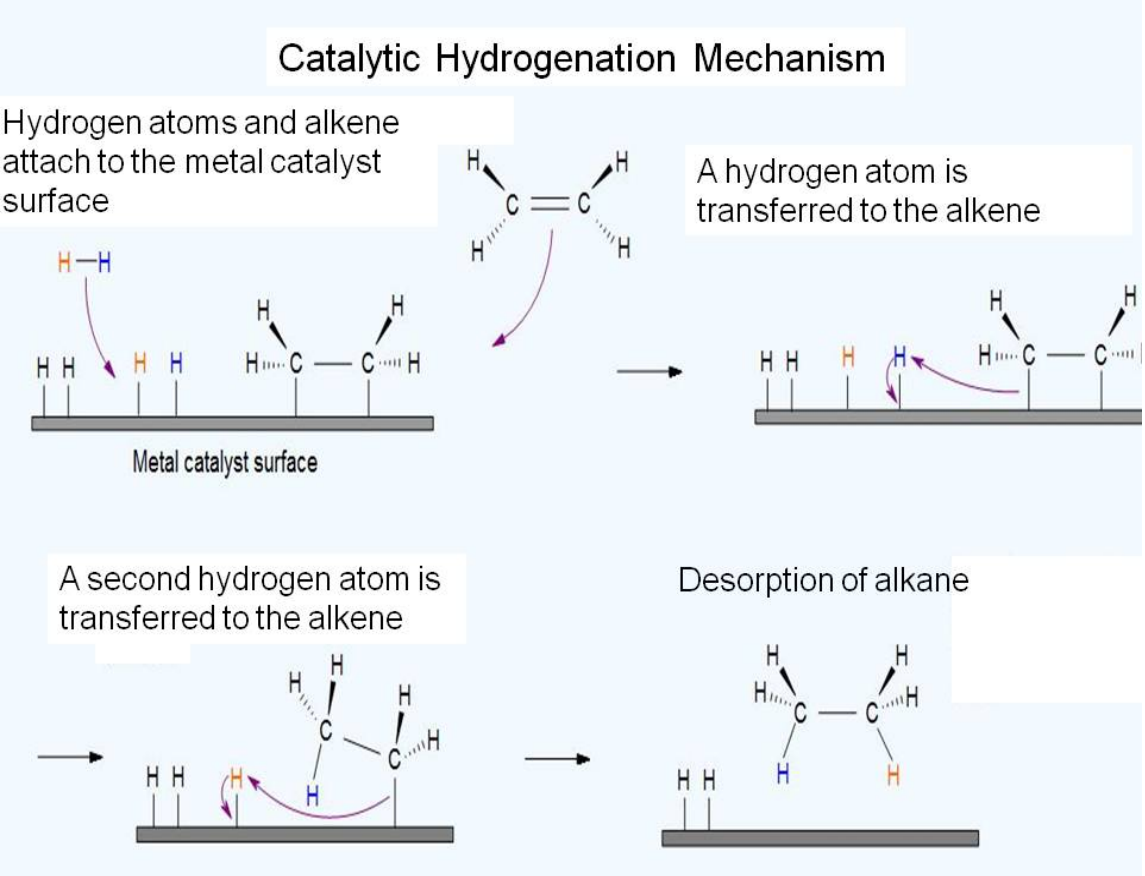

Figure 2.1 Schematic representation of catalytic hydrogenation mechanism (from website: http://chemwiki.ucdavis.edu/Organic_Chemistry/Hydrocarbons/Alkenes/Catalytic_Hydrogenation).

The catalyst structure-activity relationship is often explained on the basis of electronic and/or geometric effects (Coq and Figueras, 1998). The concept of electronic factors in catalysis deals with the interaction between the incomplete d-band of the surface metal sites with the molecular orbitals of reactants and products. The heat of adsorption of reactants and products, governed by the electronic factors, should be neither too strong nor too weak to give the optimum coverage for reactants competing at the surface, or for the products to desorb. The pioneering work of

geometric effect was conducted by Kobozev, and Boronin and Poltorak (Coq and Figueras, 1998). They showed that some reactions need more than one surface atom to proceed. Moreover, specific arrangements between these atoms are required to generate the active site. Therefore, hydrogenation rate is a function of the probability of finding an ensemble of *n* free and neighbor atoms on which the reactive adsorption of the reactants, and further transformations, can occur. Geometric and electronic influences cannot be separated as independent parameters. For instance, increasing the size of metallic particles results in an electron bandwidth increase, but the nature of the exposed planes and the topology of the surface sites change as well. The electronics and geometry effects, and further the catalytic properties of the metal catalytst depends on following factors (Kacer and Cerveny, 2002): i) type of a metal, ii) structure and morphology of metal particles; iii) surface association of two or more metals or other components; iv) surface ligands; v) role of a support; vi) effect of a metal distribution in a porous matrix of support.

2.2.1 Methods for preparing heterogeneous catalysts

There are several techniques applied in laboratory and industrial practice for catalyst preparation, such as coprecipitation, deposition/precipitation, impregnation, incipient wetness, ion-exchange, gas phase deposition method (atomic layer epitaxy), sol-gel method, metal introduction into mesoporous materials via in situ synthesis, and immobilizing homogeneous catalysts on solid supports (Augustine, 1996). Catalyst preparation method affects very much on the metal dispersion, which could be crucial for achieving high activity and selectivity.

2.2.1.1 Co-precipitation and deposition methods

Coprecipitation involves the addition of a precipitating agent to a solution containing both a support precursor and a catalyst precursor. The resulting precipitate contains both the active component and the support material. Deposition describes the application of the catalytic component to a separately produced support. A coprecipitated catalyst has the active component distributed throughout the resulting catalyst particles. With catalysts prepared by deposition, the active component can be found primarily on the surface of the supporting material. Cu/SiO_2 catalysts were synthesized by the ammonia-evaporation method, a kind of the homogeneous deposition-precipitation method which can conveniently and effectively disperse Cu species on silica, and the catalysts showed good activity in gas phase hydrogenation of dimethyl oxalate (Chen et al., 2008).

2.2.1.2 Impregnation and incipient wetness methods

Impregnation is properly defined as the adsorption of a catalyst precursor salt from solution onto a support material. The procedure calls for stirring a suspension of the support in the salt solution for a prescribed length of time followed by the separation of the modified support by filtration or centrifugation. The supported salt is then dried and, frequently, calcined before the salt is reduced to the metal. The concentration of the precursor salt, the type of salt, solvent, temperature, nature of the support, time of contact with the support and the presence of other materials can all influence both the metal loading and location of the material in the support particle. Incipient wetness, also referred to as dry impregnation, involves contacting a dry support with only enough solution of the impregnant to fill the pores of the support.

Supercritical carbon dioxide ($scCO_2$) has been used in impregnation method. Chatterjee et al. (2006) reported the formation of Au nanoparticles into the channels of mesoporous material in $scCO_2$ medium using a hydrogen reduction technique. $ScCO_2$ can provide a unique environment for stabilizing Au nanoparticles in the channels of the cubic mesoporous MCM-48 support. Furthermore, it was possible to control the desired particle size by simple tuning of the solvent density, without perturbing the support structure. The catalysts were tested in crotonaldehyde hydrogenation, which provided high selectivity to crotyl alcohol. Lee et al. (2006) reported the synthesis of Pd/SBA-15, in which the dispersion of Pd nanoparticles is highly improved by using $scCO_2$. Compare with commercially Pd catalysts deposited on Al_2O_3 or carbon supports, Pd/SBA-15 shows similar catalytic activity but significantly higher selectivity for the hydrogenation of 4-methoxycinnamic acid benzyl ester.

2.2.1.3 Ion-exchange method

Ion-exchange means the surface of the support is modified to give a surface species that can chemically react with the precursor salt. The absorption character of a support material is governed by the nature of its surface functionality. For oxides these are generally hydroxyl groups and for carbon supports they are the acidic functions such as phenols and carboxylic acids. Depending on the acidity of these surface groups and the pH of the solution in which the support is suspended, the surface can be either positively or negatively charged. When the surface is negative, cationic species are attracted to it and become adsorbed. While a positive surface interacts with negative species.

2.2.1.4 Gas-phase deposition method

Gas-phase deposition method has also been used to prepare hydrogenation catalysts. A systematic comparative study of preparing catalysts via gas phase deposition and via wet impregnation and testing in cinnamaldehyde hydrogenation was performed by Lashdaf et al. (2003). Small Pd metal crystallites were formed by gas-phase deposition method even with high metal loadings, whereas larger Pd particles were achieved via impregnation. Additionally, Pd catalysts which were prepared by gas-phase deposition method were more selective to cinnamyl alcohol formation than the impregnated catalysts with larger metal particles. Ni/Al_2O_3 and Ni/SiO_2 catalysts prepared by gas-phase deposition method were tested in citral hydrogenation (Mäki-Arvela et al., 2003). The result showed that by this method a more even metal distribution can be achieved. A higher selectivity to citronellol was obtained over this new Ni/SiO_2 catalyst than that over a conventional Ni/SiO_2 catalyst.

2.2.1.5 Sol-gel technique

A sol-gel technique means direct inclusion of a metal precursor in the sols. The sol-gel-derived Au/TiO_2 catalyst was prepared by using tetrabutoxytitanium (IV), gold acetate, methanol, and distilled water as starting components (Claus et al., 2000). The resulting Au/TiO_2 catalyst was tested in acrolein hydrogenation at 240 ^oC under 2 MPa, and the selectivity to allyl alcohol was 19% at 100% conversion. Additionally, Ag/SiO_2 (Claus and Hofmeister, 1999) catalyst was prepared by sol-gel method with Ag particle size of 4.5 nm. The Ag/SiO_2 was used in crotonaldehyde hydrogenation at 140 ^oC and 2 MPa resulting in more than 60% selectivity to crotyl alcohol.

2.2.1.6 *In-situ* metal introduction method

In-situ metal introduction into mesoporous materials method is an attractive method to prepare hydrogenation catalysts. Direct inclusion of metal particle in the synthetic gel of mesoporous materials has been studied in the cases of Ru (Kumar et al., 2004), Rh (Boutros et al., 2006), Pt (Song et al., 2006; Boualleg et al., 2009), Pd (Papp et al., 2005; Mastalir et al., 2007; Dominguez-Dominguez et al., 2008), and Ir (Albertazzi et al., 2003) in hydrogenation reactions. Metal containing mesoporous materials with MCM-41 pore architecture have been prepared via a template directed hydrolysis-polycondensation of tetraethoxysilane and rhodium (III) chloride in aqueous ammonia (Boutros et al., 2006). The resulting materials showed a good catalytic activity and stability in the hydrogenation of arene derivatives under mild pressure and temperature. Song et al. (2006) reported a preparation of Pt/SBA-15 by adding Pt colloidal solution to the synthesis gel. Monodispersed Pt nanoparticles of 1.7-7.1 nm were first synthesized by alcohol reduction methods, and then incorporated into mesoporous SBA-15 silica during hydrothermal synthesis. The Pt/SBA-15 catalysts were tested in ethylene hydrogenation, and the hydrogenation rates were invariant with particle size. This controlled growth by sol-gel process of a hierarchically organized silica matrix around a colloidal solution of metal nanoparticles using supramolecular interactions between a surfactant (used as the structure directing agents of the oxide matrix) and metal colloids could be an attractive way to get a highly disperse catalysts. Figure 2.2 showed the schematic procedure of this method (Boualleg et al., 2009). However, sometimes the catalytic performances of these catalysts are not good as expected, which is due to the incomplete metal incorporation or to circumvent the presence of tricky stabilizing ligands such as PVP in the synthetic procedures. PVP are difficult to

remove from the metal particles without their sintering and not compatible with acidic media generally used for obtaining highly structured silica matrixes.

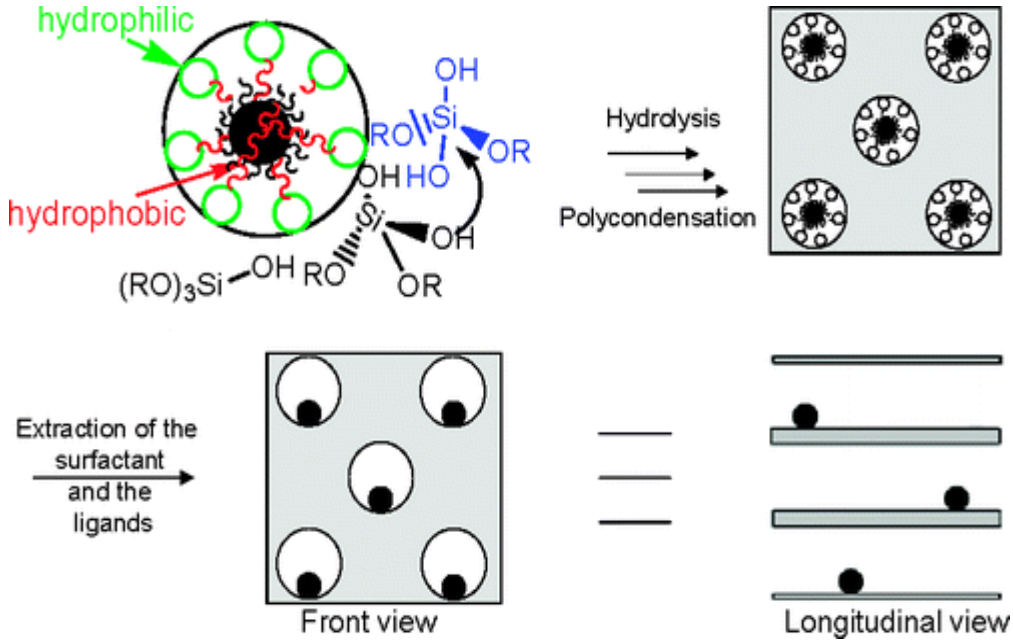

Figure 2.2 Schematic presentation of in-situ metal introduction into mesoporous materials method (Boualleg et al., 2009).

2.2.1.7 Immobilization of homogeneous catalysts on porous materials

Immobilize homogeneous catalysts in porous materials is also a promising method for the preparation of supported metal catalysts, because fine tuning of the metal complexes in terms of electronic states and steric environment is substantially easier than with the metal salts used in the conventional catalyst preparation. However, the catalytic properties of these immobilized catalysts have shown an enormous variation and in many cases were significantly below those of the homogeneous analogues (Crosman and Hoelderich, 2007). Since the reasons for these differences in performance are usually not understood, it is still of interest to test different immobilization methods and supports in order to get a systematic picture of positive and negative effect. Pt nanoparticles in the size range of 1.7-7.1 nm protected by PVP were incorporated into mesoporous SBA-15 silica using low-power ultrasonication, the

catalysts used in the hydrogenation of ethylene (Rioux et al., 2005). Using dendrimer-encapsulated metal nanoparticles as catalyst precursors offers the opportunity to control metal particle size and composition. Figure 2.3 (Lang et al., 2003) showed the schematic route to prepare dendrimer-derived supported nanoparticle catalysts. The resulting catalysts were active for both oxidation and hydrogenation reactions. Jiang et al. (2006) reported Pd nanoparticle catalysts stabilized by Gn-PAMAM-SBA-15 organic-inorganic hybrid composites, and these catalysts showed highly catalytic activity for the hydrogenation of allyl alcohol. Crosman et al. (2005) present a straightforward method for immobilizing rhodium diphosphine complexes on aluminated SBA-15 based on ionic interaction between the negatively charged Al-SBA-15 framework and the cationic rhodium of the organometallic complex.

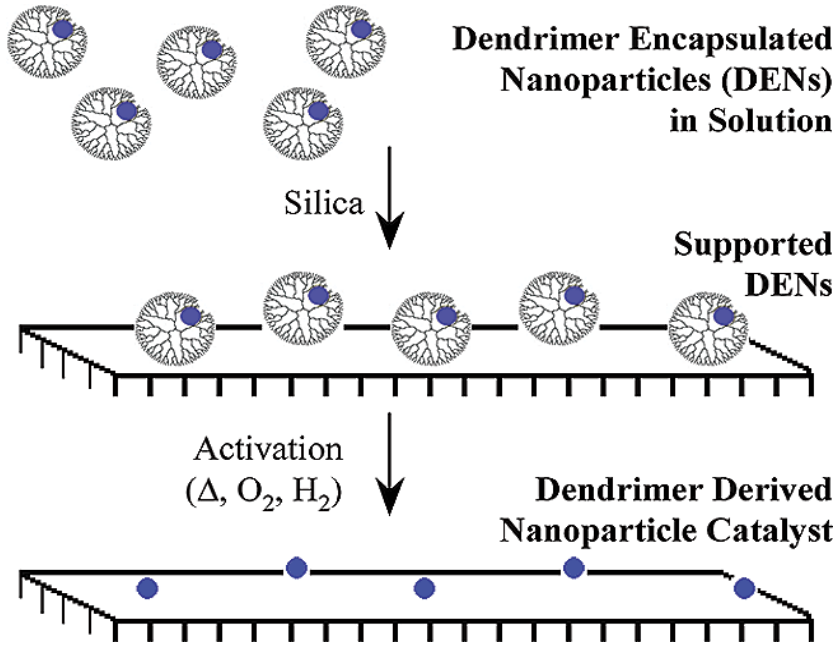

Figure 2.3 Schematic route to dendrimer-derived supported nanoparticle catalysts (Lang et al., 2003).

There is a growing interest in the application of ionic liquids in various field of catalyst preparation. For instance, Huang et al. (2004) reported the immobilization of Pd nanoparticles onto molecular sieves with a porous diameter of 6.7 nm using the ionic liquid (1,1,3,3-tetramethylguanidinium lactate) (as shown in Figure 2.4). The

catalytic system was used for solvent-free hydrogenation of olefins, and high activity and stability was achieved.

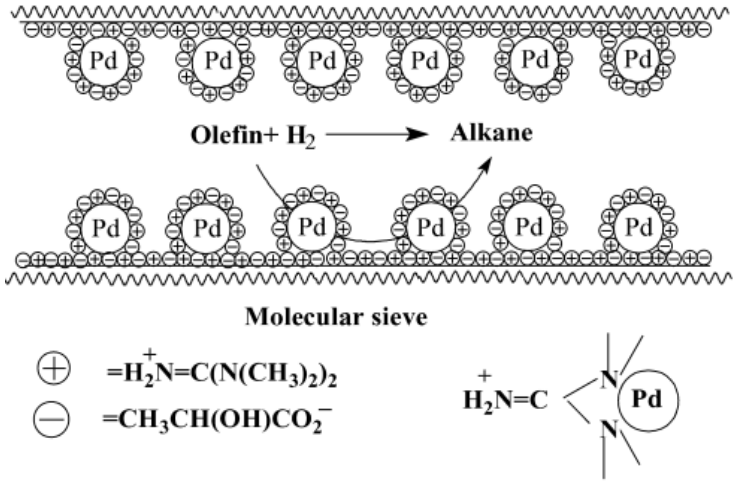

Figure 2.4 Illustration of the immobilization of Pd nanoparticles at the surface of a molecular sieve with an ionic liquid layer (Huang et al., 2004).

For these preparation methods catalyst pretreatment is often necessary, because the solid materials containing metal compounds in non-metallic state can exhibit only low catalytic activity or be catalytically inactive. Catalyst pretreatment involves the catalyst calcination, catalyst reduction, and the catalyst aging (Maki-Arvela et al., 2005). If the metal originates from chloride precursor the amount of residual chloride can be decreased with calcination. Catalyst reduction temperature has been very intensively investigated in the case of reducible supports exhibiting SMSI effect (Haller et al., 1989). However, even over conventional supports, e.g. alumina and silica the catalyst reduction temperature can have dramatic effects on the catalytic performance. The nature of the support affects the mobility of different metals during catalyst pretreatment. Catalyst pretreatment affects both catalytic activity and selectivity, since it can change metal particle size, morphology, amount of residual chloride, influence alloy formation, lead to reduction of reducible oxides, which decorate the metal surface as well as in case of carbon can alter the amount of the oxygen containing surface groups.

2.2.2 Selection of metal catalysts

The catalytic characteristics are determined mainly by the major metal component. Nickel (Ni), cobalt (Co), copper (Cu), platinum (Pt), palladium (Pd), ruthenium (Ru), rhodium (Rh), osmium (Os), iridium (Ir), and rhenium (Re) are used most often and each metal has its own activity and selectivity profile.

Ni is used extensively in hydrogenation since Sabatier's discovery of its activity. The preparation and activation of Ni catalysts have studied by numerous investigators (Fouilloux, 1983). It is frequently used in skeletal form as Raney nickel, which is produced by leaching away alumina from alloy of Ni and aluminum. The hydrogenation of almost all the functional groups can be accomplished over some form of Raney nickel.

Co catalysts have been used not so widely as Ni catalysts in the usual hydrogenations, but their effectiveness over Ni catalysts has often been recognized in the hydrogenation of aromatic amines and nitriles to the corresponding primary amines (Nishimura, 2001). The methods of preparation for cobalt catalysts are very similar to those used for the preparation of nickel catalysts.

Cu is usually not active as a hydrogenation catalyst and tends to lose its activity at high temperature. Adkins et al. (1931) have developed an efficient Cu catalyst for the liquid-phase hydrogenation by combining copper and chromium oxides, known as copper chromite oxide or copper chromite. It is active for the hydrogenation of esters to alcohols and amides to amines.

The platinum group metals-ruthenium, rhodium, palladium, osmium, iridium and platinum- have all been used as hydrogenation catalysts. Among the platinum metals, Pt and Pd have been by far the most widely used catalysts since the earliest stages of the history of catalytic hydrogenation. Compared to the base metals, these metals are

active under mild conditions. It has been recognized that the second-row group VIII metals (Ru, Rh, Pd) often show behavior different from that of the third-row group VIII metals (Os, Ir, Pt) in catalytic hydrogenation (Bond et al., 1962).

Pt is capable of promoting the hydrogenation of most functional group under relatively mild conditions. Esters, carboxylic acids, and amides are the only common functional groups not hydrogenated over this catalyst.

Pd is the best catalyst for the hydrogenation of olefins and acetylenes. It is also useful for the hydrogenation of phenol to the corresponding cyclohexanone. However, Pd is a very bad catalyst for hydrogenation of carbonyl groups, which is due to a too weak adsorption of carbonyls under reaction conditions.

Ru can promote the hydrogenation of aromatic rings without the hydrogenolysis of any amino and hydroxyl groups present on the ring even though high temperatures and pressures are required for the reaction. Ru is also particularly effective for the low pressure hydrogenation of ketones and aldehydes especially in an aqueous environment. Therefore, Ru is particularly active for the hydrogenation of aqueous sugar solutions to polyols (e.g. glucose to sorbitol) and it maintains its activity for a long period (Kluson and Cerveny, 1995).

Rh is often used for the hydrogenation of carbonyl groups, carbocyclic aromatic, and heteraromatic systems at low temperatures and pressures.

Os is a less active catalyst than the other platinum metals but it has some advantages in certain hydrogenations such as the conversion of α, β-unsaturated aldehydes to the corresponding unsaturated alcohol and the hydrogenation of halonitrobenzenes to the halo anilines with little dehalogenation.

Ir has been not widely used in catalytic hydrogenation. Recently, however, Ir-based catalysts have been shown to be effective in various hydrogenations, such as in

selective hydrogenation of α, β-unsaturated aldehydes to allylic alcohol, of aromatic nitro compounds to the corresponding hydroxylamines, of halonitrobenzenes to haloanilines without loss of halogen, and in the stereoselective hydrogenation of carbon to carbon double bonds (Savchenko et al., 1997).

Re catalysts had found little attention until their attractive catalytic properties in hydrogenation have been revealed by a systematic study by Brodbent et al. (1954). Re catalysts are effective catalysts for the hydrogenation of unsaturated carboxylic acids and amides.

2.2.3 Selection of supports

The primary role of the support is to finely disperse and stabilize small metallic particles and thus provides access to a much larger number of catalytically active atoms than in the corresponding bulk metal. The choice of a suitable support is very important, because the interaction with the active phase may play a critical role in the final performance of the catalysts. The most conventional supports are acidic or basic oxides and different types of carbons. Supports can have very different properties, like specific surface area, pore volume, acidities, electronic and geometrical properties. Additionally, the shape of catalyst particles can vary from powders and pastes to pellets, fibers and monoliths.

2.2.3.1 Oxides

The most conventional oxide supports are alumina (Al_2O_3) (Echeverri et al., 2009; Hoxha et al., 2009) and silica (SiO_2) (Chen et al., 2008; Manyar et al., 2009). Basic magnesia (MgO) (Recchia et al., 1999; Sordelli et al., 1999), a variety of reducible oxides, like titania (TiO_2) , ceric oxide (CeO_2) (Fajardie et al., 1996; Campo et al.,

2009), zirconia (ZrO_2) (Claus et al., 2000; Gaspar et al., 2008), Gallia (Ga_2O_3) (Gebauer-Henke et al., 2007) (Dominguez et al., 2005) and alloy forming oxides, i.e. zinc oxide (ZnO) (Ramos-Fernandez et al., 2008), stannic oxide (SnO_2) (Liberková and Touroude, 2002; Liberkova et al., 2002), have also been studied in hydrogenation reactions. A comparison of different oxides in hydrogenations were performed with Ru (Bachiller-Baeza et al., 2005), Pt (Kijenski et al., 2002), Pd (Pinna et al., 2001), and Cu (Saadi et al., 2000). In general oxide supports can provide stronger interactions with the main metal than carbon. Additionally, the full reduction of the metal might be more difficult on an oxide than on carbon. Furthermore, acidic oxides can promote side reactions, for instance alumina favors cyclization of citronellal in citral hydrogenation (Silva et al., 2003). Several metals supported on reducible oxides (TiO_2, CeO_2, ZrO_2, or Ga_2O_3) have been applied in hydrogenations. In these cases, the possible interaction of the noble metal with the partially reduced oxide (strong metal-support interaction effect, SMSI) or even with the metal formed upon a reduction treatment, has been proposed to be responsible for the improved selectivity in hydrogenation of unsaturated aldehyde to unsaturated alcohols. For example, selective hydrogenation of crotonaldehyde was performed on 5% Pt/SnO_2 catalysts, and the improvement of catalytic activity and selectivity of the catalysts were due to the formation of Pt-Sn alloy on the metal particles of Pt (Liberková and Touroude, 2002). The alloy formation and the state of the active metal are very much dependent on the metal precursor and the type of support.

Supports with magnetic properties can be used as the supports for catalysts and facilitate their separation from the reaction media (Hu et al., 2005; Rossi et al., 2007). However, the low surface area and easy aggregation of magnetic nanoparticles cumber their practical applications as the supports of catalysts. To overcome these drawbacks,

magnetic nanoparticles have been introduced into silica (Li et al., 2009; Panella et al., 2009) and carbon (Lu et al., 2004). These types of magnetic nanoparticle-based materials combine the advantage of both mesoporous materials and magnetic nanoparticles. Figure 2.5 showed the schematic procedure of preparation the magnetic Pt/SiO_2 catalysts. First, the magnetite nanoparticles were prepared by coprecipitation method. Then the magnetite nanoparticles were coated with silica. After coating, the $Pt/SiO_2/Fe_3O_4$ catalyst was prepared by incipient wetting impregnation. The magnetic catalyst modified with cinchonidine showed a catalytic performance (activity, enantioselectivity) in the asymmetric hydrogenation of various activated ketones in toluene comparable to the best known Pt/alumina catalyst used for these reactions. In addition, the magnetic catalyst can be easily separated from the reaction solution by applying an external magnetic field.

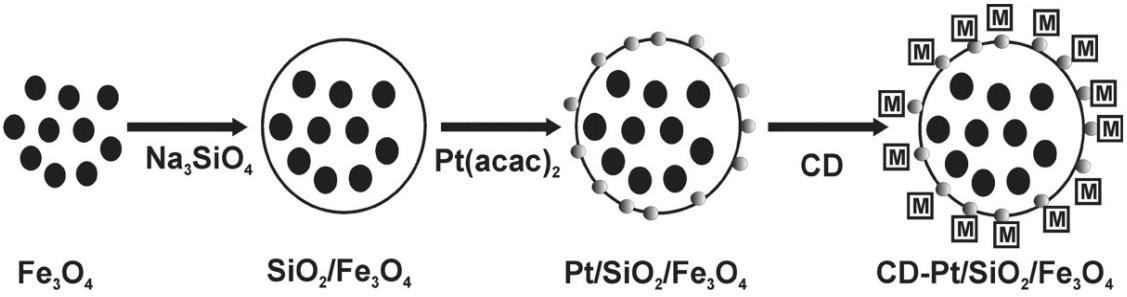

Figure 2.5 Schematic presentation of preparation of the magnetic, chirally modified $Pt/SiO_2/Fe_3O_4$ (M represents cinchonidine) (Panella et al., 2009).

2.2.3.2 Zeolites and mesoporous materials

Zeolites and mesoporous materials, which exhibit structured ordering at the nanometer scale, have been used for a long time in petrochemical applications. Due to their channel system and shape selective properties these materials have a potential for synthesis of fine chemicals. Zeolites and mesoporous alumina-silicate materials have acid sites, which arise from the presence of accessible hydroxyl groups associated with tetrahedral framework aluminum in a silica framework. The existence of acid sites

causes an enhancement in the hydrogenation rate as compared to hydrogenation in the presence of metals resting on non-acidic support, such as silica and alumina (Masalska, 2005). Two mechanisms have been proposed to explain this phenomenon. One of these involves the metal-support interactions, which modify the electronic state of the metal clusters on the support and make them more active for hydrogenation reactions. The other one, called hydrogen spillover, is based on the assumption that the hydrocarbons adsorbed on the acid sites of the support in the metal-acid interfacial region could be additionally hydrogenated by the spillover hydrogen which migrates from the surface of the metal particles to the surface of zeolite particles. The use of metal/zeolite systems in the hydrogenation reactions is of course limited to the molecules, which are small enough to enter into the zeolite pores. Zeolites such as ZSM-5, dealuminated Y zeolite, and alkali zeolite beta have been used as supports in toluene hydrogenation (Masalska, 2005), tetralin hydrogenation (Rocha et al., 2008), and chemoselective hydrogenation of citronellal (Kantam et al., 2006). Mesoporous materials have tunable pore sizes between 2 and 10 nm, therefore they can be more suitable for hydrogenation of large organic molecules than zeolite materials. Mesoporous materials such as MCM-41, MCM-48, and SBA-15 have been used in hydrogenation of alkynes (Papp et al., 2005), hydrogenation of arene derivatives (Boutros et al., 2006), hydrogenation of allyl alcohol (Jiang and Gao, 2006), propene hydrogenation (Boualleg et al., 2009), and hydrogenation of dimethyl itaconate (Crosman and Hoelderich, 2005).

2.2.3.3 Clays

Clays also serve as supports for noble-metal catalysts used in hydrogenation reactions because of their high surface area and surface polarity. Clays may be divided into two broad groups: cationic clays, widespread in nature, and anionic clays, rarer in

nature but relatively simple and inexpensive to synthesize. The cationic clays have negatively charged alumino-silicate layers, which have cations in the interlayer space to balance the charge, while the anionic clays have positively charged metal hydroxide layers with balancing anions and water molecules located interstitially (Angelo, 1998). To date, a variety of methods have been developed to introduce catalytically active noble metal species into clays. Pd nanoparticles deposited on montmorillonite with surfactants exhibit a high selectivity for the partial hydrogenation of 1-phenyl-1-pentyne to 1-phenyl-cis-1-pentene (Kiraly et al., 2001). Miao et al. (2006) reported that Ru nanoparticles were immobilized on montmorillonite by novel ionic liquid method and exhibited excellent activity for hydrogenation of benzene to cyclohexane, but Ru particles were found to tend to aggregate along the pore channels after several reaction runs. Metals supported on clays have also been used as catalysts in cinnamaldehyde (Szöllösi et al., 1998), crotonaldehyde (Kun et al., 2001), and dimethyl adipate hydrogenations (Figueiredo et al., 2009).

2.2.3.4 Functional organic polymers

Functional organic polymers can also be used as supports for metal nanoparticles in hydrogenation reactions. The polymer support can be a soluble linear or branched macromolecule or a micelle aggregate which “wraps” the metal nanoparticles in solution, thus, preventing metal sintering and precipitation. The protective polymers are usually functional macromolecules, which are able to give weak interactions with the metal nanoparticle surface in order to build a protective “shell” of polymer chains. The most commonly protective polymers are commercial poly-vinylpyrrolidone (PVP) (Yu et al., 1999), poly-ethyleneimine (PEI) (Bhattacharjee et al., 2009) and polyvinyl alcohol (PVA). Pt catalysts stabilized with PVP exhibited very high activities and

selectivities in cinnamaldehyde hydrogenation at 60 ^{o}C and 4 MPa in ethanol (Yu et al., 1999).

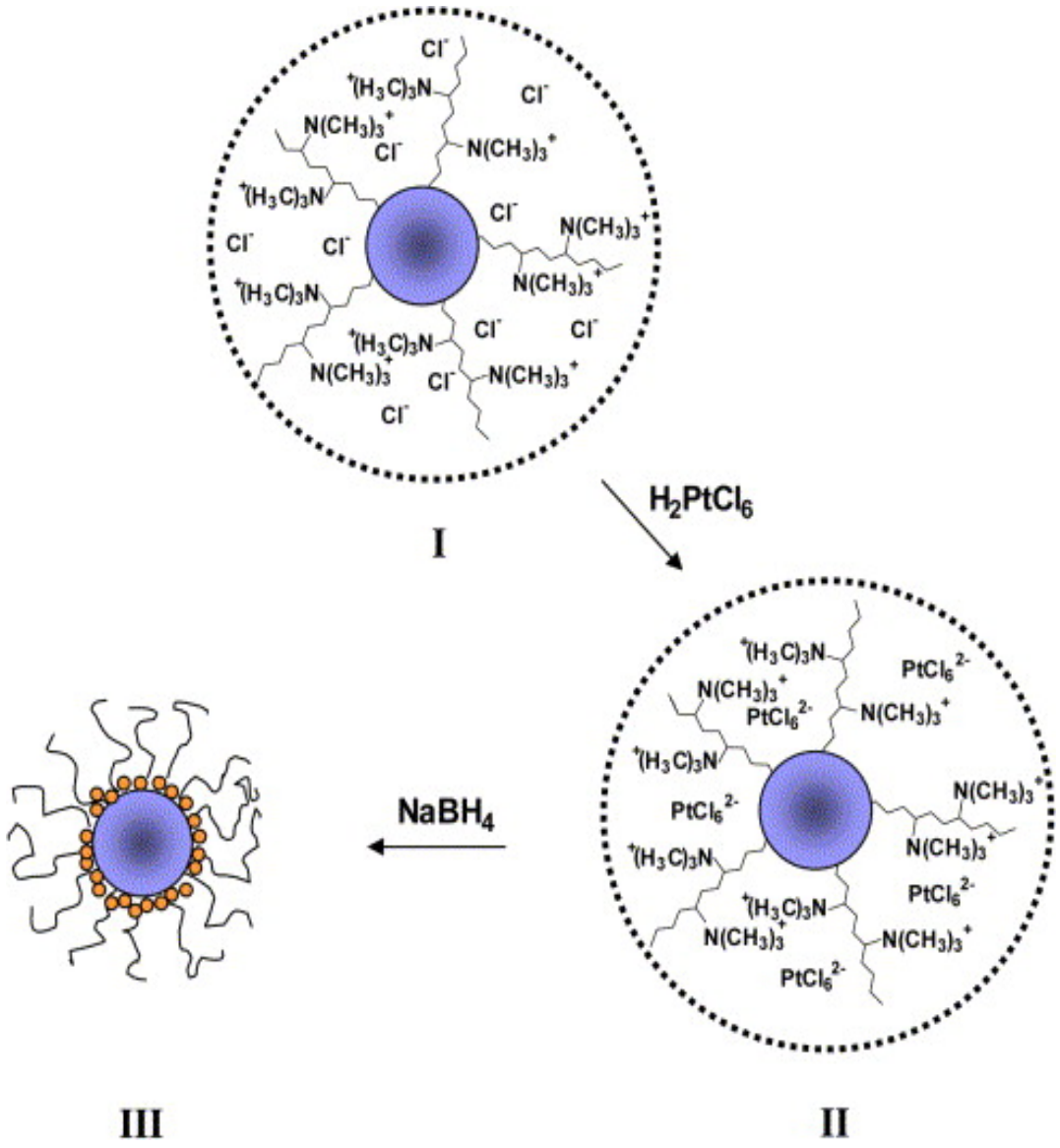

Figure 2.6 Schematic presentation of formation of Pt particles on the surface of the spherical polyelectrolyte brush particles (Sharma, et al., 2007).

On the other hand, it can be resin, i.e. an insoluble material consisting in a bundle of physically and/or chemically cross-linked polymer chains in which the metal nanoparticles are embedded (Kralik and Biffis, 2001). Resin-supported metal nanoparticles have been used in hydrogenation of citral (Centomo et al., 2005), dehydrolinalool (Sulman et al., 1999), and 2-ehtylanthraquinone (Drelinkiewicz et al.,

1999). Sharma et al. (2007) reported the preparation of the Pt nanoparticles on the surface of spherical polyelectrolyte brush particles. As shown schematically in Figure 2.6, the polyelectrolyte chains are generated on the surface of the polystyrene core with a thin shell of poly(2-methyl-propenoyloxyethyl)trimethylammonium chloride (I). (I) was exchanged with $PtCl_6^{2-}$ to give (II). After $NaBH_4$ reduction Pt nanoparticles supported on spherical polyelectrolyte brushes particles (III) were formed. The catalyst showed good catalytic activity and recyclability in hydrogenation of butyraldehyde to 1-butanol. Functional organic polymer supported metal catalysts provide the better control of the metal particles morphology (size and shape) compared to classical supported catalysts. However, there are several drawbacks for these catalysts such as their difficult preparation, a relatively low productivity and/or stability and separation problems

2.2.3.5 Carbons

Several types of carbons have been applied in hydrogenation reactions. Application of carbon support is described in more detail in Section 2.4.

2.2.4 Bi- and multi-metallic catalysts

Bi- and multi-metallic catalysts have long been an important area of catalysis research. Certain combinations of metals are known to improve activity, selectivity, or catalyst lifetime. One classical example is the Lindlar catalysts (Pd-Pb/$CaCO_3$) (Lindlar et al., 1973), where the addition of lead allows the selective hydrogenation of acetylenic bonds. Another example is the Nishimura catalyst (Rh-Pt oxide) (Nishimura, 1544) for the mild hydrogenation of aromatic rings. The improvement of the bi- and multi-metallic catalysts is primarily due to changes in their geometric and electronic

structures introduced by the second element, which can exist as an adatom (Santori et al., 2002), in an alloy state (Liberkov and Touroude, 2002; Reyes et al., 2002), in an ionic state (Santori et al., 2002; Marchi et al., 2003), and as partially oxidized form (Reyes et al., 2002).

Various typical structure models of bimetallic nanoparticles are shown in Figure 2.7. Core-shell segregated bimetallic nanoparticles (Figure 2.7a) consist of a shell of one type of atom B surrounding a core of another atom A, though there may some mixing between the shells. This mixing pattern is common to a large variety of systems. Subcluster segregated bimetallic nanoparticles (Figure 2.7b) consist of A and B subclusters, which may share a mixed interface (left) or may only have a small number of A-B bonds (right). Mixed A-B bimetallic nanoparticles (Figure 2.7c) may be either ordered (left) or random (i.e., a solid solution, right). Multishell bimetallic nanoparticles (Figure 2.7d) present layered or onion-like alternating –A-B-A- shells.

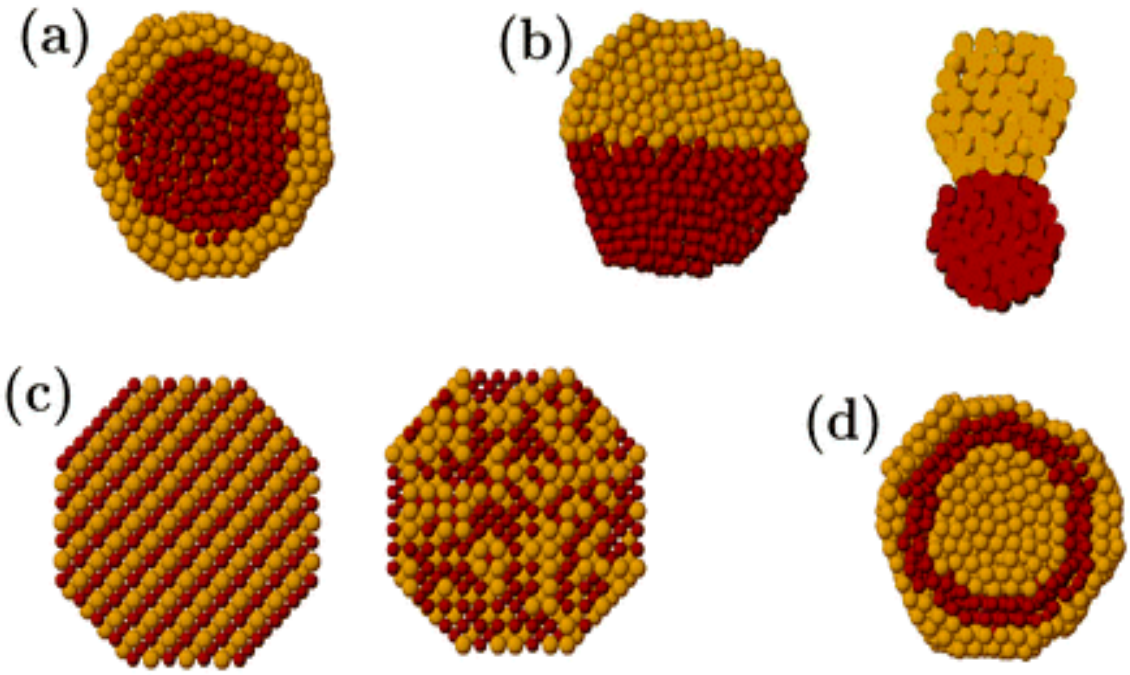

Figure 2.7 Schematic representation of some possible mixing patterns of bimetallic nanoparticles: (a) core-shell, (b) subcluster segregated, (c) mixed, (d) three shell (Ferrando et al., 2008).

The degree of mixing and atomic ordering in AB bimetallic nanoparticles depends on the following factors (Ferrando et al., 2008). First one is relative strengths of A-A, B-B and A-B bonds. If A-B bonds are strongest, this favors mixing, otherwise, segregation is favored, with the species forming strongest homonuclear bonds tending to be at the center of the bimetallic nanoparticles. Second one is surface energies of bulk elements A and B. The element with lowest surface energy tends to segregate to the surface. Third one is relative atomic sizes. Smaller atoms tend to occupy the more sterically confined core. Fourth one is charge transfer. Electron transfer from less to more electronegative elements favors mixing. Fifth, the element that binds most strongly to the support or ligands may be pulled out toward the surface.

The catalytic effect of the second metal element can often be explained in terms of an ensemble and/or a ligand effect in catalysis. When atoms surrounding a metal atom on the surface are replaced by other atoms, this will change the nature of chemisorption bond. This is called electronic or ligand effect. In the case of core/shell structured bimetallic nanoparticles, the shell element can provide a catalytic site and the core element can give an electronic effect (a ligand effect) on the shell element. The term ensemble effect refers to the number of active sites on the surface that are required for a particular reaction. It is well known that the modification of an active group VIII transition metal with IB metals greatly suppresses the catalytic activity for hydrocarbon reactions, which require a large number of neighboring surface atoms (ensembles). While the reaction, which needs one metal adsorption site, is not affected. Thus, reactions that require a large ensemble of active sites can be selectively suppressed by blocking a fraction of these active sites, improving in this way the selectivity toward reactions that require a small ensemble of active sites.

For supported bimetallic catalysts, metallic dispersion can also be modified by the addition of a second metal (Guczi, 2005). First, the formation of a mixed oxide phase could mutually prevent the surface mobility of both metals. This results in the formation of small oxide particles ultimately leading to the increased dispersion of the active metal component. Second, the formation of an oxide interface between the support and the active metal could also lead to a stabilization of the high dispersion. Third, the diminished deactivation of supported metal catalysts may lead to an increased metal dispersion. The deactivation is usually due to the formation of a large carbide phase, which needs a large ensemble size. In bimetallic particles dilution of the active metallic component with a non-active metal decreases the ensemble size, and further hinders the formation of carbide phase. In addition, enhanced amounts of weakly bound surface hydrogen also retard the surface deactivation processes.

2.2.5 Catalyst promoters

Small quantities of various substances that have favorable effects on activity, selectivity, or catalyst life may be loosely termed promoters (Rylander, 1979). The promoters are adsorbed on the catalyst, which can be solid acids, sulphur compounds, alkali metal oxide, or transition metal oxides. The beneficial effect of promoters is known for a long time, but there are many particular cases where the mechanism of promotion is still obscure. Cinchona alkaloids are efficient chiral surface promoters for enantioselective hydrogenation of various activated ketones over heterogeneous catalysts (Busygin et al., 2008). Alkali metal oxides or transition metal oxides (MgO and CeO_2) have been used as promoters in gas phase hydrogenation of crotonaldehyde and in liquid phase hydrogenation of citral (Bachiller-Baeza et al., 2001). In the hydrogenation of cinnamaldehyde, the activation of C=O was enhanced by using an

electropositive metal (Li^+, Na^+ and K^+) with respect to Pt (Koo-amornpattana and Winterbottom, 2001). Cinnamaldehyde adsorbs on the promoter surface via donation of a lone pair electrons from the oxygen atom (Figure 2.8). The possible promoting mechanisms could be an increased electron density of the metal, and presence of Lewis acid sites near the metal particle.

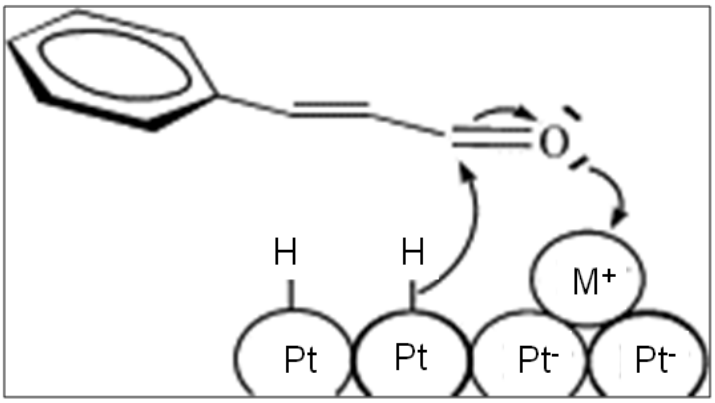

Figure 2.8 Schematic representation of promoter effect in hydrogenation of cinnamaldehyde (M^+=Li^+, Na^+, or K^+) (Koo-amornpattana and Winterbottom, 2001).

2.2.6 Amorphous alloys

Amorphous alloys represent a new class of powerful hydrogenation catalysts due to the higher activity, better selectivity, and stronger sulfur resistance than their corresponding crystalline metal catalysts (Li et al., 2007; Acosta et al., 2008; Meng et al., 2008). Amorphous alloys usually can be obtained by chemical reduction of metal salt with borohydride (BH_4^-) or hypophosphite ($H_2PO_2^-$) (Chen, 1998; Deng et al., 1999). Amorphous alloy catalysts have been used in sugar hydrogenation (Li et al., 2000; Li et al., 2008; Meng et al., 2008), benzene hydrogenation (Li et al., 2001), and acetonitrile hydrogenation (Yang et al., 2008). The high catalytic activities and selectivities as well as poison resistance can be explained by the alloying effect of the metalloids boron or phosphorus on the surface electronic states and the surface structural properties. The low thermal stability of amorphous alloys restricts their

application in industry. In order to overcome the shortcoming while retaining their attractive characteristics, supported amorphous alloys were prepared.

2.2.7 Catalyst deactivation

The main causes of the catalyst deactivation in the liquid-phase were found to be phase transformations of active components (sintering or leaching), coking, poisoning of the active site by impurities in solvents and reagents or by-products, or by deposition of less active or totally inactive metal or metal oxide on noble metal surface (Besson and Gallezot, 2003).

2.3 Hydrogenation of D-glucose

Hydrogenation of aldoses to alditols (sugar alcohols such as sorbitol, mannitol, and xylitol) has been an industrially importance process, and many patents and articles may be found in the literature. Of these sugar alcohols, sorbitol is by far the most important and is manufactured in largest scale, since it finds numerous applications in various fields such as vitamin C production, cosmetics and dentifrices, foods, surfactants and adhesives, pharmaceuticals, and many other miscellaneous uses. Sorbitol is found in many natural products such as seaweed, tobacco, edible fruits, and plants. Sorb berries and mountain ash berries are particularly rich source of the sorbitol. It was first isolated in 1872 by the French chemist, Joseph Boussingault (Fedor, 1960). Atlas Powder was the first to make sorbitol commercially based on electrolysis of glucose in the early 1930's (Fedor, 1960). In 1956 Merck entered the field using a process based on catalytic hydrogenation of glucose (Fedor, 1960). Today it is commercially produced by the hydrogenation of D-glucose and is available in both liquid and crystalline form with a world capacity of more 1 Mt/a (Eisenbeis et al., 2009).

Approximately 60% of the produced sorbitol is utilized in processed foods, confections, toothpaste and other personal care products such as humectants, stabilizers, softeners, emulsifiers and bodying agents. An additional 16% of the total market for sorbitol is utilized for the production of L-ascorbic acid (Vitamin C) (the process is shown in Figure 2.9) (Crezee et al., 2003). In tobacco industries, sorbitol may give mild effect in sniff, and avoid acrolein formation which formed in burned glycerine. Sorbitol is also used as softener and color stabilizer in textiles and as softener in leather industries. In addition, sorbitol can be efficiently converted into H_2, synthesis gas, alkanes, liquid fuels, and oxygenates (Figure 2.10 shows the essential features of the bifunctional reaction pathway for the production of alkanes from sorbitol.) (Huber et al., 2003; Davda and Dumesic, 2004; Huber et al., 2004).

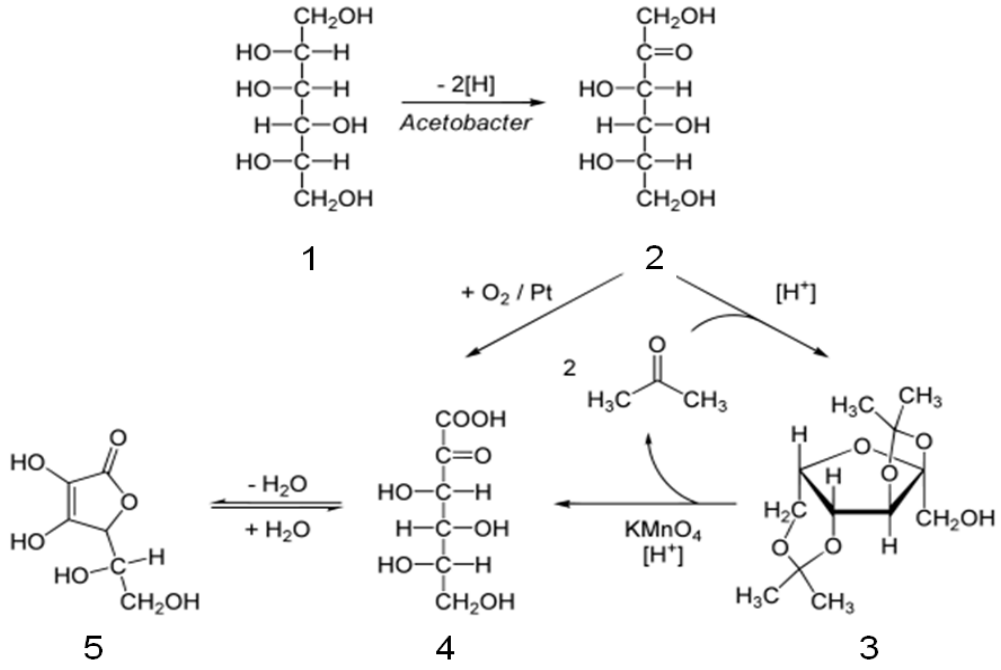

Figure 2.9 Reichstein process for the production of ascorbic acid from D-glucose (from website: http://www.absoluteastronomy.com/topics/Reichstein_process). The reaction steps are: 1) microbial oxidation or fermentation of sorbitol to L-sorbose with acetobacter with pH 4-6 and 30 ^{o}C; 2) protection of the 4 hydroxyl groups in sorbose by formation of the acetal with acetone and an acid to Diacetone-L-sorbose; 3) organic oxidation with potassium permanganate followed by heating with water gives the 2-Keto-L-gulonsäure; 4) the final step is a ring-closing step or gamma lactonization with removal of water. Intermediate 4 can also be prepared directly from 2 with oxygen and platinum.

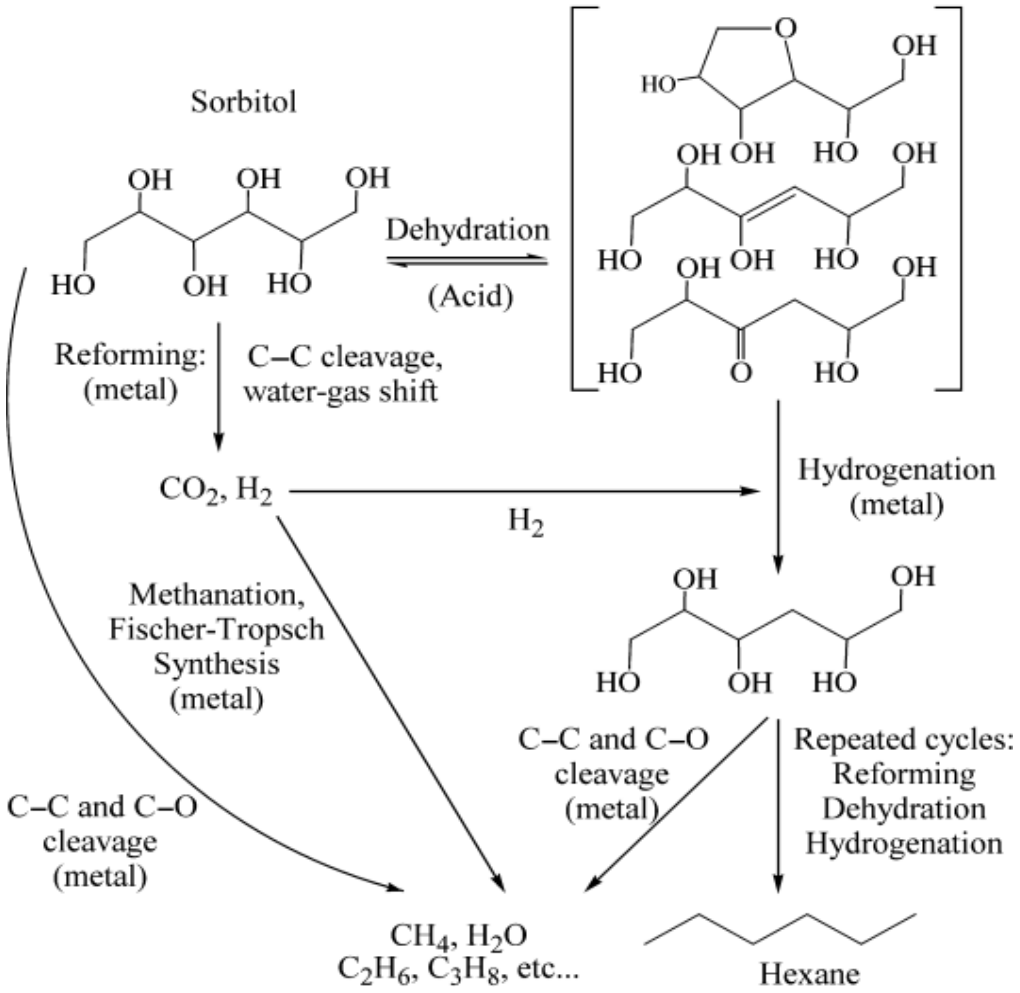

Figure 2.10 Reaction pathways for the production of alkanes from sorbitol over catalysts with metal and acidic components (Huber et al., 2004). Hydrogen is produced on the metal by cleavage of C-C bonds followed by the water-gas shift reaction. Dehydrated species such as ring compounds like isosorbide or enolic species are formed on acid sites, which migrate to metal sites where they undergo hydrogenation reactions. Repeated cycling of dehydration and hydrogenation reactions in the presence of hydrogen leads to heavier alkanes (such as hexane) from sorbitol. Formation of lighter alkanes takes place by more rapid cleavage of C-C bonds compared to hydrogenation of dehydrated reaction intermediates.

In industrial hydrogenation of glucose can typically be performed batchwise in stirred tank reactors at temperatures ranging from 80 to 150 ^{o}C, pressures of 4-18 MPa, and pH values from 4.5 to 7 with 1-6wt% catalyst (Nishimura, 2001). The use of continuously operated trickle-bed reactors is less common in industry. The hydrogenation process is in principle straightforward, but it is complicated by the generation of small amounts of by-products, such as D-gluconic acid formed by the

Cannizaro reaction and D-mannitol formed by hydrogenation of D-fructose and D-mannose (as shown in Figure 2.11a). The rate of hydrogenation of D-glucose is increased in alkaline solution, but these conditions also promote the isomerization of D-glucose to D-mannose and D-fructose (Lobry de Bruyn-van Ekenstein transformation, shown in Figure 2.11b) and the Cannizzaro reaction

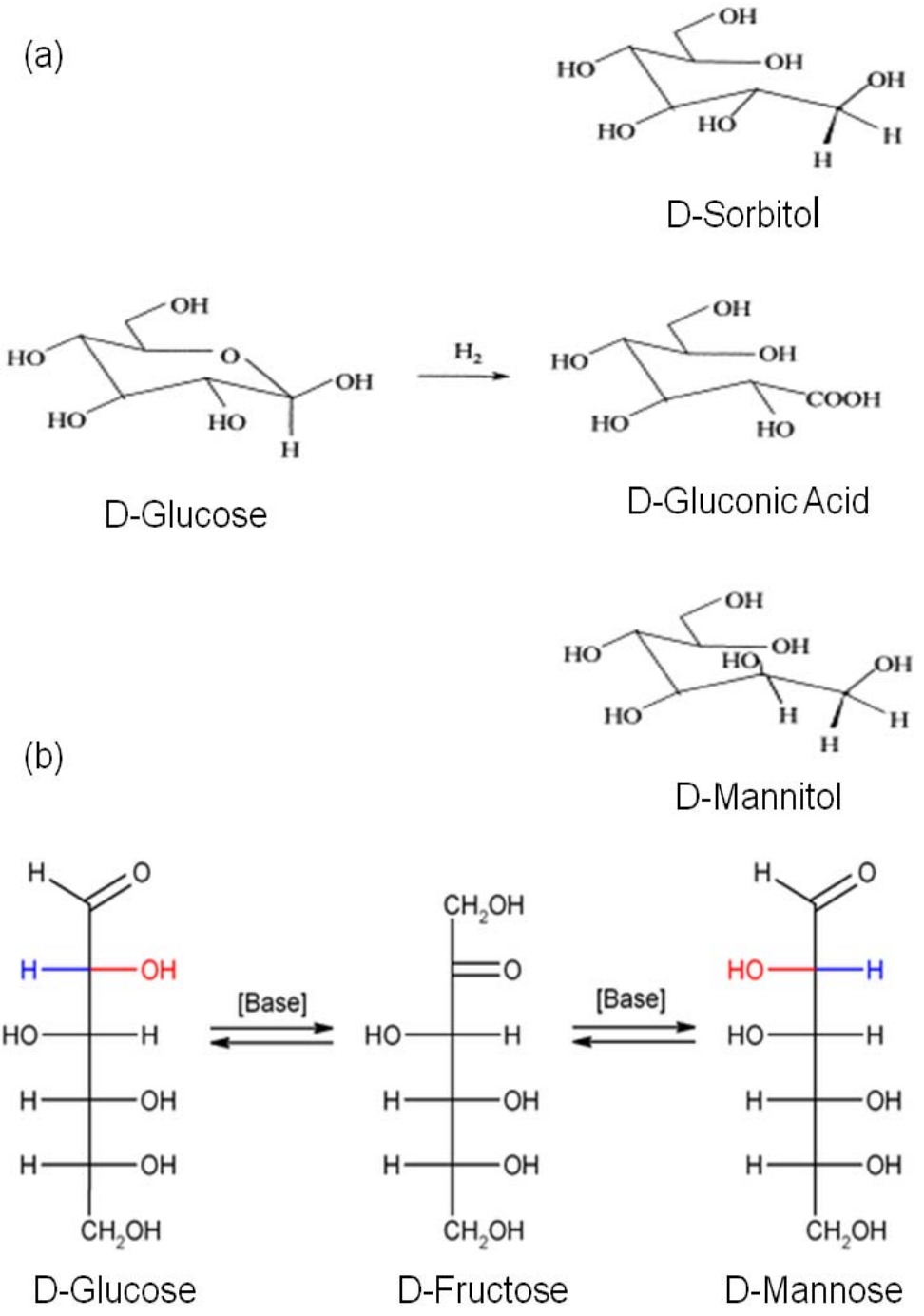

Figure 2.11 (a) Hydrogenation of D-glucose to D-sorbitol, (b) Lobry de Bruyn-van Ekenstein transformation of D-glucose (Hoffer et al., 2003).

2.3.1 Catalysts for the hydrogenation of D-glucose

The most common catalysts in D-glucose hydrogenation are based on Ni as active metal. Historically, Raney Ni was used because of its economic price. Later supported Ni catalysts were more frequently used because they are more active (Schimpf et al., 2007). To increase activity and stability, Ni was promoted with some catalyst promoters, such as molybdenum (Mo), chromium (Cr), iron (Fe), titanium (Ti), and tin (Sn) (Gallezot et al., 1994; Li et al., 2000; Hoffer et al., 2003; Schimpf et al., 2007; Acosta et al., 2008). The promoters in a low-valent state on the Ni surface act as Lewis adsorption sites for the oxygen atom of the carbonyl group which is then polarized and thus more easily hydrogenated via a nucleophilic attack on the carbon atom by hydride ions. However, due to the leaching of Ni and catalyst promoters into the product and fast deactivation of the catalyst, alternative heterogeneous catalysts have been tested, including supported metals such as cobalt (Co), copper (Cu), platinum (Pt), palladium (Pd), rhodium (Rh) and ruthenium (Ru) (Wisnlak and Simon, 1979; Makkee et al., 1985; Li et al., 2001; Perrard et al., 2007).

The general observed order of activity for the hydrogenation of D-glucose is as follows (Wisniak et al., 1974; Wisnlak and Simon, 1979): Ru > Ni > Rh > Pd. Among these catalysts, Ru is the most promising catalysts. Furthermore, Ru is not dissolved under the reaction conditions of the hydrogenation of D-glucose to D-sorbitol. Ru catalysts are most often supported on alumina, silica, titania or activated charcoal (Gallezot et al., 1998; van Gorp et al., 1999; Hoffer et al., 2003; Kusserow et al., 2003; Besson et al., 2005; Perrard et al., 2007; Yuan et al., 2008). Ru-B amorphous alloys (Guo et al., 2003) and water soluble Ru complex with sulfonated phosphine ligand (Kolaric and Sunjic, 1996) have also been used in D-glucose hydrogenation. While the low thermal stability of amorphous alloys and difficulty in removing and recovering of

the homogenous catalysts restrict their application in industry. Ruthenium (III) chloride is referred to as the most often used active component precursor. Conventional impregnation and the incipient wetness technique are the methods reported most frequently for the preparation of supported Ru catalysts.

However, these supported Ru catalysts have a common issue, namely rapid deactivation (Kusserow et al., 2003). For example, Arena (1992) investigated the hydrogenation of D-glucose over Ru/Al_2O_3, whereas Gallezot et al. (2003) studied a Ru/C catalyst. Both groups concluded that deactivation of the catalyst could be attributed, in part, to poisoning of the Ru surface by metal impurities in solution. Arena also found that byproduct formation and increased levels of alumina crystallinity contributed to catalyst deactivation. Furthermore, Gallezot et al. postulated that deactivation also involved sintering of Ru particles. Maris et al. (2006) examined D-glucose hydrogenation over Ru/SiO_2, and they found that the mechanism of particle growth involves migration of Ru species during the hydrolysis of the silica surface. Thus, the choice of catalyst support and the preparation method are crucial in the hydrogenation of D-glucose. Because of the inert nature of carbon, Ru nanoparticles supported on carbon appear to be promising catalysts for D-glucose hydrogenation.

2.3.2 Mechanism and kinetics in hydrogenation of glucose

Hydrogenation kinetics of D-glucose has been studied over Ru/C (Crezee et al., 2003), Ru/Al_2O_3 (Bizhanov and Drozdova, 1982), silica-alumina supported Ni catalysts (Dechamp et al., 1995) and Raney Ni catalyst (Brahme and Doraiswamy, 1976). Literature about D-glucose hydrogenation kinetics is nicely summarized by Crezee et al. (2003) in the introduction part. Usually a Langmuir-Hinshelwood mechanism is a good approximation for the kinetics. In aqueous solution, D-glucose

exists as a mixture of α-, β-pyranose forms and the open aldehyde form. These forms will have different adsorption constants and their own characteristic rates of hydrogenation. These factors will determine which form is preferentially adsorbed and hydrogenated. Molecular models indicate that the adsorption of the β-pyranose form will more favorable through the coordination of O-1, O-5, and O-6 (Makkee et al., 1985). It is proposed that the hydrogenation of D-glucose over Ru/C involves the formation of an ionized β-pyranose species adsorbed on the Ru surface by coordination of O-1, O-5, and O-6, which is susceptible to attack by hydrogen at the anomeric carbon (Figure 2.12).

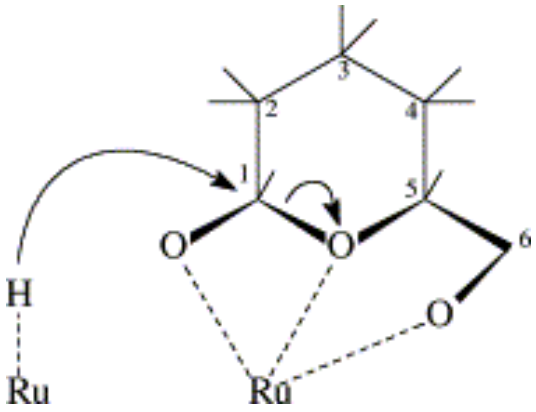

Figure 2.12 Schematic representation of the reaction mechanism between adsorbed β-D-glucopyranose and hydrogen (Crezee et al., 2003).

2.4 Porous carbon as a catalyst support

Among the different types of supports used in heterogeneous catalysis carbon materials attract a growing interest due to their specific characteristics which are mainly: (i) resistance to acid/basic media, (ii) possibility to control, up to certain limits, the porosity and surface chemistry, (iii) easy recovery of precious metals by support burning resulting in a low environmental impact, and (iv) although carbon is usually hydrophobic, the chemical nature of the surface can be modified to increase the hydrophilicity, and even carbons with ion-exchange properties can be prepared.

Numerous publications have been written about carbon and its use as catalyst support or catalyst in its own right (Auer et al., 1998; Rodríguez-reinoso, 1998). The most common carbon support materials are activated carbon and carbon black. Besides the commercially used carbon, the appearance of novel carbon materials, such as carbon nanotubes (CNTs), carbon nanofibers (CNFs), and templated-synthesized porous carbons, has attracted tremendous attention.

Although carbon is considered to be an inert material in comparison with other catalyst supports such as alumina and silica, its surface has a proportion of active sites, constituted by unsaturated valences at the edges and defects of the graphitic hexagonal crystallites (graphene layers). The proportion of these active sites will increase as porosity and surface area increase. The presence of heteroatoms (mainly oxygen, hydrogen, and nitrogen) also introduces active sites on the carbon surface, and consequently the carbon surface is not as inert as it could be expected. The functionalities present on the carbon surface in the form of surface oxides (e.g. carboxylic groups, phenolic groups, lactonic groups, etheric groups) are responsible both for the acid/base and the redox properties of the activated carbon (Figure 2.13). These surface groups act as nucleation centers for the generation of highly dispersed metallic crystallites.

The preparation of carbon-supported catalysts is carried out mainly by impregnation, incipient-wetness or ion-exchange, thus the interaction of the solution with the carbon surface is critical. The adsorption capacity is determined by both the porous structure and the chemical nature of the surface. Thus carbons having the same surface area but prepared by different methods may show markedly different adsorption characteristics. Since carbon is essentially non-hydrophilic nature, it has a very low affinity for solvents of polar character such as water and high affinity for non-polar solvents such

as acetone. The metal precursor will be mostly located at the external surface of the carbon particle when using water, but it will penetrate to the interior of the porosity when using acetone, thus leading a more uniform distribution throughout the carbon particle.

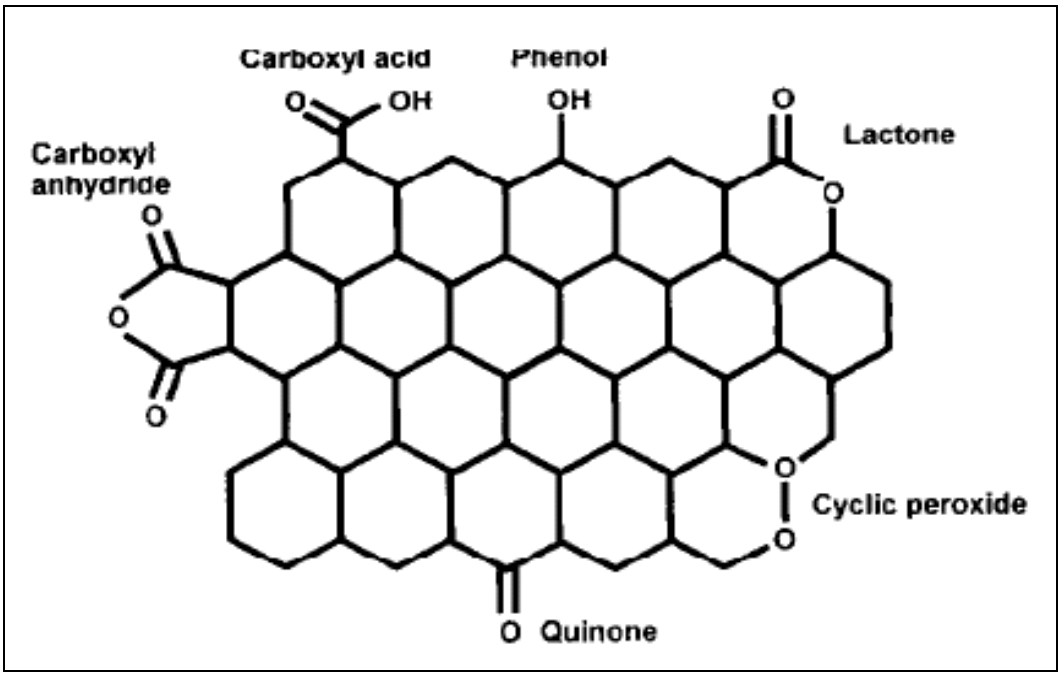

Figure 2.13 Some types of oxygen surface groups in activated carbon (Rodríguez-reinoso, 1998).

2.4.1 Activated carbons and carbon blacks

Activated carbons and carbon blacks are the most common carbon support materials. Activated carbons have a porous structure, usually with a relatively small amount of chemically bonded heteroatoms (mainly oxygen and hydrogen). The high surface area of activated carbons is mainly concentrated in microporosity, and this may be an inconvenience for both the preparation of the catalyst and the catalytic activity when in both cases large molecules are involved. Furthermore, the active phase particles placed on the support porosity can cause problems of micropore accessibility to reactants and products, thus limiting the effectiveness of microporosity. Activated carbon-supported Pt catalysts were highly active and selective for the production of crotyl alcohol in the

vapor-phase hydrogenation of crotonaldehyde (Coloma et al., 1997), and the metal particle size is related with the amount of oxygen surface groups. H_2 spillover was observed at ambient temperature on activated carbon-supported Pt in benzene hydrogenation (Srinivas and Rao, 1994). Carbon blacks are manufactured by the pyrolysis of hydrocarbons such as natural gas or oil fractions from petroleum processing (Auer et al., 1998). Compared to activated carbons, carbon blacks only possess limited specific surface area in the range of 100-1500 m^2/g, the porosity is built up from three-dimensional agglomeration of very small (5-100 nm), non-porous primary particles into branched chains and clusters. Carbon blacks supported Pd catalysts were prepared by an incipient wetness impregnation method and tested in benzene hydrogenation (Jen et al., 2007). The deactivation is found to be accompanied by Pd sintering, and the Pd sintering is due to the loss of Pd-C interaction.

2.4.2 Carbon nanofibers (CNFs) and carbon nanotubes (CNTs)

CNFs and CNTs as supports have been carried on different catalytic reactions (De Jong and Geus, 2000; Serp et al., 2003). Such structures can display unusual behaviors compared to classical supports, especially for liquid-phase reactions, in which the diffusion of the reactants and products are significantly influenced by the external size of particles. The carbon nanofilaments are grown from carbon-containing gases using a metallic catalyst. Figure 2.14 showed the different types of CNFs and CNTs. In 1994, Rodriguez et al. (1994) first published an article in which they introduced active phase (Fe or FeCu) onto the CNFs via an incipient-wetness technique, followed by calcination and reduction. In comparison with alternative supports (γ-alumina and activated carbon), the FeCu/CNFs catalyst displayed an order of magnitude higher activity for ethene hydrogenation. This activity enhancement was due to a unique

metal-support interaction between the FeCu particles and the basal-plane regions of the CNFs. In the same year, Planeix et al. (1994) first reported the carbon nanotubes as supports for 3-7 nm Ru nanoparticles in the hydrogenation of cinnamaldehyde. Although the mechanism still remains unclear, the reaction involved a noticeably higher selectivity (>92%) for cinnamyl alcohol generation as compared with the use of Ru supported either on Al_2O_3 (20-30%) or active carbon (30-40%). Since then, the vast majority of applied studies involving metal-nanoparticle deposition on CNTs and CNFs have associated with Pt, Pd, Ru, Ag and Au (Pham-Huu et al., 2001; Vu et al., 2006). Because as-synthesized CNFs and CNTs materials are hydrophobic, it is difficult to emplace an active phase. Therefore, pre-treatment procedures are needed to achieve optimal interaction between the support and the catalyst precursor (Toebes et al., 2003; Castillejos et al., 2009).

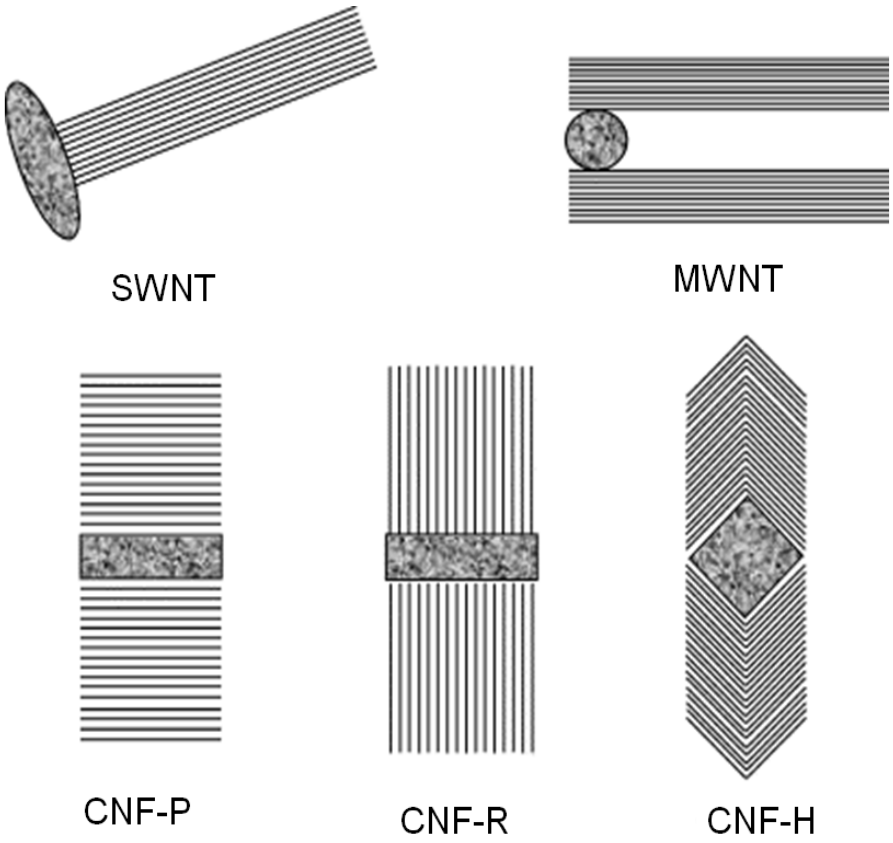

Figure 2.14 Different types of CNTs and CNFs.

2.4.3 Templated-synthesized porous carbons

Templated-synthesized porous carbons with a uniform pore size, high surface area and interconnected network are a better catalysts carrier than traditional porous carbons (Zhao et al., 2006). There are two types of templates allowing one to achieve the template strategy, namely soft template and hard template as schematically illustrated in Figure 2.15. The former refers to those organic species, which can be subsequently removed by calcination or solvent extraction. The latter refers to porous structures, such as zeolites, mesoporous silicas, and colloidal crystals that are used to form porous frameworks. Using the preparation of porous carbons as an example, the hard template method works this way. First, the template pores are filled with a carbon precursor such as sugar, benzene, and furfuryl alcohol. After carbonization under proper conditions followed by removal of the template framework, a porous carbon with pores replicated from the template framework is obtained.

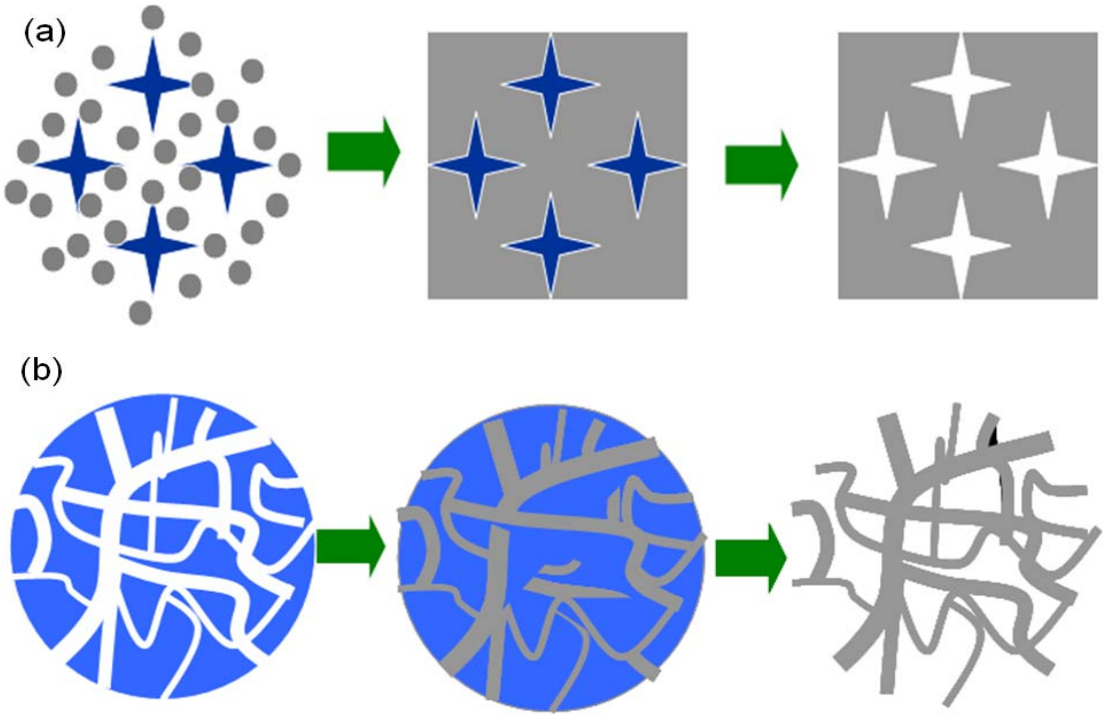

Figure 2.15 Scheme of synthesis of the porous materials with the (a) soft template; (b) hard template.

Hard templates that can be used include zeolites, ordered mesoporous silicas and colloidal crystals. Knox et al. (1986) were the first to use the hard template method to synthesize porous glassy carbon. Since then, there have been rapid advances in template synthesis of ordered porous carbons, ranging from microporous to mesoporous carbons, and further to macroporous carbons. There are two strategies via which carbon precursors may be introduced into the pore channels of porous silica or aluminosilicate templates: liquid impregnation or chemical vapor deposition (CVD). Liquid impregnation is usually followed by polymerization and pyrolysis (carbonization) steps or cycles. In CVD, a carrier gas is used to deliver the carbon precursors into the pore channels of the porous template followed by thermal treatment at a target temperature to form the carbon framework. This allows the polymerization and carbonization of the carbon precursor to occur simultaneously in the pore channels of templates.

Zeolites are microporous crystalline aluminosilicates with a channel-like and/or cage-like pore structure of pore-opening sizes in the range of 0.3-1.0 nm. The spatially periodic pore structure and well-defined nanospaces of zeolites offer one to control the nanostructure and morphology of microporous carbon materials at the nanometer level. In the past decades, many zeolite templates (e.g., zeolite Y, zeolite β, and ZSM-5) and carbon precursors (e.g., furfuryl alcohol, phenol-formaldehyde, and sucrose) have been employed to fabricate microporous carbons with a high specific surface area, a large pore volume, and various morphologies (Kyotani et al., 1997; Ma et al., 2000; Ma et al., 2001; Meyers et al., 2001; Ma et al., 2002; Barata-Rodrigues et al., 2003; Kyotani et al., 2003; Su et al., 2004; Hou et al., 2005; Matsuoka et al., 2005; Su et al., 2005; Su et al., 2005; Su et al., 2005; Tosheva et al., 2005). Figure 2.16 showed the structural models of ordered microporous carbons prepared using different zeolite templates.

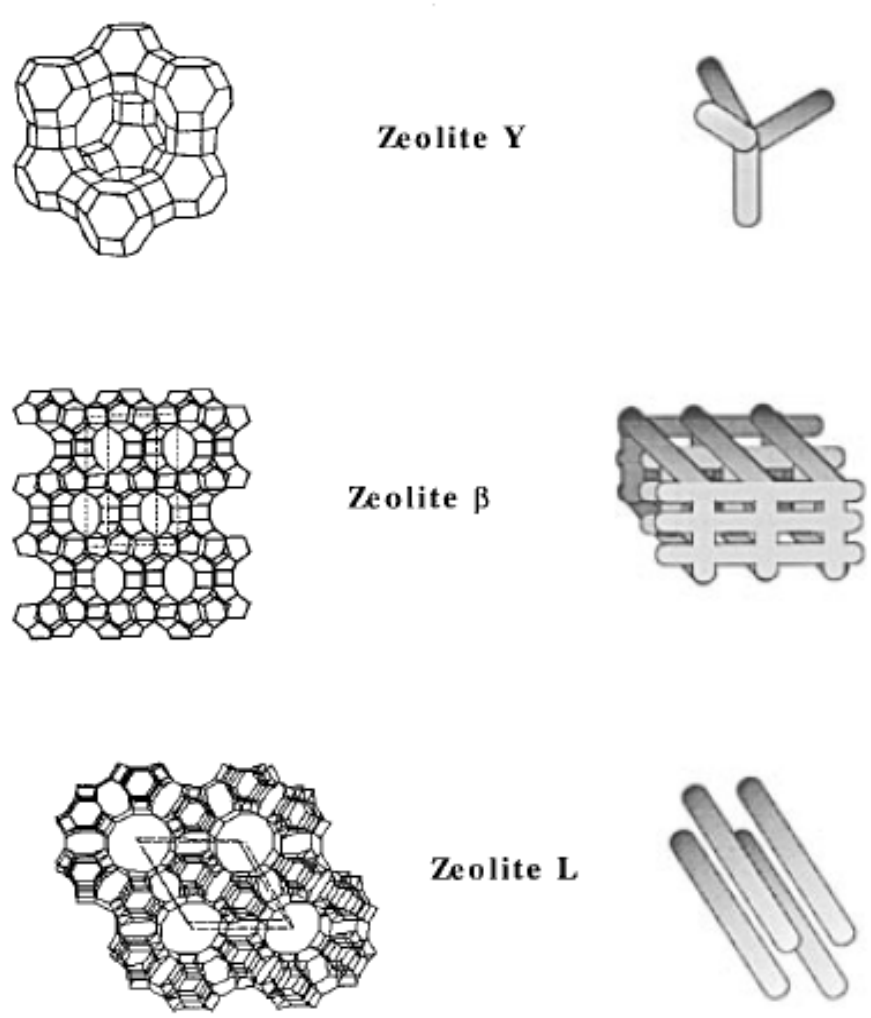

Figure 2.16 Structural models of ordered microporous carbons prepared using different zeolite templates (Ma et al., 2001).

The ordered mesoporous carbon is a unique porous carbon material that was first prepared by Ryoo et al. (1999) by hard templating method. Ordered mesoporous carbon (denoted CMK-1) was synthesized by using MCM-48 silica, which exhibits porous structures consisting of two disconnected interwoven three-dimensional (3-D) pore systems. Following the first report on the synthesis of ordered mesoporous carbons using the MCM-48 silica template, various mesoporous carbon materials with different pore structures were synthesized using a variety of different mesoporous silica templates (Ryoo et al., 2001; Lee et al., 2006; Liang et al., 2008). Hexagonally ordered mesoporous silica SBA-15 was used as a template for a mesoporous carbon

designated as CMK-3 (Jun et al., 2000). Unlike CMK-1, the ordered structure of the CMK-3 carbon was the exact inverse replica of the SBA-15 silica without the structural transformation during the removal of the silica template. CMK-3 is composed of carbon nanorods arranged in a hexagonal pattern, with connecting bridges between them. The pore size of an ordered carbon material synthesized with a hard template is primarily determined by the pore wall thickness of the inorganic templates, which can be tailored by the synthetic conditions (Lee et al., 2002). Figure 2.17 showed the structural models of ordered mesoporous carbons prepared using MCM-48 and SBA-15 as template, respectively.

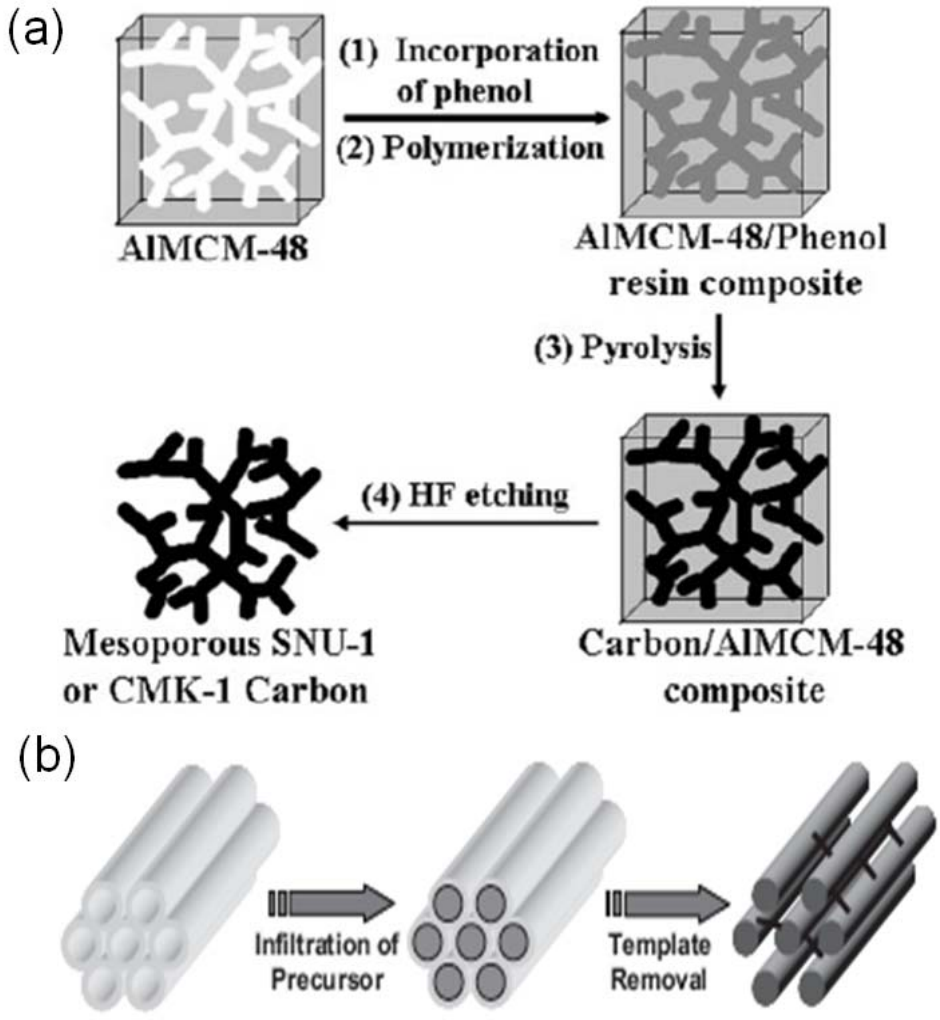

Figure 2.17 Structural models for ordered mesoporous carbons synthesized by using (a) MCM-48 as template (Lee et al., 1999); (b) SBA-15 silica as template (Lu and Schüth, 2006).

Colloidal-crystal-templated ordered macroporous carbon was first synthesized by Zakhidov et al. (1998), whereby using colloidal crystals as the template to fabricate highly ordered 3-D macroporous carbon. As schematically illustrated in Figure 2.18, spherical colloidal particles can self organize into a colloidal crystal, then the colloidal crystals serve as templates to fabricate ordered macroporous materials. Using volume-templating approach, a carbon precursor is infiltrated into the interstitial space between the colloidal spheres. Carbonization and removal of the opal template leave behind a three dimensional periodical carbon structure. Normally, liquid-phase carbon precursors such as phenolic resin (Chai et al., 2004) and sucrose solution (Lei et al., 2001; Yu et al., 2002) are used for infiltration. Alternately, CVD technique can be employed to enhance carbon infiltration. Both graphitic and diamond macroporous carbons were synthesized by using CVD and plasma techniques (Zakhidov et al., 1998).

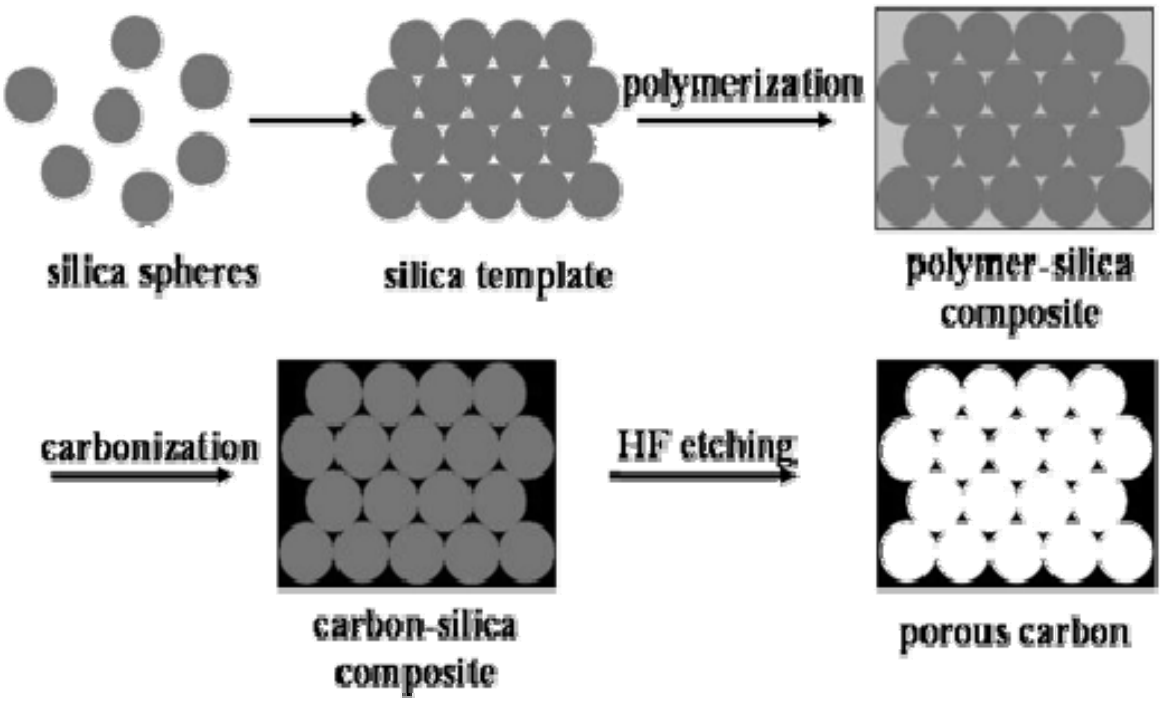

Figure 2.18 Synthetic procedures for uniform porous carbons of tunable pore sizes through colloidal crystal template approach (Chai et al., 2004).

A few studies have examined templated-synthesized porous carbons as heterogeneous catalysts during the last few years. Typical preparation method to incorporate metal particles on carbon support involves loading with metal precursors by ion exchange, impregnation and incipient-wetness methods, followed by catalyst activation. Since such methods always involve contact between a precursor solution and the carbon surface, it is often necessary to perform some surface functionalization on the porous carbons to increase the hydrophilicity of the surface and guarantee efficient wetting of the templated-synthesized porous carbons, in particular for aqueous precursors. Ryoo et al. (2001) incorporated Pt into nanoporous carbon structures using the incipient wetness technique with hexachloroplatinic acid to generate nanoparticles of Pt within the pore structure. The Pt cluster diameter can be controlled to below 3 nm, and the high dispersion of these metal clusters gave rise to promising electrocatalytic activity for oxygen reduction. Ferdi et al. (2004) introduced ferromagnetism in carbon particles which made the catalyst powder to be easily separated from solution and possessed the high catalytic reproducibility. The catalyst of Pd loaded on magnetic ordered mesoporous carbon displayed a good performance in the hydrogenation of octene to octane. When performance advantages over other carbon supports are observed, they are usually related to enhanced catalytic dispersion and easy diffusion of reagent/product through the mesoporous carbon.

Metal precursors can be introduced with carbon precursors at the templating stage to produce carbon-based nanocomposites with metals, such as Co, Pd, Pt, Ru (Holmes et al., 2005; Choi et al., 2005; Liu et al., 2006; An-Hui Lu et al., 2007; Su et al., 2007, Su et al., 2008). During carbonization in an inert atmosphere, metal salts/oxides are spontaneously reduced to metal nanoparticles. The growth and aggregation of the metal nanoparticles were hindered inside the confined mesoporous channels, resulting

in the formation of highly dispersed nanoparticles. For example, Pt nanoparticles studded in the mesoporous carbon nanorods were synthesized using direct conversion method (Choi et al., 2005). Figure 2.19 shows the schematic drawing of two methods: a presents the Pt nanoparticles supported on CMK-3 prepared by conventional impregnation method, while b displays the PtC nanocomposite prepared by directly conversion method. The size of the Pt nanoparticles prepared by directly conversion method was smaller than the channel size of the SBA-15 silica, while the size of Pt nanoparticles synthesized by conventional impregnation on CMK-3 was larger than the channel size of SBA-15. The Pt nanoparticles of PtC nanocomposite were accessible to CO, which indicated that they were exposed to the gas via the micropores in the carbon rods. These PtC nanocomposite showed an excellent performance in direct methanol fuel cells.

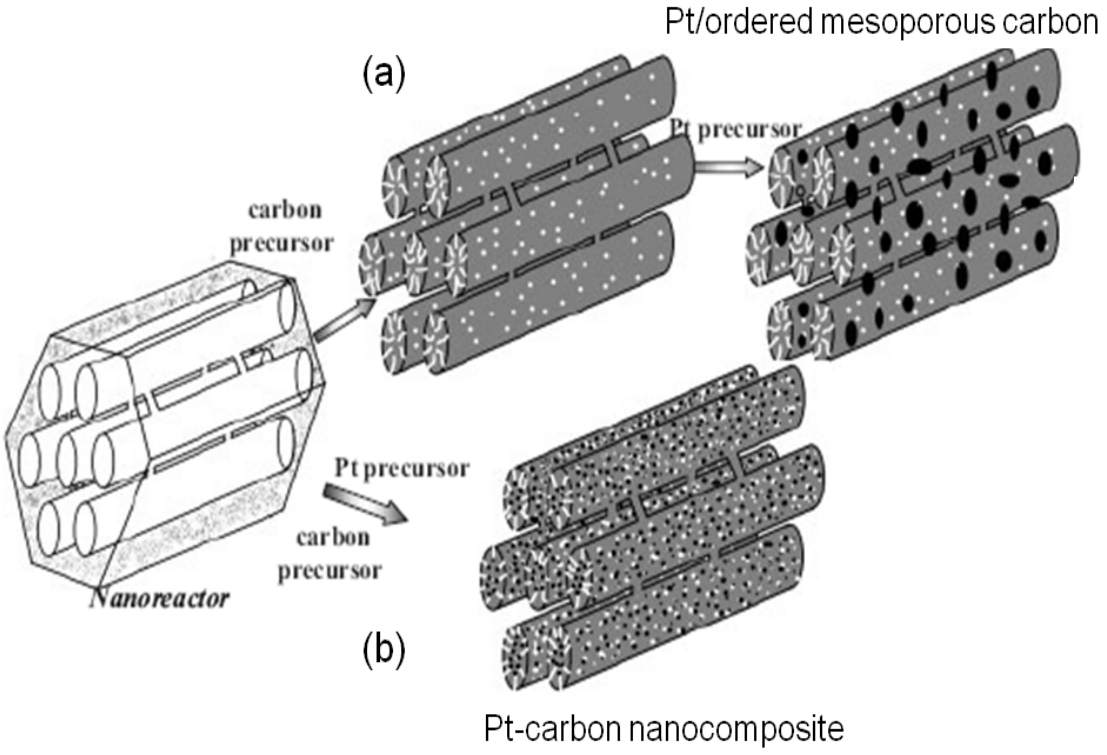

Figure 2.19 Schematic drawing of a) Pt/ordered mesoporous carbon prepared by a convention method, and b) the PtC-nanocomposite array synthesized using an SBA-15 template nanoreactor (Choi et al., 2005).

Despite the achievements reached by the aforementioned method, the synthesis of atomically dispersed metallic nanoparticles on ordered porous supports is still a challenge. For example, for many target compositions, the chemistry of the target material is not compatible with the conditions of the template-removal process. In addition, increasing metal loading without destroying structure is also a challenge. Furthermore, it is necessary to ensure a rigid structure, thus avoiding collapse of the pore system after removal of the template. Especially in the case of noble metals, it is important to prepare them with sizes as small as possible and highly dispersed throughout the support, in order to improve the catalytic efficiency and to minimize the cost.

2.4.4 Nitrogen-containing carbons

Nitrogen-containing carbons are exciting materials, as the inclusion of nitrogen can improve the properties of bulk carbon, such as the conductivity, basicity, wettability, oxidation stability, and catalytic activity (Czerw et al., 2001; Matsuoka et al., 2004; Hou et al., 2005; Gorgulho et al., 2009; Ismagilov et al., 2009). The performance of these materials crucially depends on the amount of nitrogen in the carbon host as well as its mode of integration. Two classes of C, N materials can be identified: nitrogen-rich compounds (CN_x, $x \geq 1$) and nitrogen-doped carbon. Nitrogen-rich compounds, such as carbon nitride (C_3N_4), have recently gained much attention because of their promising properties, such as "superhardness" (predicted for cubic β-C_4N_4) or semiconductivity (for the graphitic form g-C_3N_4). The synthesis of these nitrogen-rich carbon nitrides generally includes thermal condensation of nitrogen-rich precursors. Nitrogen-doped carbons can be obtained using the following several methods (Lu et al., 2004; Xia and Mokaya, 2004; Gorgulho et al., 2009): (i) reaction of porous carbon

with N-containing gases; (ii) co-carbonization of N-free and N-containing precursors; and (iii) carbonization of raw material containing N atoms.

X-ray photoelectron spectroscopy (XPS) and x-ray absorption spectroscopy (XAS) measurements (Machnikowski et al., 2004; Huang et al., 2009) suggest that nitrogen atoms in the carbon networks could occupy five chemically different sites: (a) pyridinic, (b) pyrrolic, (c) pyridonic, (d) quaternary, and (e) oxidized nitrogen (Figure 2.20).

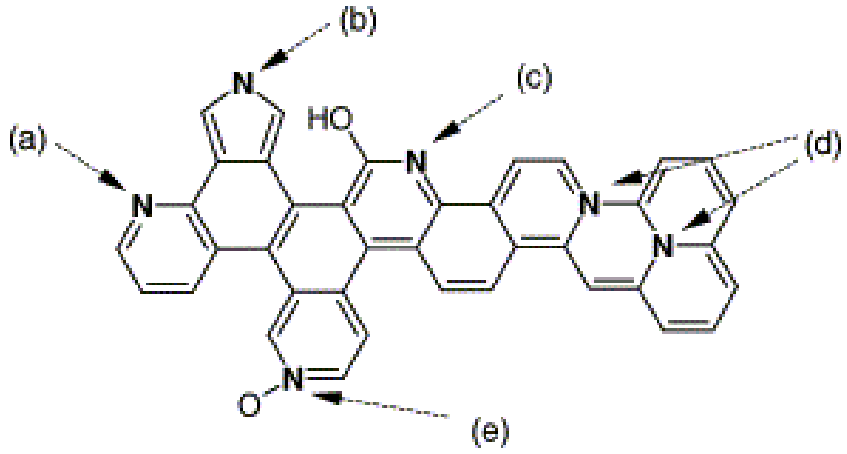

Figure 2.20 Nitrogen functionalities occurring in carbonaceous materials: a) pyridinic, b) pyrrolic, c) pyridonic, d) quaternary, and e) oxidized nitrogen (Machnikowski et al., 2004).

The variation in the relative intensity of these signals was found to be correlated with the catalytic activity. Pyridinic nitrogen bound to two carbon atoms at the edge of a layer retains a lone pair of electrons inducing electron donor properties to the layer. The quaternary nitrogen bound to three carbon atoms, either inside or at the periphery of the layers, is believed to generate a positive charge and acceptor properties. The pyridinic and quaternary nitrogen are the major forms distinguishable using XPS in the carbons produced between 800 and 1000 ^{o}C. The N-oxide and quaternary nitrogen are unreactive to chelate metal precursors, while pyrrolic nitrogen and pyridinic nitrogen are nitrogen groups that can efficiently anchor metal precursors and stabilize the final

nanocrystals (Li et al., 2006). CVD temperature will change chemical structures of nitrogen-doped carbon (Yang et al., 2001). Basically pyridinic nitrogens are formed at lower CVD temperature, and then converted to quaternary ones, which have higher thermal stability. In particular, the presence of quaternary nitrogens indicates alloying of nitrogen on the carbon.

The catalytic activity of nitrogen-containing carbon has been studied for more than 20 years, and I will summarize the existing literatures, which have compared the catalytic behavior of nitrogen-doped versus non-doped carbon supports. Amadou et al. (2008) reported a remarkable improvement of the catalytic activity in the liquid phase hydrogenation of cinnamaldehyde when Pd was supported on nitrogen-doped carbon nanotubes compared to catalysts based on Pd supported on carbon nanotubes and activated charcoal. The activity improvement was attributed to possible electronic or morphologic modifications of the active phase leading to a higher turnover frequency of the catalytic site. Nieto-Márquez et al. (2010) studied Ni supported on carbon and nitrogen-doped carbon nanospheres in the gas phase hydrogenation of butyronitrile, and the higher electron density on the surface of the supports delivered by nitrogen inclusion resulted in an enhanced catalytic activity. Furthermore, nitrogen, essentially in its quaternary form, led to an electron-enriched carbon surface, promoting the mobility of the metal and subsequent sintering. Raymundo-Piñero et al. (2003) reported the catalytic oxidation of SO_2 over activated carbon fibers, where nitrogen incorporation, mainly in the form of pyridinic groups, increased the catalytic activity. García-García et al. (2010) reported the catalytic activity of Ru-carbon in the ammonia decomposition, the catalytic activity of Ru particles was significantly improved when supported on nitrogen-doped carbon nanotubes. The presence of nitrogen atoms in the graphitic structure of the bamboo-like carbon nanotubes improves the basicity and the

electronic density of the support, and nitrogen atoms also act as an important promoter of Ru nanoparticles increasing their activities in the ammonia decomposition reaction. Nitrogen inclusion in different carbon structures has also been reported to enhance the catalytic behavior towards oxygen reduction and methanol oxidation in fuel cells (Choi et al., 2007; Kim et al., 2007; Chetty et al., 2009; Lyth et al., 2009; Kim et al., 2010). These results open an exciting research path, where a controlled tuning of nitrogen functionalities may conduct to a catalytic improvement, both in terms of activity and selectivity.

CHAPTER 3

EXPERIMENTAL SECTION

3.1 Chemicals

The chemicals used in this project are summarized in Table 3.1. All the chemicals were used as received without further purification.

Table 3.1 Chemical used in this thesis work.

Chemicals	Grade	Supplier
Alumina nitrate hydrate	98.5%	Merck
Benzene	≥99%	Sigma-Aldrich
Copper (II) chloride dihydrate	99+%	Sigma-Aldrich
Ethanol	99.5%	Aldrich
Glucose	ACS reagent	Sigma-Aldrich
Glucose	HPLC	Sigma-Aldrich
H-form zeolite Y (HY)		Zeolyst International Co.
Hydrochloride acid	37%	Merck
Hydrofluoric acid	48-51%	Tyco
Ni65		Sigma-Aldrich
Pyridine	99%	Sigma-Aldrich
5RuC		Sigma-Aldrich
Ruthenium (III) chloride hydrate	99.9%	Strem
Sorbitol	HPLC	Sigma-Aldrich
Sulfuric acid	98%	Merck
Triblock copolymer P123	Mw ~ 5800	Aldrich
Tetraethyl orthosilicate	98%	Aldrich
Urea	ACS reagent	Sigma-Aldrich

3.2 Synthesis methods

3.2.1 Preparation Ru nanoparticles embedded in templated porous carbon

H-form zeolite Y (HY) was purchased from Zeolyst International Co. Mesoporous SBA-15 silica template was synthesized following the procedure described by Zhao et al (1998). In a typical synthesis, 8g of P123 (Aldrich, typical M_n=5800) was dissolved in 60 mL of deionized water and 240 g of hydrochloride acid solution (0.74M) to form a clear solution, to which 17.6 g of TEOS was added. The suspension was stirred for 24 h at 40 ^oC. The final mixture was transferred to a Teflon-lined stainless-steel autoclave and placed in an oven at 100 ^oC for 24 h. After the hydrothermal treatment, the white precipitate was filtered, washed with deionized water, and dried at 80 ^oC in a vacuum oven for 24 h. The obtained sample was furthered calcined in air at 550 ^oC for 8 h with a heating rate of 2 ^oC/min.

Preparation of Ru/C catalysts. First, 0.5g of a dried hard template (either zeolite HY or SBA-15 silica) was impregnated with 2 mL of an aqueous solution containing 0.075g of ruthenium chloride, and the suspension was dried in air at 120 ^oC overnight. Secondly, the Ru-impregnated solid was then placed in a quartz tube and heated from room temperature to 900 ^oC at 5 ^oC /min under a pure N_2 flow (30cm^3/min) (as shown in Figure 3.1). Subsequently, infiltration of carbon was conducted in the tube with benzene as a precursor using the CVD method for 3 h. During this step, the Ru species was thermally reduced to Ru metal by carbon species and/or hydrogen gas released from benzene dehydrogenation at 900 ^oC. Finally, the black sample was treated with a 20% HF solution to remove the template, washed with deionized water, and dried at 120 ^oC overnight. The Ru catalyst obtained using HY as template is designated as RuC(HY). The Ru catalysts obtained using SBA-15 as hard template are designated as Ru6C3, Ru8C3, and Ru12C3, indicating 6wt%, 8wt%, and 12wt% loadings of Ru on

the SBA-15 silica template, respectively, and 3 h of CVD time at 900 ^{o}C. Another two catalysts, designated as Ru8C2 and Ru8C4, were similarly prepared using SBA-15 silica template with a Ru loading of 8wt%, CVD times of 2 and 4 h, respectively, at 900 ^{o}C.

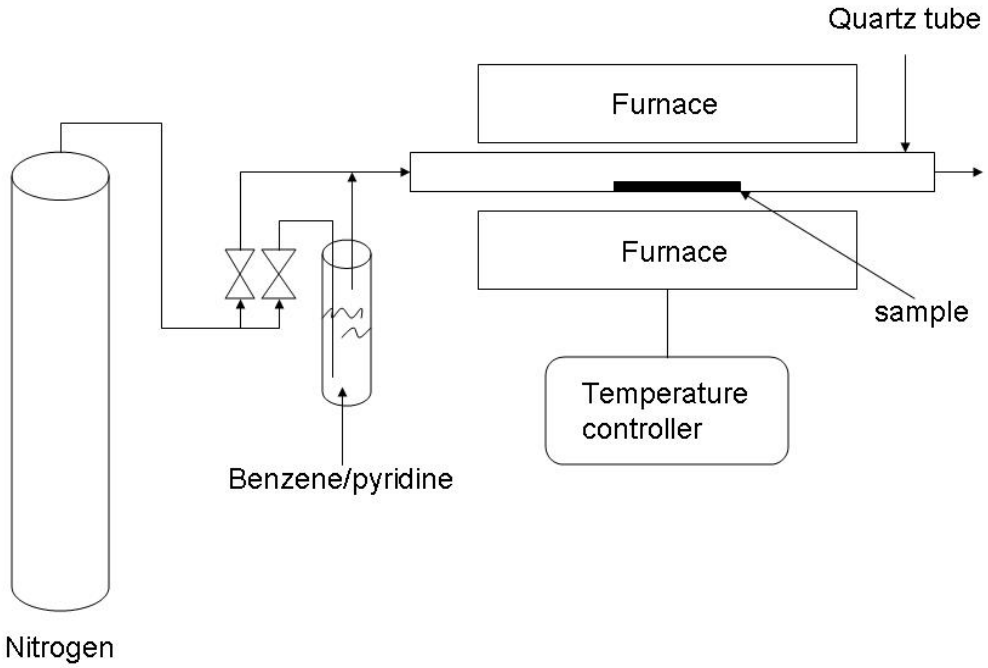

Figure 3.1 A scheme showing the CVD setup used in this work.

For comparison purposes, four Ru catalysts supported on zeolite HY- and SBA-15-silica-templated carbons, zeolite HY, and SBA-15 silica were prepared using a conventional catalyst preparation method. 0.5g of supports HY, SBA-15, HY- and SBA-15-silica-templated carbons were impregnated with 2 mL of an aqueous solution containing 0.075g of $RuCl_3$ followed by drying at 120 ^{o}C overnight. Hydrogen reduction was carried out at 300 ^{o}C for 2 h to obtain catalysts Ru/C-HY-H, Ru/C-SBA15-H, Ru/HY-H, and Ru/SBA15-H, in which "H" denotes hydrogen reduction. Two commercial catalysts Ni65 (~65wt% Ni supported on silica/alumina) and 5RuC (~5wt% Ru supported on activated charcoal) were used in this study for comparison purposes.

3.2.2 Preparation Ru-Cu bimetallic nanoparticles embedded in porous carbon

The preparation of bimetallic catalysts is described below. First, mesoporous SBA-15 silica was impregnated with 0.1 M ruthenium chloride solution and 0.1 M copper chloride solution under sonication for 0.5 h. The ratio of the volume of $RuCl_3$ solution over the mass of the solid was 4 mL over 1 g. The volume of $CuCl_2$ solution used was varied to change the amount of Cu in the resultant catalysts. Second, the suspension was dried in air at 120 ^oC overnight. Third, a 0.5 g of Ru/Cu-impregnated solid was placed in a quartz tube and heated from room temperature to 900 ^oC with a heating rate of 5 ^oC /min under a pure N_2 flow (30 mL/min). CVD was subsequently conducted at this temperature using benzene vapor for 2 h, which was carried into the tube by N_2 flow (30 mL/min) containing 5 wt% benzene. Finally, the black sample was treated with a 20 wt% HF solution to remove the silica template, washed with deionized water, and vacuum-dried at 120 ^oC overnight. The monometallic catalysts are designated as RuC and CuC. The RuCu bimetallic catalysts are designated as RuCu0.3C, RuCu0.5C, RuCu1.0C, and RuCu1.5C, indicating the molar ratio of Cu/Ru is 0.3, 0.5, 1.0, and 1.5.

The results and discussion can be referred to chapter 5 and chapter 6.

3.2.3 Preparation mesoporous carbon microfibers supported Ru catalysts.

Preparation of porous alumina microfibers. The porous alumina microfibers (AFs) were synthesized according to our previous report (Bai et al., 2007). In a typical synthesis, 4.52 g of P123 (Aldrich, typical M_n=5800) was dissolved in 65.0 mL of deionized water to form a clear solution, to which 15.0g of $Al(NO_3)_3 \cdot 9H_2O$ (Merck, 98.5%) was added. After the alumina salt was totally dissolved, 24 g of urea (ACS reagent, Sigma-Aldrich, 99.0-100.5%) was added. The final mixture was transferred to a Teflon-lined stainless-steel autoclave and placed in an oven at 100 ^oC for 24 h. After

the hydrothermal treatment, the white precipitate was filtered, washed with deionized water, and dried at 80 ^{o}C in a vacuum oven for 24 h. The obtained sample was further calcined in air at 500 ^{o}C for 2 h with a heating rate of 1 ^{o}C/min.

Preparation of mesoporous carbon microfibers supported Ru catalysts. In a typical synthesis, 1g of dried AFs was impregnated with 4 mL of ruthenium chloride solution (0.1M) under ultrasonic sonication for 0.5 h. The suspension was dried in air at 120 ^{o}C overnight. The dried Ru-impregnated solid was placed in a quartz tube and heated from room temperature to 900 ^{o}C at a heating rate of 5 ^{o}C /min under a pure N_2 flow (30 mL/min). CVD of carbon was subsequently conducted at 900 ^{o}C using benzene (or pyridine) vapor for 2 h. The vapor was carried into the tube by N_2 flow (30 mL/min) containing 5 wt% benzene (or pyridine). Finally, the black sample was treated with a 20 wt% HF solution to remove the alumina template, washed with deionized water, and vacuum-dried at 120 ^{o}C overnight. The Ru catalysts obtained using AFs as templates are designated as RuCMF, RuCMFN, where "N" denotes pyridine as carbon precursor. For comparison purpose, AFs, multi-walled carbon nanotubes (CNTs, Aldrich), and carbon microfibers (CFs) (Qingdao, China) were also used as Ru supports. In a typical synthesis, 1g of AFs, CNTs or CFs was impregnated with a 4 mL of 0.1 M $RuCl_3$ solution followed by drying at 120 ^{o}C overnight. The Ru-impregnated solids were treated at 300 ^{o}C for 2 h under hydrogen to obtain catalysts Ru/AF-H, Ru/CNT-H, and Ru/CF-H, in which "H" denotes hydrogen reduction.

3.3 Characterization techniques

Both the physical and the chemical structure of a catalyst must be known if relationships between the material structure of the catalyst and activity, selectivity, and

lifetime are to be revealed. Here, we will briefly introduce techniques for characterizing our catalysts.

3.3.1 Nitrogen adsorption-desorption isotherms

The study of the textural properties of catalyst supports is of primary importance in terms of understanding the catalytic phenomena. Gas (N_2, CO_2, Ar, etc.) sorption measurements are usually carried out for the determination of pore texture, such as the specific surface area, the specific pore volume, the shape of the pores and the pore size distribution (PSD). In N_2 adsorption analysis, a sample is exposed to N_2 gas of different pressures at a given temperature (usually at -196 ^oC, the liquid-nitrogen temperature). Increasement of pressure results in increased amount of N_2 molecules adsorbed on the surface of the sample. The pressure at which adsorption equilibrium is established is measured and the universal gas law is applied to determine the quantity of N_2 gas adsorbed. Thus, an adsorption isotherm is obtained. If the pressure is systematically decreased to induce desorption of the adsorbed N_2 molecules, a desorption isotherm is obtained. The desorption isotherm can rarely be superimposed over the adsorption isotherm, this irreversibility in terms of adsorption shows up as a hysteresis phenomenon. The forms of the isotherms and the hysteresis loops have been subject to a classification initially proposed by Brunauer and taken up by the IUPAC (Kruk et.al., 2001). The interpretation of adsorption-desorption isotherms provides a wealth of information on the texture of the adsorbent. Specific surface areas are calculated by application of the Brunauer-Emmett-Teller (BET) method to nitrogen adsorption isotherms. Total pore volume is calculated by a single-point measurement at a high relative gas pressure (p/p_0=0.99). Mesopore- and micropore-size distributions

are established by the Barrett-Joyner-Halenda (BJH) and Horvath-Kawazoe (HK) methods.

In this project, the N_2 sorption/desorption at the liquid-nitrogen temperature was carried out on an automatic volumetric sorption analyzer (Quantachrome, NOVA 1200) and a surface area and porosity analyzer (Micromeritics, ASAP2020). Before the measurement the sample was degassed at 200 ºC for 5 h.

3.3.2 Chemisorption of hydrogen (H_2) and carbon monoxide (CO)

While the specific surface area of supports is often determined by using physical adsorption, the active phase of the catalysts (metal) can be studied by selective chemical adsorption. Chemical adsorption can be either dissociative: the molecule is adsorbed in a dissociated form- or associative: the atoms comprising the probe molecule remain bonded. This character depends on the probe molecule – active center combination and the temperature. The H_2 and CO chemisorption can be used to determine the strong chemisorption uptake, the active metal area, the metal dispersion (ratio of surface metal to total metal content), and the average size of the metal crystallites. This method consists of adsorbing, on surface atoms of the active phase (e.g. a metal), a molecule likely to give rise to a balanced chemical reaction. The volume measured at saturation, converted to standard conditions, and corresponding to the formation of a complete monolayer, is used to determine the metallic surface, the average size of the crystallites and the dispersion of the metal, with the aid of the following equations:

- Metallic surface area (m^2/g): $S = \frac{\sigma n v N}{V_M}$ (3.1)
- Dispersion (%): $D = \frac{v n M}{V_M}$ (3.2)
- Average diameter of the crystallites assumed to be spherical:

$$d = \frac{6 \times 10^{3}}{\rho S} \qquad (3.3)$$

where:

n is the number of metal atoms on which a gas molecule is chemisorbed (The value of n depends on the nature of the gas and metal under consideration.)

ρ is the specific mass of the metal (g/cm^3)

N is Avogadro's constant

v is the volume adsorbed per g of metal (cm^3/g)

σ is the surface area of a metallic atom (m^2/atom)

M is the molar mass of the metal (g/mol)

V_M is the molar volume (cm^3/mol)

In this project, the measurement of chemisorption of H_2 and CO was carried out on a ChemBET *Pulsar* system (Quantachrome) (as shown in Figure 3.2) operated at room temperature. Prior to each analysis, an activation step is carried out. 0.1g of catalyst sample was reduced using 5%H_2 in N_2 at 120 ^oC for 2 h, followed by degassing at 300 ^oC under N_2 for 4 h, then cooling to room temperature. Measured pulses of H_2 were then introduced from the built-in gas-sampling loop into the carrier gas stream and passed through the catalyst bed. The total volume of hydrogen not adsorbed was measured by thermal conductivity detector (TCD). After the H_2 titration, the catalyst sample was degassed at 300 ^oC under helium for 4 h, cooled to room temperature, and titrated with CO. The Ru dispersion values was obtained using a stoichiometric ratio Ru:CO of 1:1, and the average particle size was calculated employing spherical model, d=0.45/D (Garcia et al., 2010).

Figure 3.2 Photo of ChemBET *Pulsar* system (Quantachrome).

3.3.3 Thermogravimetric analysis (TGA)

Thermogravimetric analysis (TGA) is a thermal analysis technique used to measure changes in the weight (mass) of a sample as a function of temperature under a controlled atmosphere. As materials are heated, they can loose weight from a simple process such as drying, or from chemical reactions that liberate gasses. Differential thermal analysis (DTA) is used to obtain information on the variation in temperature in a sample subject to heat treatment. It provides information on the thermal effects that accompany the heating of the sample. These are often linked to mass transfers between the liquid or solid phase and the gas phase (such as dehydration, oxidation, etc.). They may also appear without any variation in mass in the case of structural transformations (for example: phase transitions in crystals, glass transition in polymer, etc.).

In this project, TGA was carried out on a thermal analyzer, TGA 2050 (Thermal Analysis Instruments, USA), with an air flow rate of 100 mL/min and a temperature

ramp of 10 ^{o}C/min. The Ru content in Ru-carbon catalysts can back calculated from residual weight (RuO_2) above 700 ^{o}C as following:

$$Ru\% = \frac{W_{RuO_2} \times \frac{MW_{Ru}}{MW_{Ru}+2\times MW_O}}{1-W_{RuO_2} \times \frac{MW_{Ru}}{MW_{Ru}+2\times MW_C}} \times 100\% \qquad (3.4)$$

where:

W_{RuO2} is residue weight of the sample above 700 ^{o}C

MW_{Ru}=101, is molecular weight of Ru

MW_O=16, is molecular weight of oxygen.

3.3.4 Inductive-coupled plasma atomic mass spectrometer (ICP-MS)

ICP-MS is a type of mass spectrometry that is highly sensitive and capable of the determination of a range of metals and several non-metals at concentrations below one part in 10^{12}. It is based on coupling together inductively coupled plasma as a method of producing ions (ionization) with a mass spectrometer as a method of separating and detecting the ions.

An inductive-coupled plasma atomic mass spectrometer (ICP-MS) (Agilent 7500 ICP-MS) was used to quantify the composition of bimetallic catalysts in this project. Before the analysis the solid catalysts were converted into liquids via acid digestion. The concentrations of Ru and Cu were quantitatively determined based on the standard calibration curve obtained prior to every analysis. The wavelengths used for Ru and Cu measurements were 100.9 nm and 324.7 nm, respectively.

3.3.5 X-ray diffraction (XRD)

X-ray diffraction techniques are based on the elastic scattering of X-rays from structures that have long order. The diffraction pattern generated is used to study surface-supported nanoparticles, affording information on the crystal phase, lattice

constant, and average particle size of nanoparticles. In the case of bimetallic nanoparticles, XRD is important to confirm whether the bimetallic nanoparticles adopt alloy structure or not. Generally, an alloy consisting of two kinds of metals shows the diffraction peaks between those of two pure metals.

In this project, the structure of the Ru based catalysts were characterized by using X-ray diffraction technique (XRD-6000, Shimadzu, Japan) with Cu Kα radiation (λ=0.15418 nm). Measurement condition: voltage 40.0 kV, current 30.0 mA, divergence slit 1.00 (deg), scatter slit 1.00 (deg), receiving slit 0.30 (mm), scan range 20.0-80.0, scan speed 4.00 (deg/min), sampling pitch 0.02 (deg).

3.3.6 X-ray photoelectron spectroscopy (XPS)

XPS is based on the photoelectric effect, whereby absorption of light by an atom results in the ejection of electrons, provided that the photon energy is sufficient to overcome the binding energy of the electron. The core electron binding energies are characteristic of each element, and the peak areas can be used to determine the composition. As the peak shape and binding energy are sensitive to the oxidation and chemical state of the emitting atom, XPS can also provide chemical bonding information. Generally XPS technique provides a compositional estimate of only the outermost layers, with a penetration depth of ca. 5-15 nm.

In this project, the surface chemical compositions of the samples were determined using XPS (Kratos Analytical Ltd., U.K., AXIS HIS 165 spectrometer) with an Al Kα X-ray source (1486.71 eV protons), operated at 15 kV and 10 mA. The pressure in the analysis chamber was maintained below 10^{-8} torr during each measurement. The spectral regions of the Ru3p, O1s, C1s, Cu2p, N1s peaks were acquired. All spectra were fitted by a software package XPSpeak 4.1 with the subtraction of Shirley (for

transition metals) or linear background (for other elements) and a ratio of 20% Lorentzian-Gaussian. In charge-up correction, the calibration of binding energy (BE) of the spectra was referenced to the C1s electron bond energy corresponding to graphitic carbon at 284.5 eV.

3.3.7 X-ray absorption Spectroscopy (XAS)

XAS is essentially a form of electron spectroscopy. X-rays absorbed by matter (metals and non-metallic solids, liquids or gases) excite and promote an absorbing atom's core electron to higher unoccupied states or into a free unbound state (the continuum). The X-ray absorption spectrum of an element contains absorption edges corresponding to the excitation of electrons from various electronic states at energies characteristic of that element, i.e., K edges arise from the excitation of electrons from 1s states, and LI, II, III edges from excitations from 2s, 2p 1/2, and 2P 3/2 states. When the X-ray energy is increased above an edge, oscillations (fine structure) are observed in the absorption coefficient over an energy range of several hundred to over a 1000 eV above the edge. Since these oscillations arise from the interference between waves associated with the emitted photoelectrons and photoelectrons backscattered from neighboring atoms, they contain useful information on the environment of the absorbing atom. Each element's X-ray absorption spectrum is unique and provides information about the elements present in the nanoparticles, the local atomic environment, oxidation state, coordination number, and interatomic distances (Ferrando et al., 2008). The XAS spectrum can be approximately divided into three regions (Figure 3.3): X-ray Absorption Near Edge Structure (XANES), Near Edge X-ray Absorption Fine Structure (NEXAFS), and Extended X-ray Absorption Fine

Structure (EXAFS). In practice there is not an obvious division of these regions and the XANES and NEXAFS regions are often modeled together.

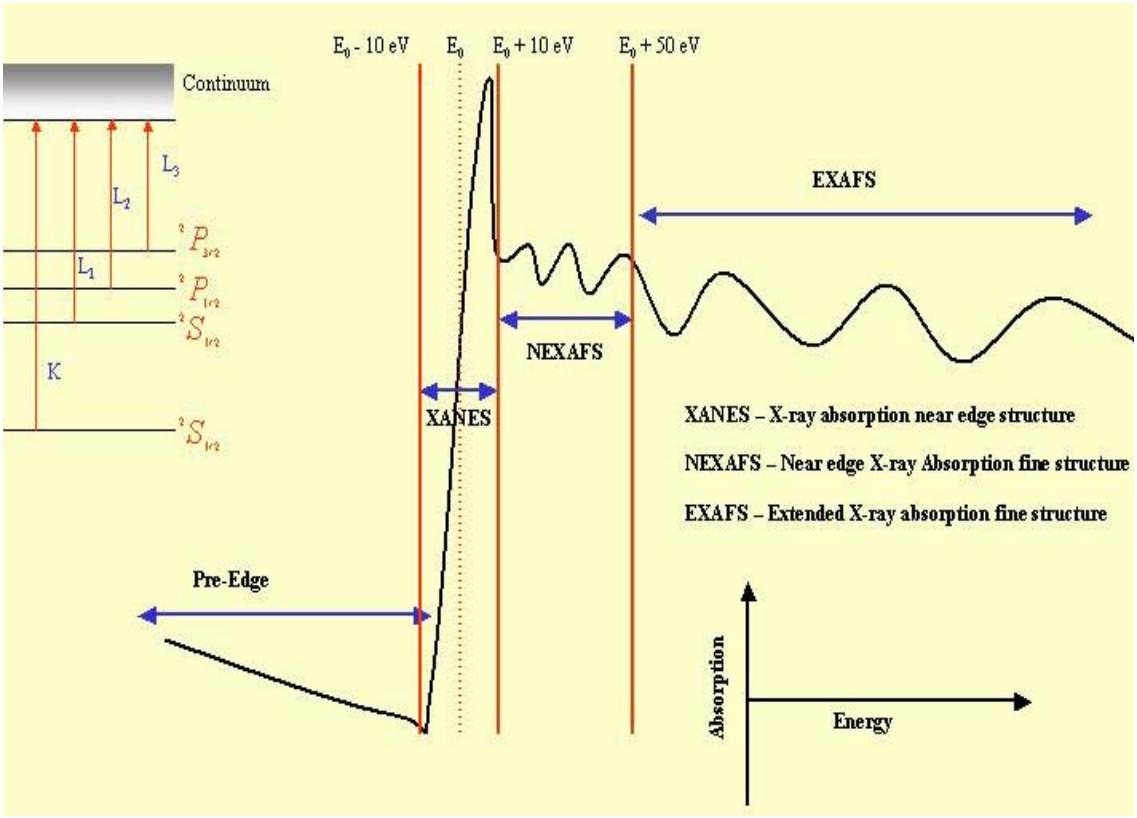

Figure 3.3 The three regions of the XAS spectrum
(http://www.chemphys.lu.se/research/techniques/xrayxas/).

XANES: The energy of incoming X-rays is sufficient to transfer core electrons to higher unoccupied valence states. Analysis of this part of the spectrum (around the edge) provides information concerning the oxidation state of the absorbing atom and its site symmetry.

NEXAFS: The core electron is excited into the continuum, but the photoelectron has low kinetic energy and is strongly backscattered by all of the neighboring atoms. This part of the spectrum is sensitive to the number, kind and symmetry of atoms adjacent to the absorber atom.

EXAFS: The energy of the photoelectron is high enough that its de Broglie wavelength becomes comparable to the distance to neighboring atoms. The photoelectron wave is weakly backscattered by and among the neighboring atoms (as shown in Figure 3.4). The analysis of this part of the absorption spectrum gives information regarding the number, kind and distance of neighboring atoms from each other and the absorber.

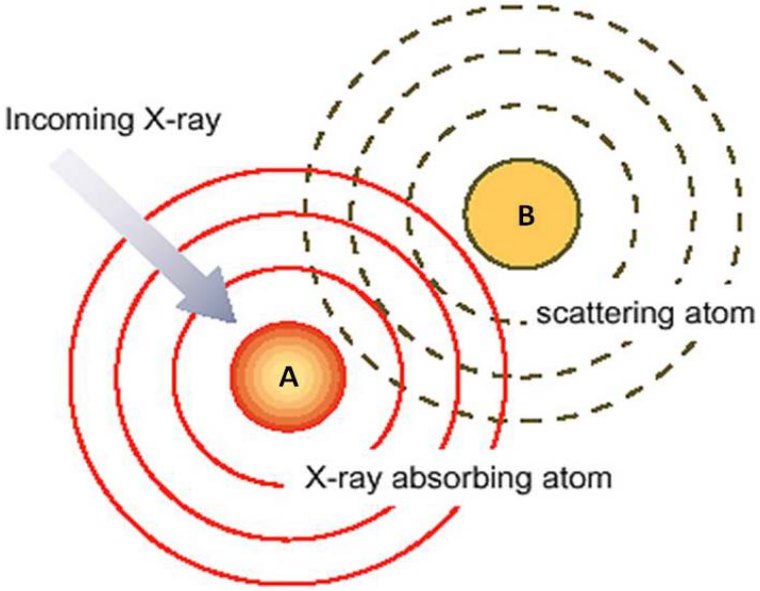

Figure 3.4 Schematic diagram of the photoelectron wave leaving atom A is backscattering by the neighbor atom B. An EXAFS oscillation originates from the interference between the outgoing and the incoming waves (Lynch, 2003).

The XAS measurments at the Cu K-edge (8.979 keV) and Ru L_3-edge (2.838 keV) were performed at room temperature at the XDD (X-ray Development and Demontrate) beamline available in the Singapore Synchrotron Light Source (SSLS) center where a pair of channel-cut Si (111) crystals was used in the monochromator. All spectra were collected in the fluorescence mode using a Lytle-type detector. Standard spectra for Cu foil, powdered Cu_2O, CuO, Ru metal and RuO_2 were used to assess bulk oxidation states.

3.3.8 Scanning electron microscopy (SEM), Energy-Disperse X-ray microanalysis (EDX) and Field-emission scanning electron microscopy (FESEM)

Scanning electron microscopy is a local chemical and textural characterization technique for solid materials which is based on the interaction of these materials with a focused electron beam with energies of between 0.5 and 35 kV. The various radiations emitted under the impact of the electron beam (secondary electrons, scattered electrons and X-rays) are used to form images showing the various properties of the material (topography, heterogeneities of composition and local elemental composition, respectively). Depending on the signal used, the information extracted reveals the following properties of the material:

- Its morphology and texture are described by the secondary electron images.
- The distribution of phases in the material is described by backscattered electron images (atomic number contrast).
- The composition of the phases is deduced from the analysis of characteristic X-rays emitted by the sample (local elemental analysis).

In this thesis work, SEM images were measured on a JEOL-6700F scanning electron microscope, which was operated at an acceleration voltage of 10kV and filament current of 60 mA. Before measurement, the samples were stuck onto a double-face conducted tape mounted on a metal stud. The non-conductive samples were coated with platinum using a sputter coater (JEOL JFC-1300 Auto fine coater) before the test. The energy dispersion X-ray spectroscopy (EDX) was obtained at 15.0 kV in the SEM measurements. The morphologies of the samples were also imaged by using a field emission scanning electron microscope (FESEM) (JSM-6700F, JEOL Japan INC) with an accelerating voltage 10.0 kV. The elemental distribution maps of Ru-Cu bimetallic

catalysts were obtained using a scanning electron microscope (JEOL 6701F, JEOL, Japan) operated at 15kV kV equipped with an energy-dispersive spectrometer.

3.3.9 Transmission electron microscopy (TEM) and high resolution transmission electron microscopy (HRTEM)

When crossing a sample, an electron beam may be partially adsorbed and partially deflected. Via the use of electromagnetic lenses, a certain fraction of these electrons, and of those that have not been deflected, can be recombined to form an image. The use of transition electron microscopy is based on controlling the electrons involve in image formation. The transmission electron microscope thus offers an image of the sample that depends on the electron-matter interaction. One of the major uses of TEM in the area of catalysts is the measurement of particle size distributions for supported metals. In TEM, the electrons pass through the sample, generally requires the samples to be dispersed onto an electron-transparent substrate, such as a thin copper-coated microgrid. HRTEM offers resolution down to the Ångstrom level and enables information to be obtained on the structure (atomic packing) rather than just the morphology of the nanoparticles.

In this thesis work, the microscopic features of the samples were observed with TEM (JEM 2010, JEOL, Japan) operated at 200 kV, and HRTEM (JEM-2100F, JEOL, Japan) operated at 200 kV.

3.3.10 Fourier transform infrared (FTIR) spectroscopy

FTIR spectroscopy was used to determine functional groups on carbon structures. FTIR spectroscopy records the interaction of infrared radiation with sample measuring the frequencies at which the sample absorbs the radiation and the intensities of the

absorptions. Chemical functional groups are known to absorb light at specific frequencies. Thus the chemical structure can be determined from the frequencies records.

In this these work, FTIR spectra were collected on an IR Prestige-21 (Shimadze, Japan) with a resolution of $4cm^{-1}$ in the wavelength range of $400\text{-}4000cm^{-1}$. A powder sample was mixed with potassium bromide, KBr in a weight of 1:99, and then pellets were formed using a Pike Specac.

3.4 Evaluation of catalytic properties

The evaluation of the catalytic properties of the catalysts for hydrogenation of D-glucose was performed in a Parr batch reactor (Parr 4560) (Figure 3.5). About 0.05 g of a solid catalyst and 30 mL of 40 wt% D-glucose solution in water were placed in the reactor. Subsequently, the reactor was purged with highly pure H_2 (>99.9995%, Singapore Oxygen Air Liquide Pte. Ltd.) three times. The reaction was conducted at 100 ^oC with a total H_2 pressure of 8 MPa. The stirring rate was 1000 rpm, which had been confirmed to be sufficient to eliminate the effect of mass transfer resistance across liquid-solid film on the overall reaction rate. After 3 h, the reactor was cooled to room temperature in an ice-water bath and the pressure in the reactor was released. The reactant and product were analyzed using an isocratic high-performance liquid chromatograph (Agilent 1100 series HPLC) system with an Agilent 1100 quaternary pump, Agilent 1100 refractive index detector, and Aminex HPX-87H column (300 mm × 7.8 mm). The concentration of D-glucose was quantitatively determined based on the standard calibration curve obtained prior to every analysis using an eluent of 5 mM H_2SO_4 at a flow rate of 0.05 mL/min under isobaric conditions. The catalytic data showed that D-sorbitol was the only product in the presence of the Ru-C catalysts used

in this project. Therefore, the catalytic activity was calculated on the basis of the mole of D-sorbitol produced per mole of Ru per second after 3 h of reaction.

Figure 3.5 Photo of Par batch reactor (Parr4560).

The Ru leaching of the catalysts experiment was carried out as follows: around 0.05g of catalyst placed in 30 mL of water was ultrasonication for 2 h, and after filtration of the suspension solution, the Ru concentration was determined using an ICP-MS.

CHAPTER 4

Ru nanoparticles embedded in templated porous carbon and there catalytic performance in D-glucose hydrogenation

4.1 Introduction

As mentioned before Ru supported catalysts suffer from rapid deactivation, partially due to sintering and migration of the Ru nanoparticles. The supports were also responsible for the deactivation. For example, Arena (1992) found that the increased levels of alumina crystallinity contributed to catalyst deactivation. Maris et al. (2006) found that the mechanism of particle growth involves migration of Ru species during the hydrolysis of the silica surface. Thus, the choice of catalyst support and the preparation method are crucial in the hydrogenation of D-glucose. Because of the inert nature of carbon, Ru catalysts supported on carbon appear to be promising catalyst for D-glucose hydrogenation. In this study, we examined the catalytic properties of the Ru nanoparticles embedded in templated porous carbon in D-glucose hydrogenation and compared the catalytic activity with that of Ru catalysts supported on carbon, silica, and aluminosilicates prepared using conventional method, and the commercial Ni and Ru catalysts. In addition, the effect of the particle size and pore structure on the glucose hydrogenation were investigated. The synthesis process can be found in section 3.2.1.

4.2 Characterization of Ru nanoparticles catalysts

FESEM Observation. The morphologies and microstructures of the catalysts were studied by means of the field-emission electron microscope (FESEM) and

transmission electron microscopy (TEM). The FESEM image of RuC(HY) (Figure 4.1b) showed rhombic, cubic, hexagonal and triangle crystal morphologies, similar to that of its parent template zeolite HY (Figure 4.1a), suggesting a faithful morphology replication. Compared with that of the parent template, the particle size (< 1μm) of the obtained RuC(HY) samples were slightly smaller. Both the template silica SBA-15 (Figure 4.1c) and the catalyst Ru6C3 (Figure 4.1d) consisted of well-ordered hexagonally arrayed bundles length up to dozens of micrometers.

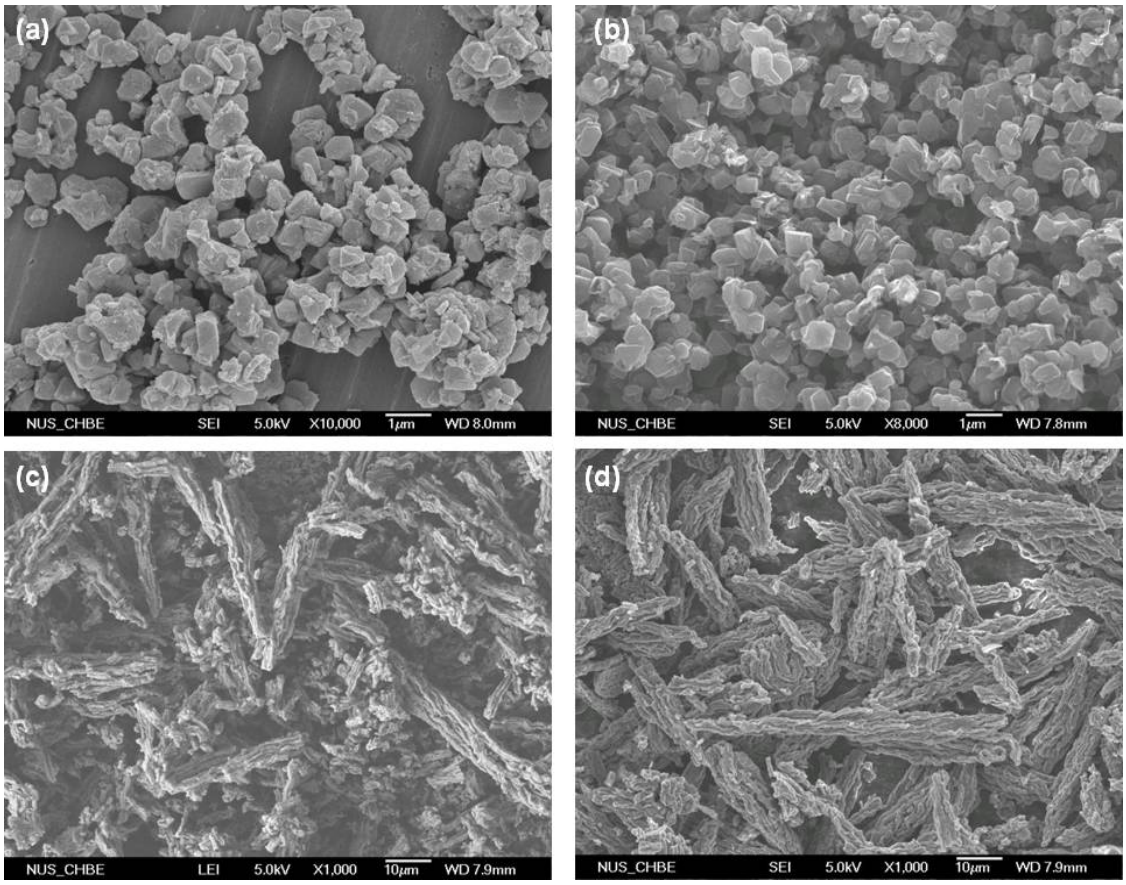

Figure 4.1 FESEM images of (a) hard templates zeolite HY, (b) catalysts RuC(HY), (c) SBA-15, (d) Ru6C3.

TEM Observation. Figure 4.2 showed TEM images of RuC(HY), Ru6C3, Ru/C-HY-H, and Ru/C-SBA15-H. The dark dots on the grey carbon background were due to the Ru nanoparticles.

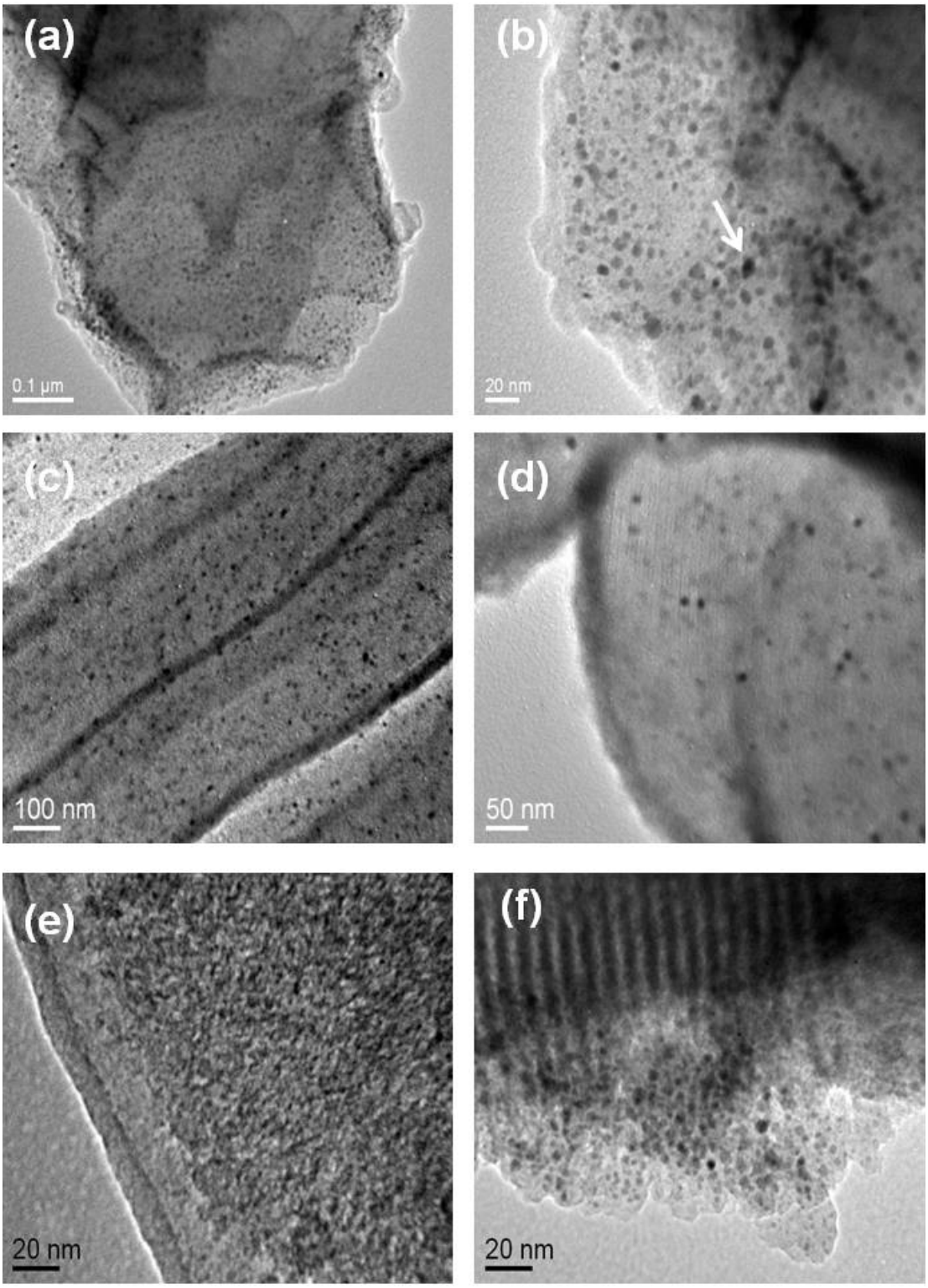

Figure 4.2 TEM images of catalysts (a, b) RuC(HY), (c,d) Ru6C3, (e) Ru/C-HY-H, (f) Ru/C-SBA15-H.

TEM images of RuC(HY) (Figure 4.2a) and Ru6C3 (Figure 4.2c) showed that uniform Ru nanoparticles highly dispersed in the carbon matrix. It can be seen from the high-magnification TEM image of RuC(HY) (Figure 4.2b) that using zeolite HY as

template, Ru particles were around 1-2 nm which was comparable to that of pore channel or cage of HY (1-2 nm). While using SBA-15 as template, Ru nanoparticles in Ru6C3 were around 7-8 nm, corresponding to the pore channel size of SBA-15 (7-8 nm). TEM image of Ru6C3 (Figure 4.2d) revealed that most of the Ru particles were studded inside the composite nanorods and did not block the openings of the mesopores. Thus, Ru particle size could be controlled by the template pores. The formation of several big Ru particles on RuC(HY) (Figure 4.2b, highlight by arrow) could be ascribed to the fact that they were not subjected to the restriction of template pore channels before CVD process. For comparison, TEM images of Ru/C-HY-H, Ru/C-SBA15-H (Figure 4.2e, 4.2f) showed randomly dispersed irregular Ru cluster, and most Ru nanoparticles were supported on the exterior surface of carbon rather than on the walls of the pores.

XRD Analysis. The structures of catalysts were further characterized by XRD, and the recorded XRD patterns were shown in Figure 4.3. The peaks at 38.3, 42.2, 44.0, 58.3, 69.5, and 78.4 degree two theta observed on catalysts RuC(HY) and Ru6C3 can be assigned to (100), (002), (101), (102), (110), and (103) diffraction planes of bulk hexagonal Ru metal. No diffraction peaks due to ruthenium oxides can be seen on the two samples, suggesting a complete reduction of ruthenium oxide species to Ru by carbon species and/or hydrogen gas released from benzene dehydrogenation during the CVD process (Sun et al., 2005; Villani et al., 2006). The relatively sharp peaks in XRD patterns could be ascribed to the few large Ru particles formed n the external surface of the template. In contrast, no peaks associated with Ru metal are seen in the XRD patterns of Ru/C-HY-H and Ru/C-SBA15-H, probably due to the small Ru particle size (see Figure 4.3c and d). These two catalysts were prepared using the conventional impregnation method followed by hydrogen reduction with template microporous

carbon C(HY) and template mesoporous carbon C(SBA-15) as the supports. It should be noted that the hydrogen reduction for these two catalysts can not carried out at 900 ^{o}C due to the methanation or gasification of carbon at high temperatures catalyzed by Ru (Koopman et al., 1979).

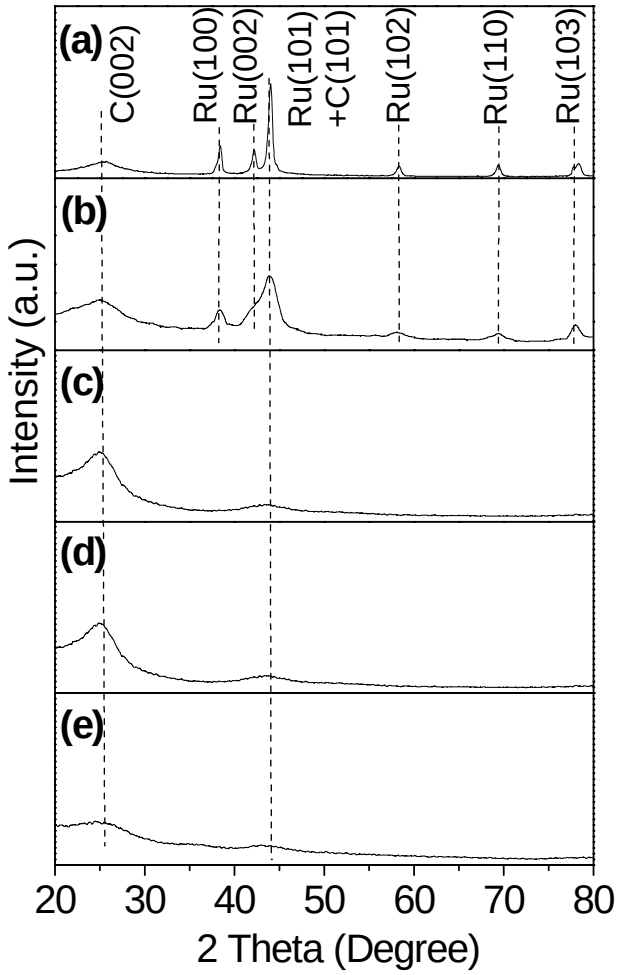

Figure 4.3 XRD patterns of (a) RuC(HY), (b) Ru6C3, (c) Ru/C-HY-H, (d) Ru/C-SBA15-H, and (e) 5RuC.

Nitrogen Adsorption. The pore structure of the catalyst plays an important role in the transport of the reactant and product. The N_2 adsorption-desorption isotherms of all the samples were shown in Figure 4.4, and the pore structure parameters of all samples were summarized in Table 4.1. The nitrogen sorption isotherms of RuC(HY), Ru/C-HY-H, Ru/HY-H, and 5RuC (see Figure 4.4a, c, e, g) exhibited very high adsorption

below P/P_0=0.1, which was ascribed to micropore filling. This suggests that a large proportion of the pore channels in the catalysts are micropores. The isotherms of RuC(HY), Ru/C-HY-H (see Figure 4.4a and c) also exhibited some nitrogen uptake at P/P_0>0.1, which may be attributed to adsorption into larger pores arising from the shrinkage of carbon during carbonization and/or incomplete filling the voids of the zeolite pores. Ru6C3, Ru/C-SBA15-H, and Ru/SBA15-H (Figure 4.4b, d, f) showed a type IV isotherm, indicating they are mesoporous materials. The catalyst Ru/SBA15-H displayed an H1 hysteresis loop, indicating cylindrical pore geometry with the average pore size around 7.2 nm. The isotherms of both Ru6C3 and Ru/C-SBA15-H exhibited an H2 hysteresis loop, indicating an ink-bottle-like pore structure with the average pore size of about 3.2 nm. The isotherm of Ni65 (Figure 4.4h) also exhibited hysteresis loop in mesopore range, indicating mesoporous material with the average pore size about 4.7 nm.

Table 4.1. Physicochemical properties of Ru catalysts.

Sample	Metal content (wt %)	Surface area (m^2/g)	Pore volume (cm^3/g)	Average pore diameter (nm)
RuC(HY)	6.1	951	1.14	1.9, 3.7
Ru6C3	6.3	834	1.10	3.1
Ru/C-HY-H	6.1	1234	1.41	1.9
Ru/C-SBA15-H	5.9	389	0.56	3.2
Ru/HY-H	5.4	626	0.46	1.1
Ru/SBA15-H	5.7	616	0.90	2.1, 7.2
Ru/C	5	690	0.48	1.4
Ni65	65	129	0.30	4.7

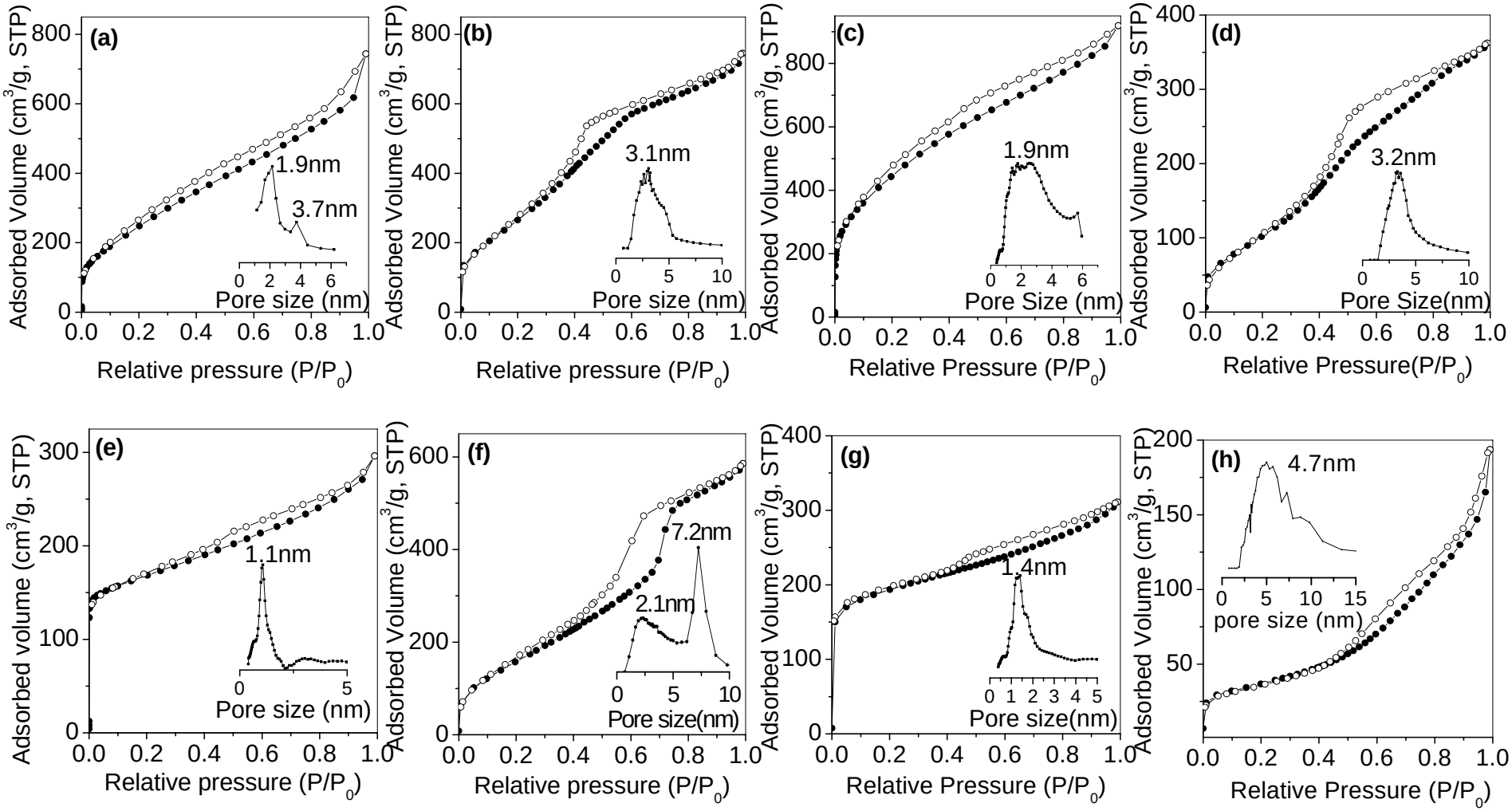

Figure 4.4 N_2 adsorption-desorption isotherms and pore size distribution curves (inset) of catalysts (a) RuC(HY), (b) Ru6C3, (c) Ru/C-HY-H, (d) Ru/C-SBA15-H, (e) Ru/HY-H, (f) Ru/SBA15-H, (g)Ru/C, (h) Ni65.

TGA Analysis. The thermogravimetric behaviors of catalysts RuC(HY) and Ru6C3 in air were shown in Figure 4.5. The TGA curves showed that the carbons were completely burnt off in air when temperature was raised to about 700 °C. The unchanged residual mass can be considered to be the mass of RuO_2. Since the templates (HY and SBA-15) can be completely removed by the aqueous HF solution (20%), the Ru content in RuC(HY) and Ru6C3 can be back calculated from residue weight (RuO_2) above 700 °C as Eq. (3.1). An analysis of EDX spectra showed that the Ru contents were about 6wt% in RuC(HY), 6wt% in Ru6C3, consistent with that of TGA data that the Ru contents in catalysts RuC(HY) and Ru6C3 were estimated to be about 6.1wt% and 6.3wt%, respectively.

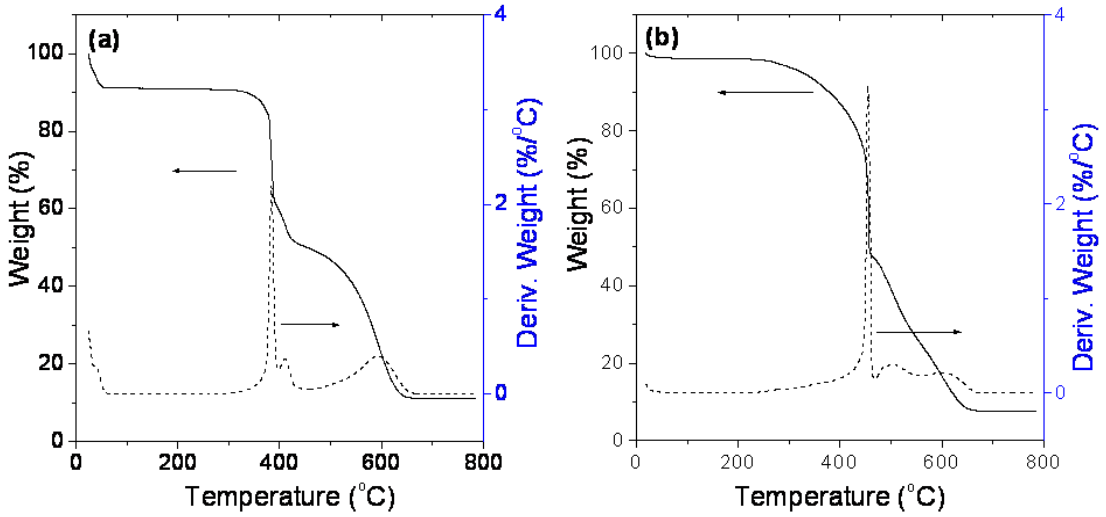

Figure 4.5 Weight loss curve of catalysts (a) RuC(HY) and (b) Ru6C3.

4.3 Catalytic properties

4.3.1 The catalytic activity of the catalysts

The catalytic properties of the catalysts prepared in this work and the two commercial catalysts in liquid-phase D-glucose hydrogenation were showed in Figure 4.6. All Ru catalysts exhibited a catalytic activity at lease 20 times higher than that of the commercial Ni catalyst, showing that metallic Ru is catalytically more active than

Ni in liquid-phase D-glucose hydrogenation (Hoffer et al., 2003). Among the Ru catalysts, the most effective in terms of activity were the sandwiched Ru-C catalyst and the commercial catalyst. In addition, HPLC analysis data showed that D-sorbitol was the only product obtained when Ru6C3 and RuC(HY) were used as the catalysts, demonstrating 100% selectivity to D-sorbitol.

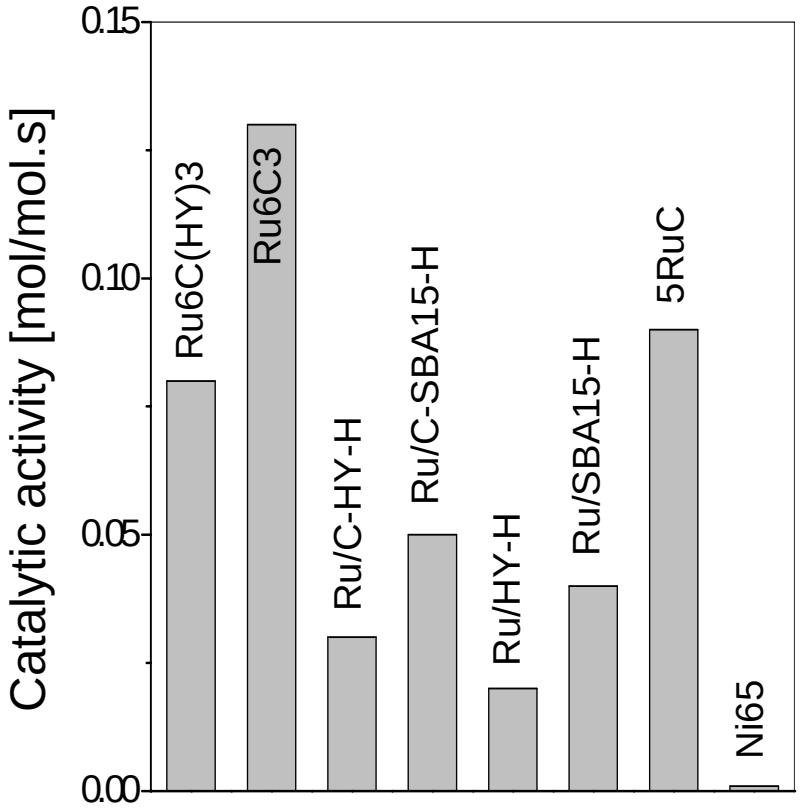

Figure 4.6 Catalytic activities of the catalysts.

Several factors could account for the observed high catalytic activity and selectivity for the Ru6C3 catalyst prepared using the thermal reduction method, such as the unblocked pores of the catalyst, the graphitic nature of the carbon, and the unique contact between the Ru nanoparticles and carbon support.

First, the thermal reduction method plays a critical role in enhancing the catalytic activity. During the CVD process, Ru particles were embedded in graphitic carbon matrix, enhancing the Ru-C contact. This contact may stimulate the hybridization of the p_z orbital of graphene (π-bonded states) and the d orbital of Ru, resulting in

electron transfer from Ru to the graphene of the carbon substrate. As a result, the Ru metal particles were less easily oxidized by oxygen than the nanoparticles lying on a planar surface (Pan et al., 2007). Such a unique contact between Ru nanoparticles and carbon support may also favor hydrogen spillover (Wang and Yang, 2008). It is well known that hydrogen spillover exerts a great influence on the catalytic activity of many heterogeneous catalysts in hydrogenation reactions (Conner and Falconer, 1995). In the present case, hydrogen can adsorb dissociatively on the exposed Ru surface to form atomic H species, followed by spillover throughout the carbon support. The spillover hydrogen from Ru can make carbon active for hydrogenation of D-glucose, resulting in the observed high catalytic activity. The lower catalytic activity of Ru/C-HY-H, Ru/C-SBA15-H, Ru/HY-H, and Ru/SBA15-H may also be due to the presence of residual chlorine species. EDX analysis of the four samples proved the existence of the chlorine species. When using a Ru chlorine salt as a catalyst precursor, the residual chlorine species could block and/or poison the active Ru surface to some degree. Removal of such species during low temperature hydrogen reduction seems difficult (Wu et al., 1992). In contrast, the thermal reduction method has no temperature limitation, which can remove the chlorine species at all.

In addition, the pore structures of catalyst in the transport of the reactant and product play an important role. The lower catalytic activity of Ru nanoparticles supported on the microporous carbon (catalyst RuC(HY)) than that of Ru nanoparticles supported on the mesoporous materials (catalyst Ru6C3) may be due to the effects of steric hindrance imposed by the molecular sizes of the reactants relative to the pore sizes of thermal-reduced Ru catalysts on the diffusion and accessibility of the reactants to the Ru domains confined inside the pores (Kusserow et al., 2003).

4.3.2 Effect of metal loading and CVD time on catalytic activity

To maximize of the catalytic activity of the Ru catalysts, the effect of metal loading and CVD time were investigated. It can be observed from Figure 4.7 that the mean catalytic activity increases with the increment of Ru loading up to 8wt%, and then slightly decreased with further addition of Ru. Prolong the CVD process the catalytic activity decreased, two hours is the best time.

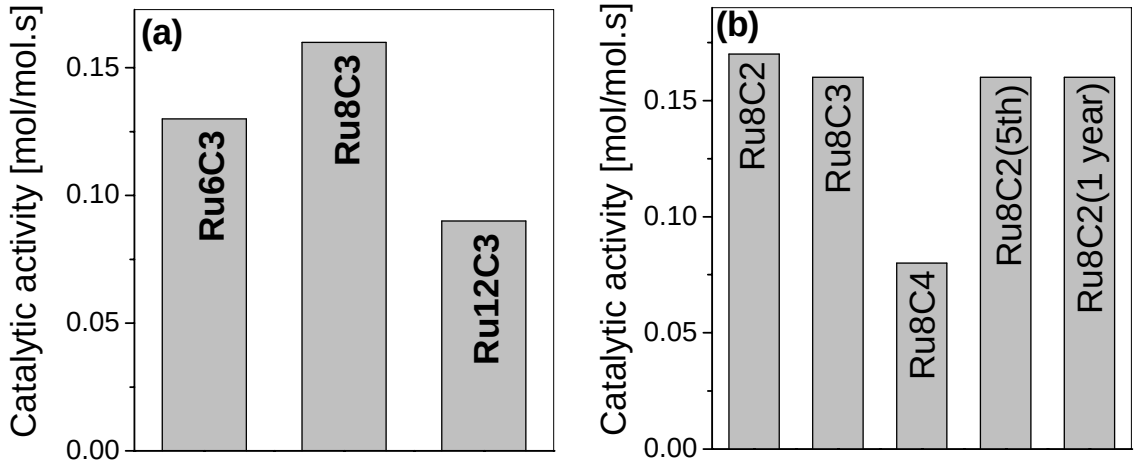

Figure 4.7 Catalytic activities of RuC catalysts prepared under different experimental conditions: (a) different metal loading, (b) different CVD time.

XRD patterns in Figure 4.8 showed that with the increasing of Ru loading, the peaks at 38.3, 42.2, 44.0, 58.3, 69.5, and 78.4 degree two theta became narrower, these peaks assigned to the (100), (002), (101), (102), (110), and (103) diffraction planes of bulk hexagonal Ru metal. The narrower peak means the larger the crystallite size of Ru, therefore increasing the Ru loading resulted in increments of Ru particle size. This can be further confirmed by the TEM image depicted in Figure 4.9. Big particles with sizes of over 10 nm were also seen on catalyst Ru12C3. Since the SBA-15 silica template limits the particle size in the range of 7-8 nm, it is possible that more big nanoparticles clusters formed on the external surface of the carbon when the Ru loading increased up to 12wt%. This may be decreasing the Ru surface interaction with the support and

decreasing the catalytic activity. Therefore the good dispersion of the Ru nanoparticles was obtained and was maintained up to 8 wt%.

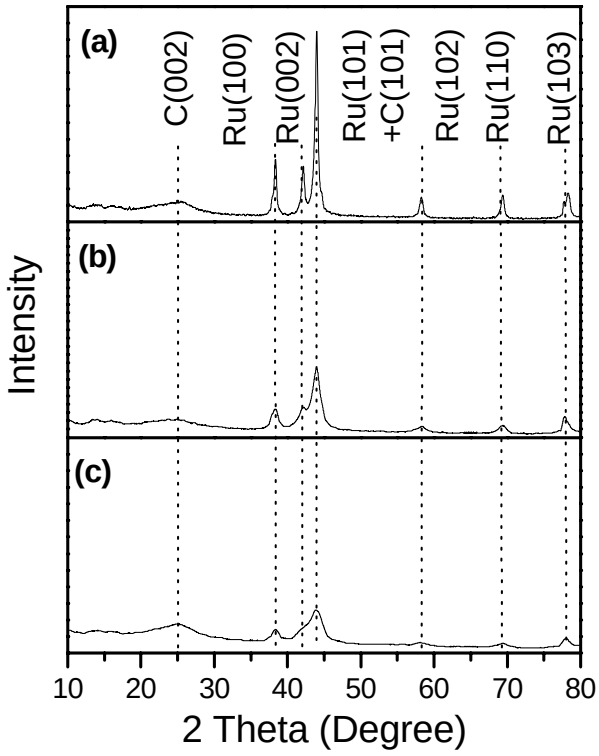

Figure 4.8 XRD patterns of (a) Ru12C3, (b) Ru8C3, and (c) Ru6C3.

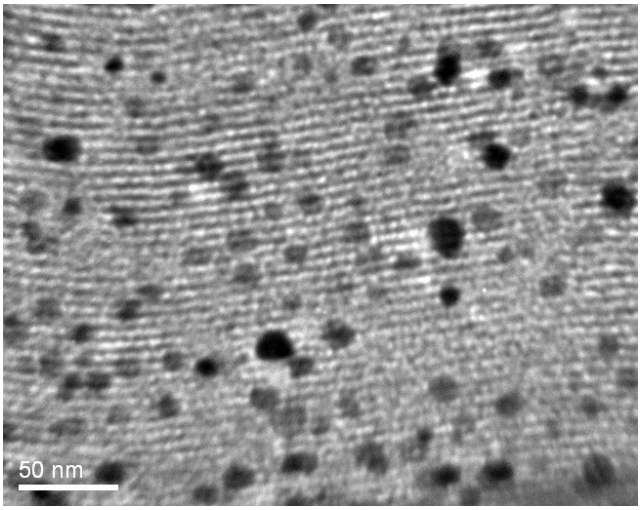

Figure 4.9 TEM image of Ru12C3.

All the RuC composites which were templated from silica SBA-15 displayed similar nitrogen isotherms and pore size distribution, indicating that incorporation Ru nanoparticles inside the carbon matrix did not destruct the structure of the carbon

support. Table 4.2 summarized the pore parameter of these samples. The BET surface area and pore volume increased with increasing Ru content, implied that Ru could facilitate the carbon deposition. While the BET surface area and pore volume decreased with increasing the CVD time, which could be attributed to the mass increase in carbon deposited with increasing the CVD time. The deposition of pyrolytic carbon took place primarily in the mesopores of the SBA-15 rather than on the external surface. The carbon deposition in the pores ceased when the pore size became smaller than the kinetic size of benzene (0.36 nm). With prolonged CVD times, carbon deposition occurred on the external surface of the template forming a layer of dense carbon, decreased the catalytic activity. Thus precise control over CVD time is important in this work.

Table 4.2. Physicochemical properties of Ru catalysts prepared under different experimental conditions.

Sample	Metal content (wt %)	Surface area (m^2/g)	Pore volume (cm^3/g)	Average pore diameter (nm)
Ru6C3	6.3	834	1.10	3.1
Ru8C3	8.3	1004	1.15	3.1
Ru12C3	12.3	1077	1.18	3.1
Ru8C2	8.5	1116	1.26	3.1
Ru8C4	4.3	404	0.56	3.1

4.3.3 Stability of catalyst Ru8C2

The stability of catalyst performance is of extreme importance in industrial hydrogenations. An industrial catalyst must be stable against sintering and poisoning.

After the first reaction run, catalyst Ru8C2 was washed with deionized water, dried at 120 ^{o}C in air, and reused without further treatment. As can be seen in Figure 4.7, little loss in catalytic activity occurred in the fifth run. In addition, long-term storage (1 year) under ambient conditions did not lead to obvious deterioration in catalytic performance. Neither aggregation of Ru nanoparticles nor loss in Ru content after five runs was observed. The TEM images of Ru8C2 before and after five runs were shown in Figure 4.10. It can be seen that most of the Ru nanoparticles are still present in the form of crystallites with diameters less than 8 nm. EDX analysis confirmed that the Ru content of Ru8C2 did not change after five runs, indicating negligible leaching of Ru.

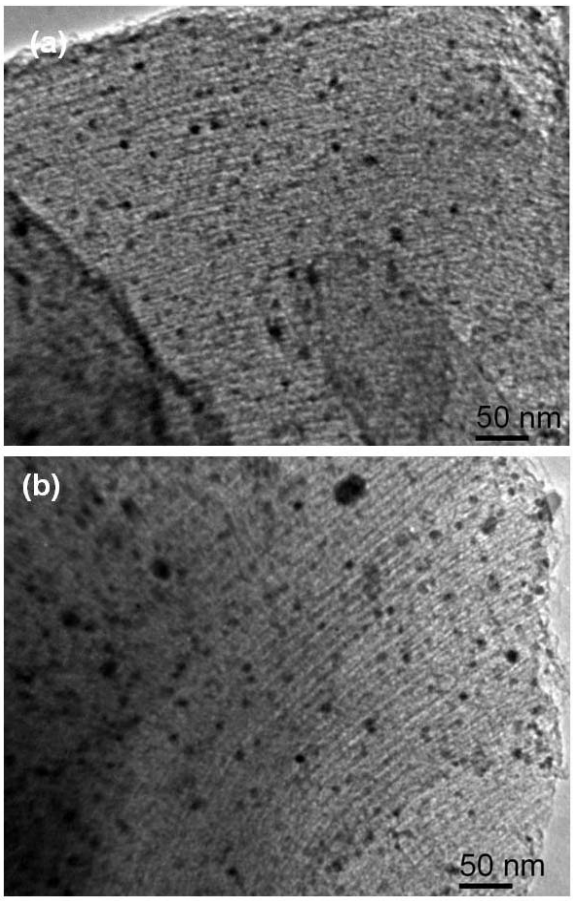

Figure 4.10 TEM images of (a) fresh Ru8C2 and (b) after five-reaction runs.

4.4 Summary

This study reports that Ru nanoparticles sandwiched in the pore walls of templated carbons exhibit high catalytic activity and stability in the hydrogenation of D-glucose. The following points are highlighted:

1. Comparison with the Ni-based catalyst shows that the mean activity of Ru-C nanostructured catalysts (Ru6C(HY)3, Ru6C3) were approximately 20 times higher than those of Ni catalysts. In addition to their higher activity, the Ru-C nanostructured catalysts (Ru6C(HY)3, Ru6C3) had the crucial advantage that they are stable against leaching and poisoning.
2. Compared with other Ru-C catalysts, Ru-C nanostructured catalysts exhibit higher catalytic activity because of the enhanced contact between the Ru nanoparticles and the carbon matrix, together with the unblocked pores of the catalysts. The Ru-C nanostructured catalysts created a highly intimate contact between the Ru nanoparticles and the carbon support because of the carbon deposition on the Ru surface via CVD. Such intimate contact may favor the hydrogen spillover, which greatly enhanced the transfer rate of H species. Therefore, more hydrogen could be adsorbed on the Ru-C nanostructured catalysts, which in turn enhanced its hydrogenation activity.
3. The pore structure of the Ru-C nanostructured catalysts had a significant influence on the catalytic results. In Ru-C nanostructured catalysts with zeolite HY as template, the transport of D-glucose was significantly hindered.

CHAPTER 5

Bimetallic Ru-Cu nanoparticles sandwiched in porous carbon

5.1 Introduction

Bimetallic catalysts have been shown to exhibit improved catalytic properties for many chemical reactions than a single-metal one (Guczi, 2005). The improvement is considered to be primarily due to changes in their geometric and electronic structures introduced by the second element, which can exist as an adatom (Santori et al., 2002), in an alloy state (Liberkov and Touroude, 2002), in an ionic state (Marchi et al., 2003), and as partially oxidized form (Reyes et al., 2002). Among all bimetallic catalysts reported so far, Ru-Cu catalysts supported on high-surface-area supports, including silica (Rouco et al., 1983; Smale and King, 1989; Smale and King, 1990), zeolite (Alvarez-Rodriguez et al., 2006; Alvarez-Rodriguez et al., 2008) , and carbon (Asedegbega-Nieto et al., 2006; Asedegbega-Nieto et al., 2006) , have received the great interest, in spite of the fact that these two metals do not form a solid solution in bulk. Study (Sinfelt, 1973) showed that there are strong interactions at the interface of Ru and Cu particles, the Cu atoms form an adsorbed layer on the Ru kernel. A structural model for describing the bimetallic catalyst was subsequently proposed (Sinfelt et al., 1980; Smale and King, 1990; Chen and Goodwin, 1996). According to the model (Figure 5.1), in a bimetallic Ru-Cu catalyst, Cu preferentially populates the edge and corner sites of Ru crystallites. When these sites were completely filled with Cu, low index planes of Ru start to be covered with Cu. In addition to the geometric (or ensemble) effect, the electronic (or ligand) effect is believed to be another important factor determining the catalytic behaviors of the supported bimetallic Ru-Cu

catalysts (Rouco et al., 1983; Bond and Yide, 1984; Shastri et al., 1986; Schoenmakerstolk et al., 1987). For hydrogenation reactions, another important effect that should be considered is the hydrogen spillover from Ru to Cu (King et al., 1986). The interactions between the two metals and how the interactions determine the physicochemical and catalytic properties of the bimetallic catalyst are influenced by the metal-support interactions (Guczi, 2005).

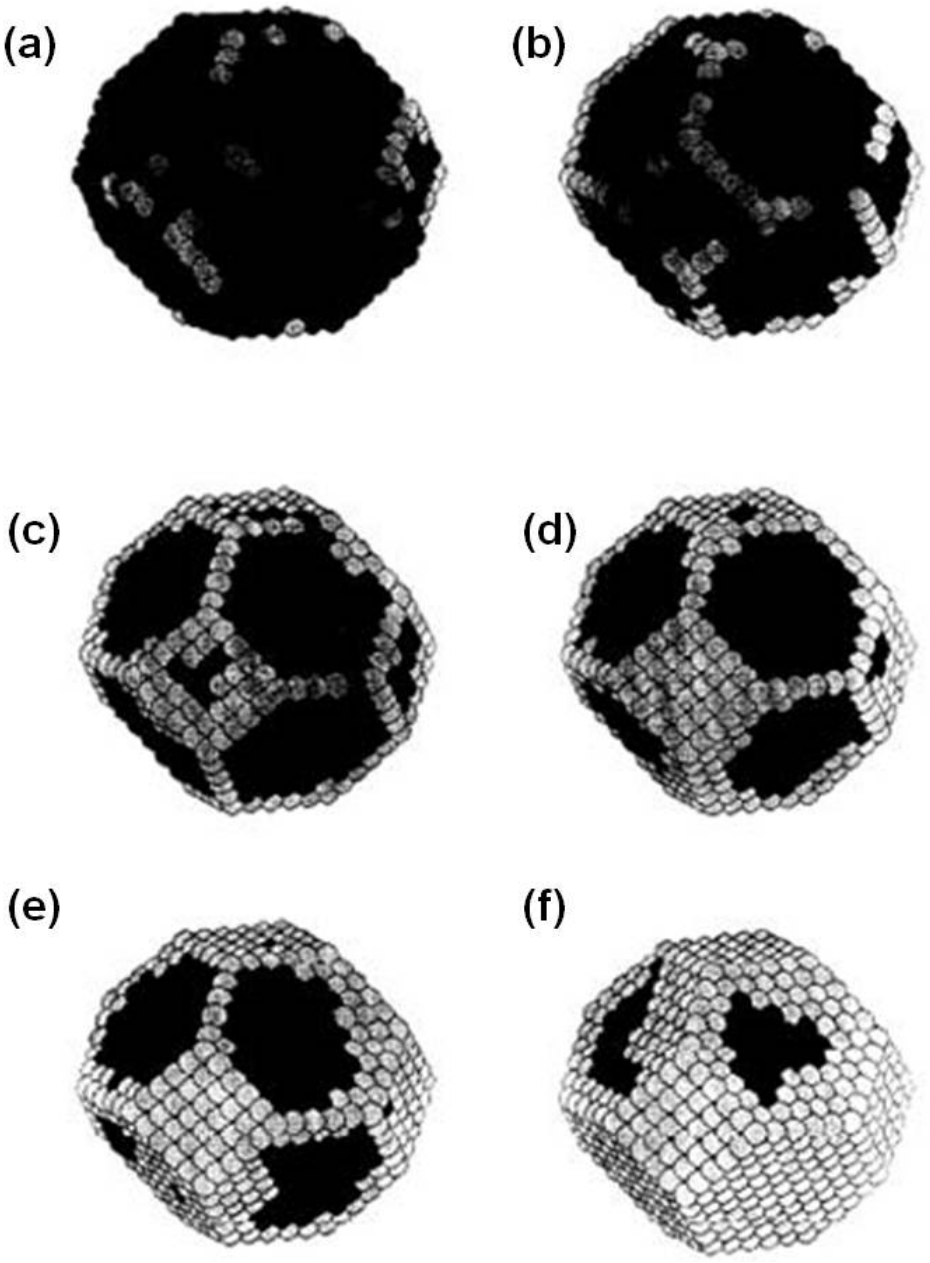

Figure 5.1 Monte Carlo simulation results for Ru-Cu/SiO_2 catalysts with a total metal dispersion of 30%; (a) 2% Cu, (b) 5% Cu, (c) 10% Cu, (d) 15% Cu, (e) 20% Cu, (f) 30% Cu (Smale. et al., 1989)

With the consideration of the bimetallic effects and the advantage of lowering the cost of catalyst by partially replacing Ru with Cu, the bimetallic Ru-Cu catalysts were prepared by using the template preparation method. The catalytic properties of the bimetallic catalysts were evaluated using the reaction of D-glucose hydrogenation. The experimental results demonstrated that the bimetallic displayed a significantly improved performance than both single-metal catalysts. A number of characterization techniques were employed to characterize the catalysts for elucidating the experimentally observed catalytic properties. The synthesis process can be found in section 3.2.2.

5.2 Characterization of bimetallic Ru-Cu catalysts

Nitrogen Adsorption. Figure 5.2 showed the isotherms of the RuC, RuCuC and CuC. The pore parameters of the samples were compiled in Table 5.1. It can be seen that all samples showed a type IV isotherms, but with different pore geometries. RuC and all the bimetallic RuCuC catalysts exhibited a H2 hysteresis loop, indicating an ink-bottle-like pore structure. The average pore sizes of all the samples were estimated to be about 3.3 nm. Sample CuC, however, displayed an H3 hysteresis loop, indicating a slitlike pore structure. The average pore size was about 3.6 nm (see Figure 5.2f). The lower surface area and pore volume of sample CuC suggests that the Cu may have largely hindered the deposition of pyrolytic carbon during the CVD process, leading to the formation of a poor porous structure. For all bimetallic catalysts and catalyst RuC, their surface areas, pore volumes, and pore sizes are comparable.

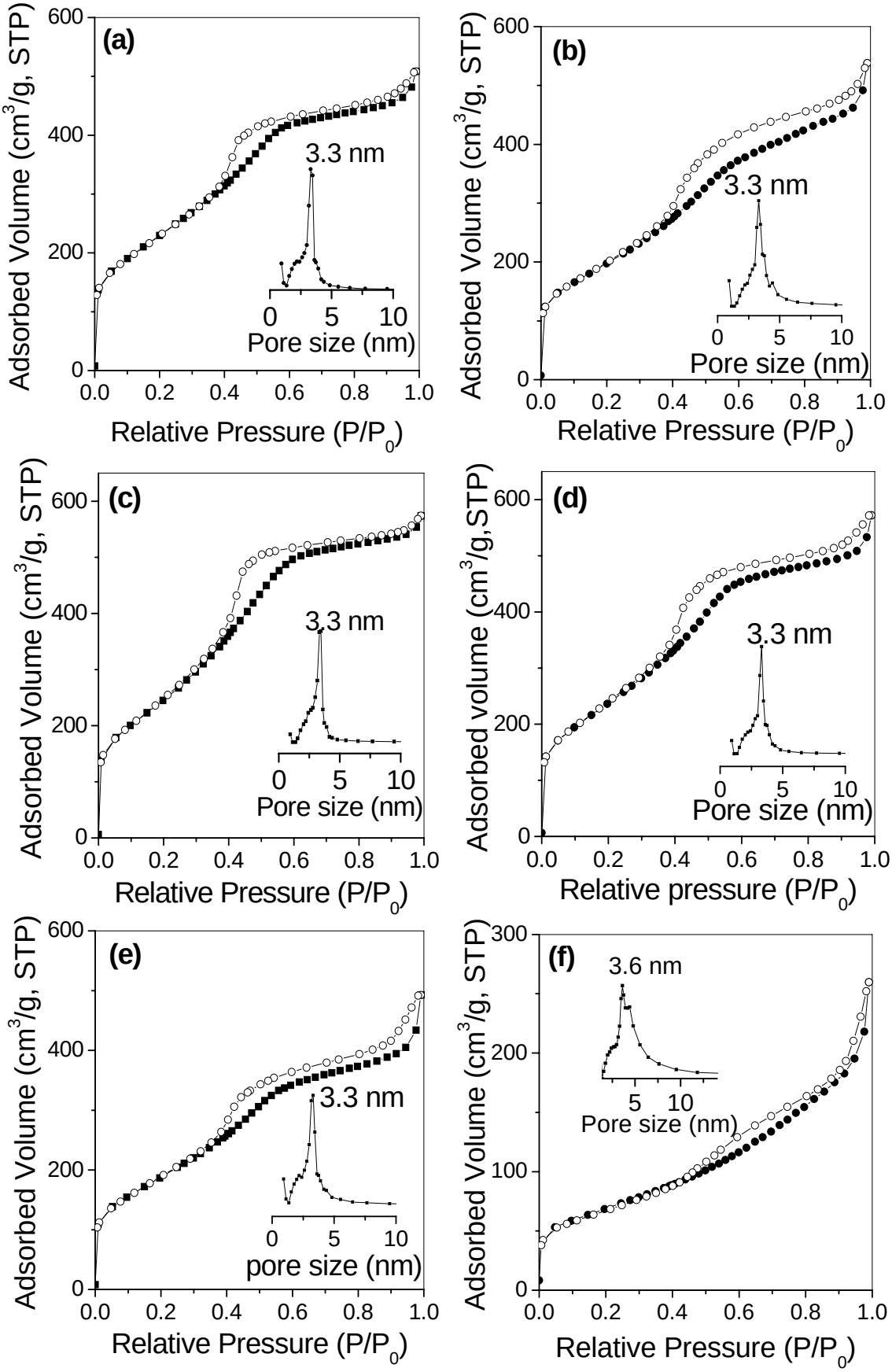

Figure 5.2 N2 adsorption-desorption isotherms and PSD (the inset) of catalysts: (a) RuC, (b) RuCu0.3C, (c)RuCu0.5C, (d) RuCu1.0C, (e) RuCu1.5C, and (f) CuC.

Table 5.1 Physicochemical properties of the Ru-Cu catalysts.

Catalyst	Ru content (wt%)	Cu content (wt%)	Cu/Ru (atom/atom)	A (m^2/g)	V (cm^3/g)	d (nm)
RuC	7.3	0	0	834	0.78	3.3
RuCu0.3C	5.6	1.1	0.3	712	0.83	3.3
RuCu0.5C	5.6	1.8	0.5	897	0.88	3.3
RuCu1.0C	5.4	3.4	1.0	864	0.88	3.3
RuCu1.5C	5.9	5.6	1.5	682	0.76	3.3
CuC	0	7.2	-	246	0.40	3.6
5RuC	5	-	-	690	0.48	3.7
Ni65	65[a]	-	-	129	0.30	4.7

[a] Ni content is 65wt%.

XRD Analysis. Figure 5.3 compared the XRD patterns of the bimetallic catalysts with that of single-metal catalysts RuC and CuC. The broad peak centered at 25 degree two theta corresponded to the interlayer distance of 0.36 nm, which may be indexed to the (002) diffraction of the graphite structure (Kim et al., 2003; Xia and Mokaya, 2004). These catalysts contained stacked grapheme sheets as the result of CVD treatment at 900 ^{o}C. For sample RuC, the peaks at 38.3, 42.2, 44.0, 58.3, 69.4, and 78.4 degree two theta were respectively due to the diffractions of the (100), (002), (101), (102), (110), and (103) planes of hexagonal close-packed (hcp) Ru metal (ICDD-JCPDS card No. 06-0663). For sample CuC, the peak at 43.3 degree two theta can be assigned to the reflection of (111) plane of metallic Cu (ICDD-JCPDS card No. 04-0836). The broad reflection peak implied small size of Cu particles. Compared with the XRD pattern of RuC catalysts, the peaks number and the location of the RuCuC

catalysts were not changed. XRD analysis provided clear evidence that the incorporation of Cu does not alter RuC structure. Previous study on silica supported Ru-Cu bimetallic catalysts has shown that the Cu atoms tend to cover the surface of Ru particles (Strohl and King, 1989; Smale and King, 1990; Sprock et al., 1992; Lenarda et al., 1996). On the basis of this description we envisage that the RuCuC catalysts were made up of a hcp core of Ru covered by Cu atoms, retaining a coherent hcp structure.

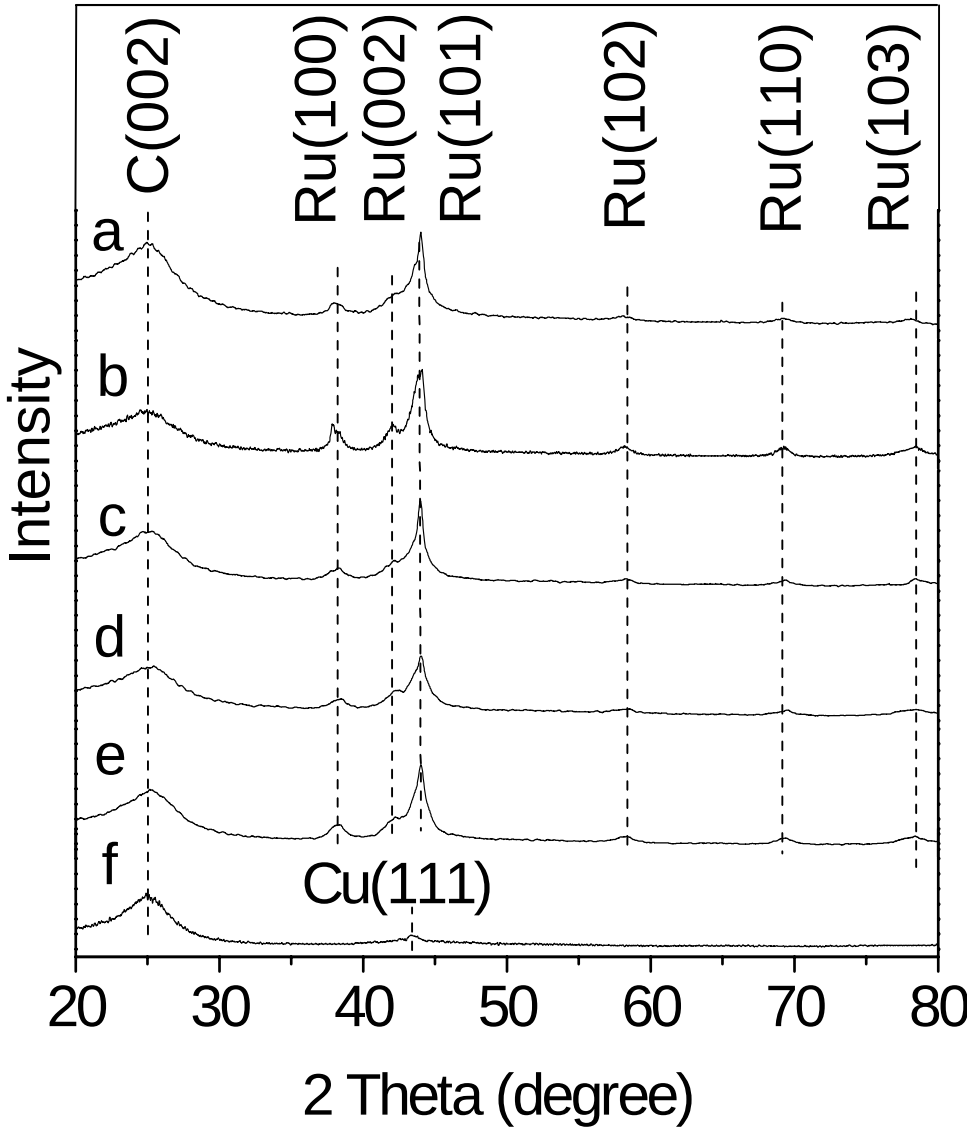

Figure 5.3 XRD patterns of (a) RuC, (b) RuCu0.3C, (c) RuCu0.5C, (d) RuCu1.0C, (e) RuCu1.5C, (f) CuC.

TEM Observation. Figure 5.4 shows the TEM images of samples RuC, CuC, and RuCu0.5C. The dark dots seen on the grey carbon background were due to the metal nanoparticles.

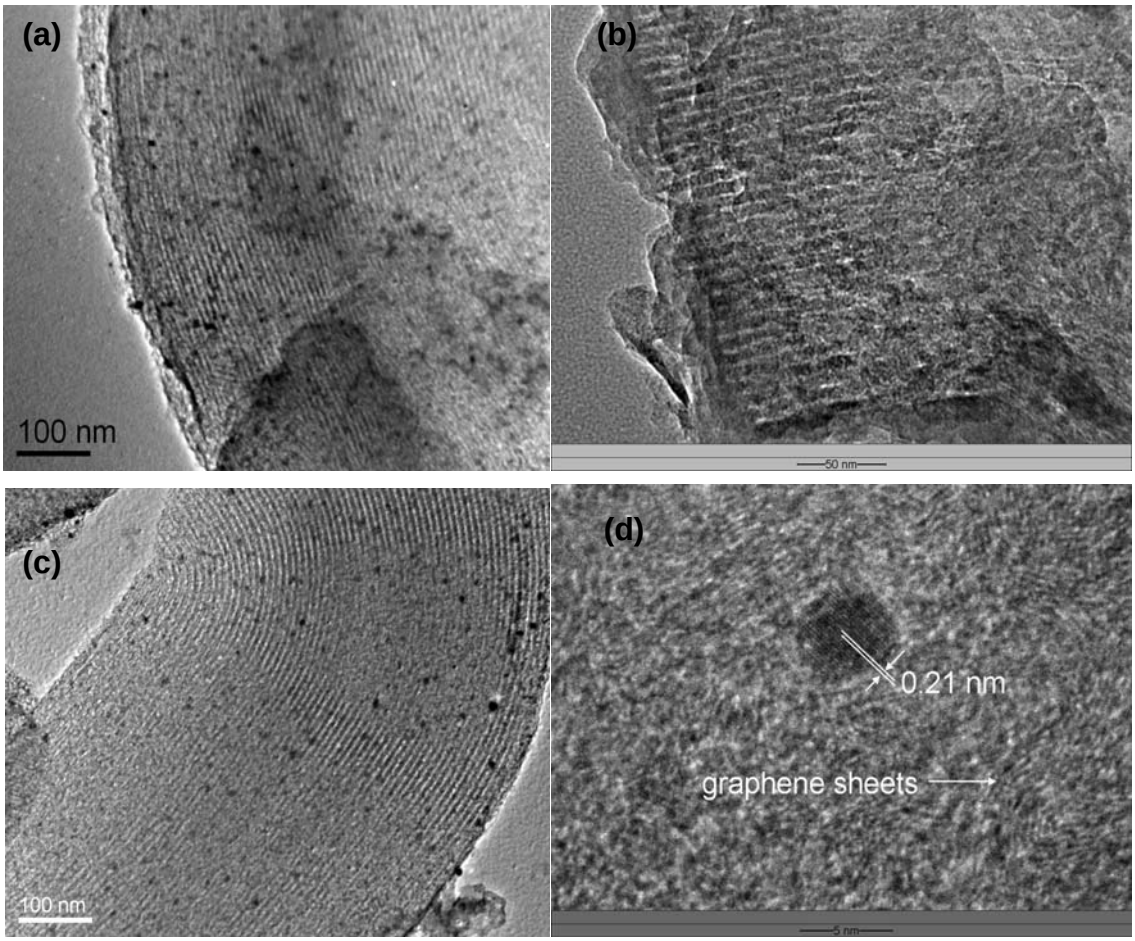

Figure 5.4 TEM images of catalysts (a) RuC, (b) CuC, (c) RuCu0.5C, and (d) HRTEM image of RuCu0.5C showing the stacking of graphite sheets [$d_{(002)}$=0.36 nm].

It can be seen from Figures 5.4a and 4c that both Ru and RuCu nanoparticles were uniformly dispersed within the carbon framework, and most of Ru and RuCu nanoparticles were sandwiched in the carbon nanorods. The carbon nanorods were derived from the pore channels of SBA-15 template (Jun et al., 2000). The diameters of these carbon nanorods were in the range of 5-7 nm, consistent with the pore diameter of the template. It can be seen from Figure 5.4c that the some channels in CuC sample collapsed, further demonstrated that Cu may have largely hindered the

carbon deposition during the CVD process. Figure 5.4d showed a spherical RuCu nanoparticle with a diameter of about 5 nm embedded in the carbon substrate. The lattice spacing in the RuCu particle was 0.21 nm corresponding to the Ru (101) planes (Hansen et al., 2001). This image also indicated a stacking of the discoid graphene sheets with a spacing of about 0.36 nm around the RuCu nanoparticles, which was in accordance to the XRD results. The chemical composition of the RuCu0.5C was examined by EDX and elemental mapping analysis (Figure 5.5). The EDX spectrum testified the existing of the Ru and Cu element. The corresponding elemental maps revealed that the Ru element is relatively uniform distributed in carbon framework.

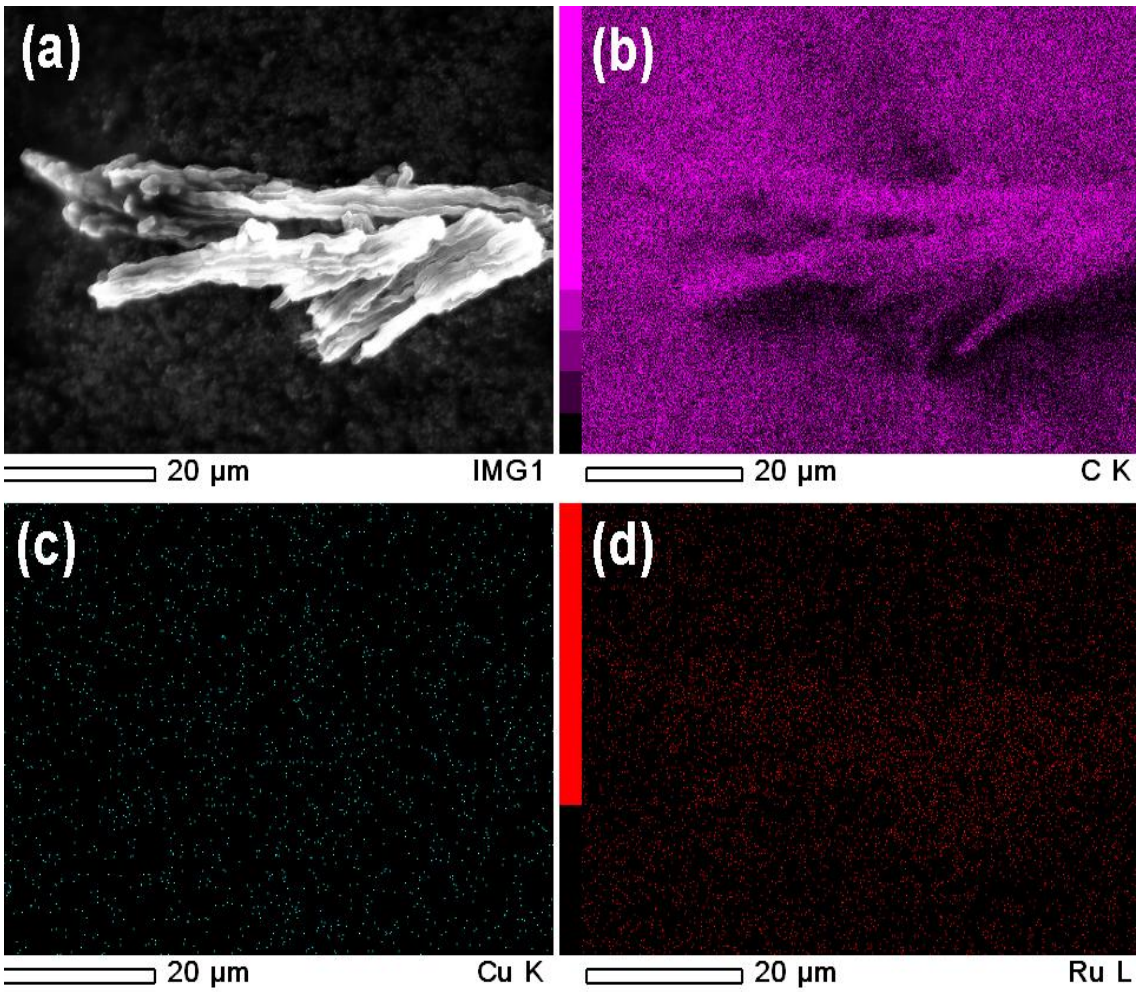

Figure 5.5 (a) the SEM image of the RuCu0.5C sample, and elemental mapping of C (b), Ru (c) and Cu (d), respectively, correspond to (a).

XAS Analysis. Figures 5.6a and 5.6b showed the Ru L_{III}-edge and Cu K-edge XANES spectra of the bimetallic catalysts together with reference samples. It can be seen that the spectra of catalyst RuC and RuCu0.5C were similar (Figure 5.6a), suggesting a similar coordination of Ru in both catalysts. The Cu K-edge spectra of RuCuC catalysts (Figure 5.6b) resembled that of CuO, suggesting that most of the Cu was present in an average oxidation state close to Cu (II).

The EXAFS data of Cu K-edge of RuCuC catalysts at room temperature and the associated Fourier transforms, which were taken over the range of wave vectors $2.2 \leq K \leq 11.2$ $Å^{-1}$, were shown in Figures 5.7a and 5.7b. The interatomic distances measured for Cu-O and Cu-Cu in reference samples were highlighted by line A and B, which had a phase shift of about 0.4 Å (Ru_{Cu-O}=1.87 Å, R_{Cu-Cu}=2.55 Å). The Fourier transforms of RuCuC catalysts displayed a broad shoulder in the range of 2-2.8 Å (after phase correction), which implied multiple interatomic absorber-scatterer interactions besides Cu-O. This is likely to be caused by the presence of the neighbors, which are Cu and Ru atoms around the Cu atom (Sinfelt et al., 1980; Shephard et al., 1998; Bromley et al., 2001; Highfield et al., 2009). Based on the above discussions, there are bimetallic entities in the RuCuC catalysts. In addition, the multiple interatomic interactions between Cu with neighboring elements (O, Cu and Ru) imply that the Cu presented as a layer on the surface of Ru. The outerlayers of the Cu clusters were oxidized, leaving the interior Cu atoms coordinated to Ru as well as Cu atoms. Furthermore, the incorporation of Cu did not change the Ru crystal structure, which is in accordance with the XRD results.

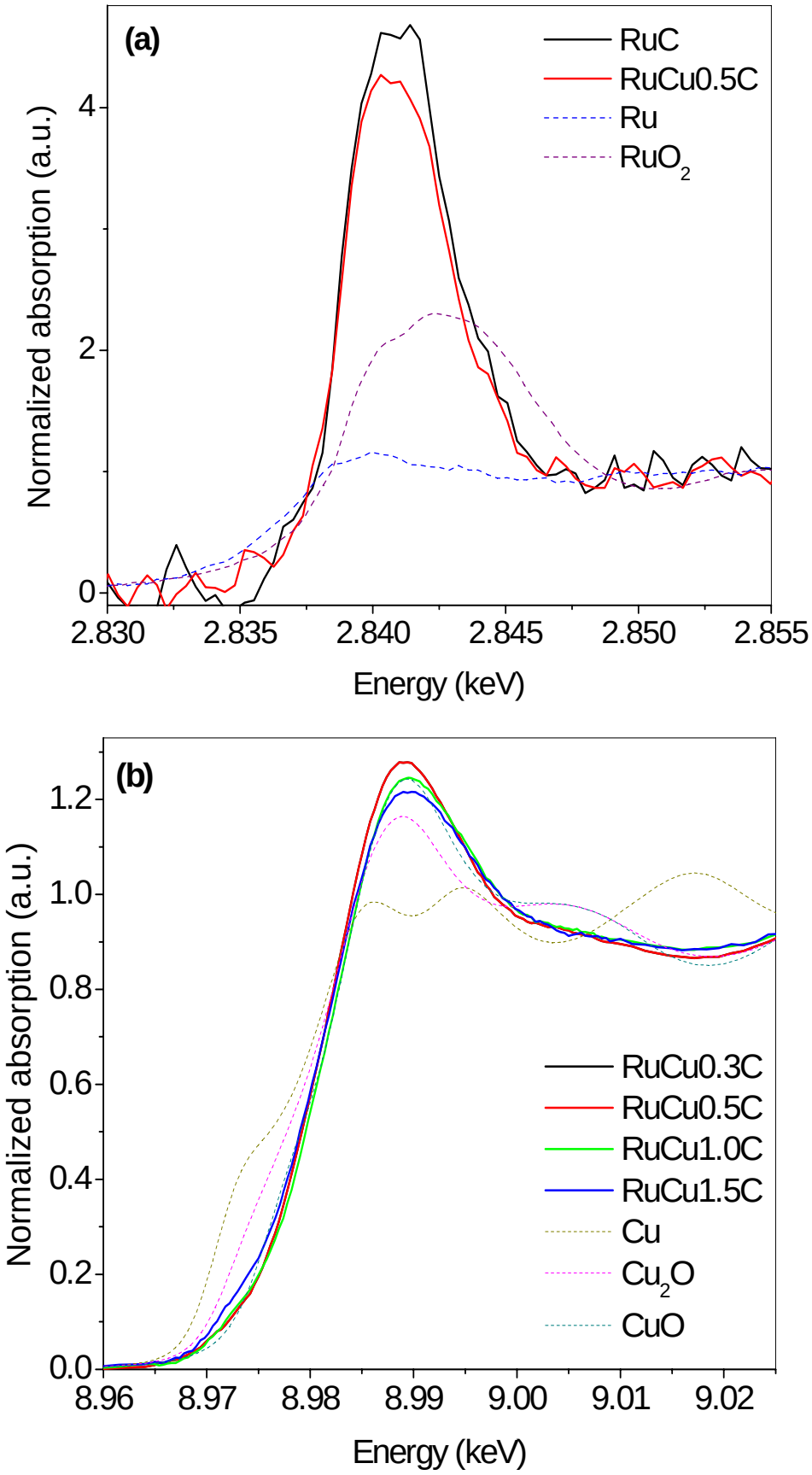

Figure 5.6 (a) Ru L_{III}-edge XANES spectra of RuC and RuCu0.5C catalysts, (b) Cu K-edge XANES spectra of RuCuC catalysts,

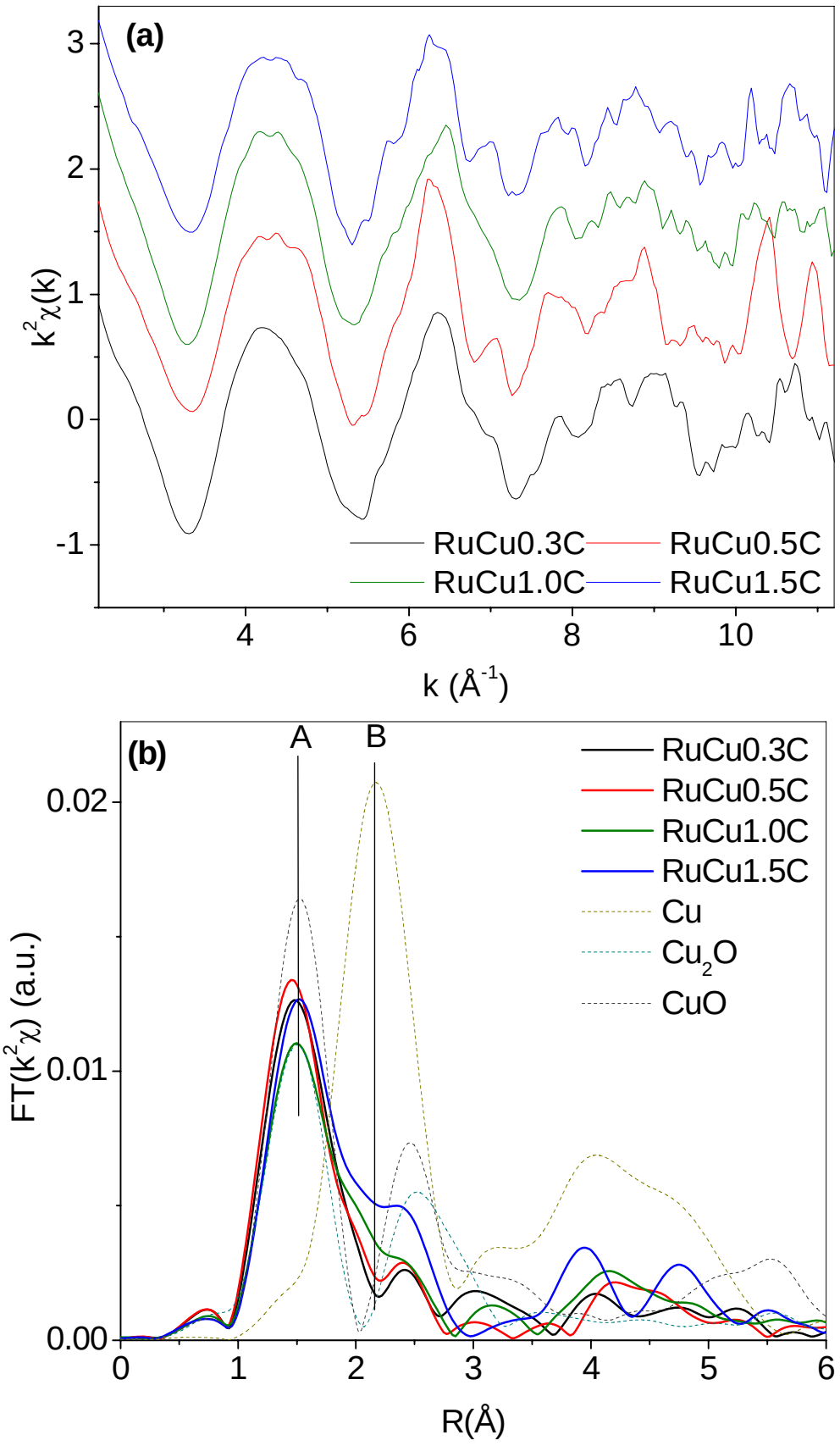

Figure 5.7 (a) Cu K-edge EXAFS data, (b) k2-Weighted Fourier-transform (not phase-corrected) for RuCuC catalysts at the Cu K-edge (A: Cu-O, B: Cu-Cu from Cu metal).

H_2 and CO chemisorption. Figure 5.8 and 5.9 showed the H_2 and CO pulse titration peaks of the samples, respectively. The chemisorption results were summarized in Table 5.2.

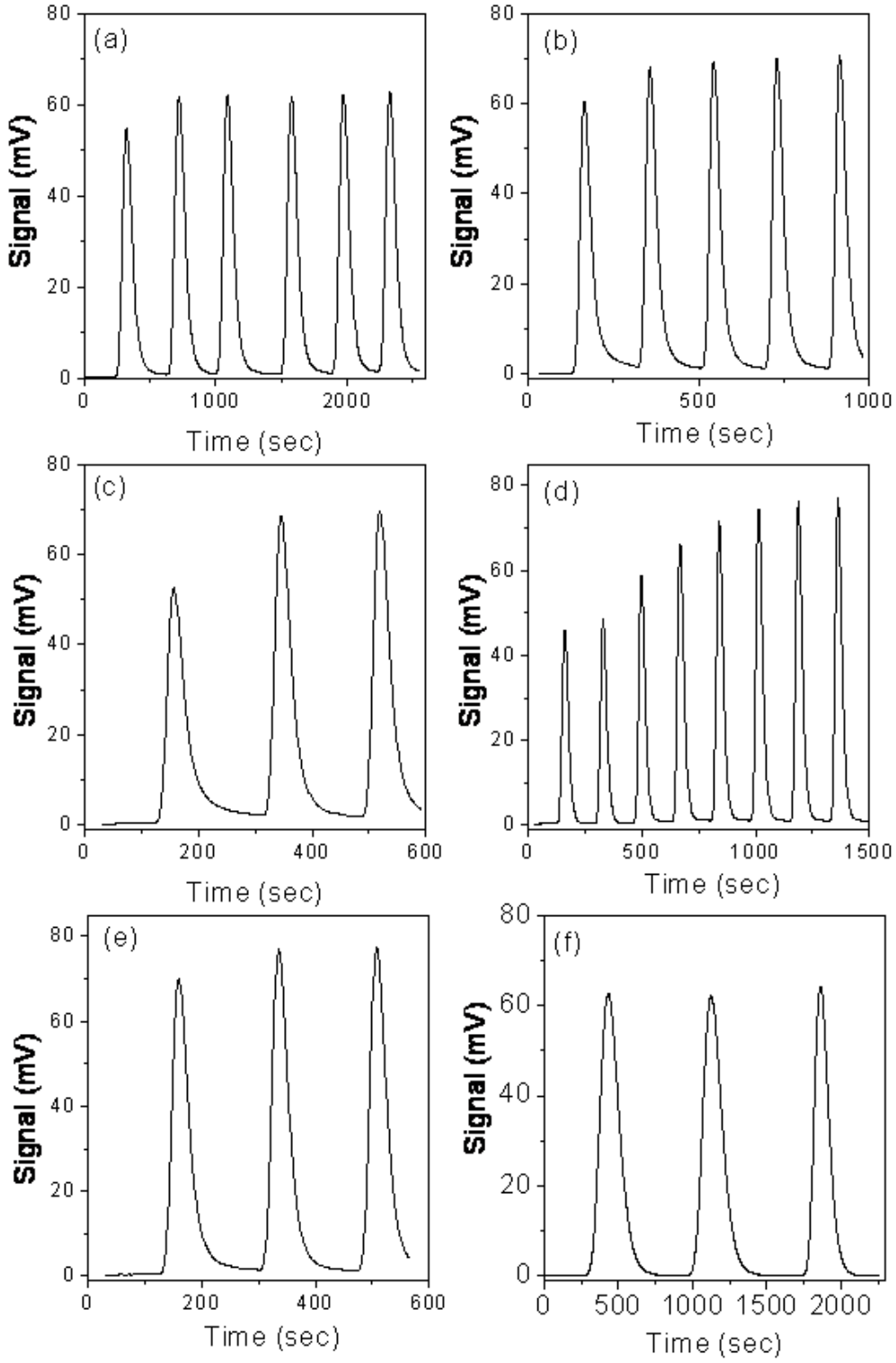

Figure 5.8 H_2 pulse titration peaks of (a) RuC, (b) RuCu0.3C, (c) RuCu0.5C, (d) RuCu1.0C, (e) RuCu1.5C, (f) CuC.

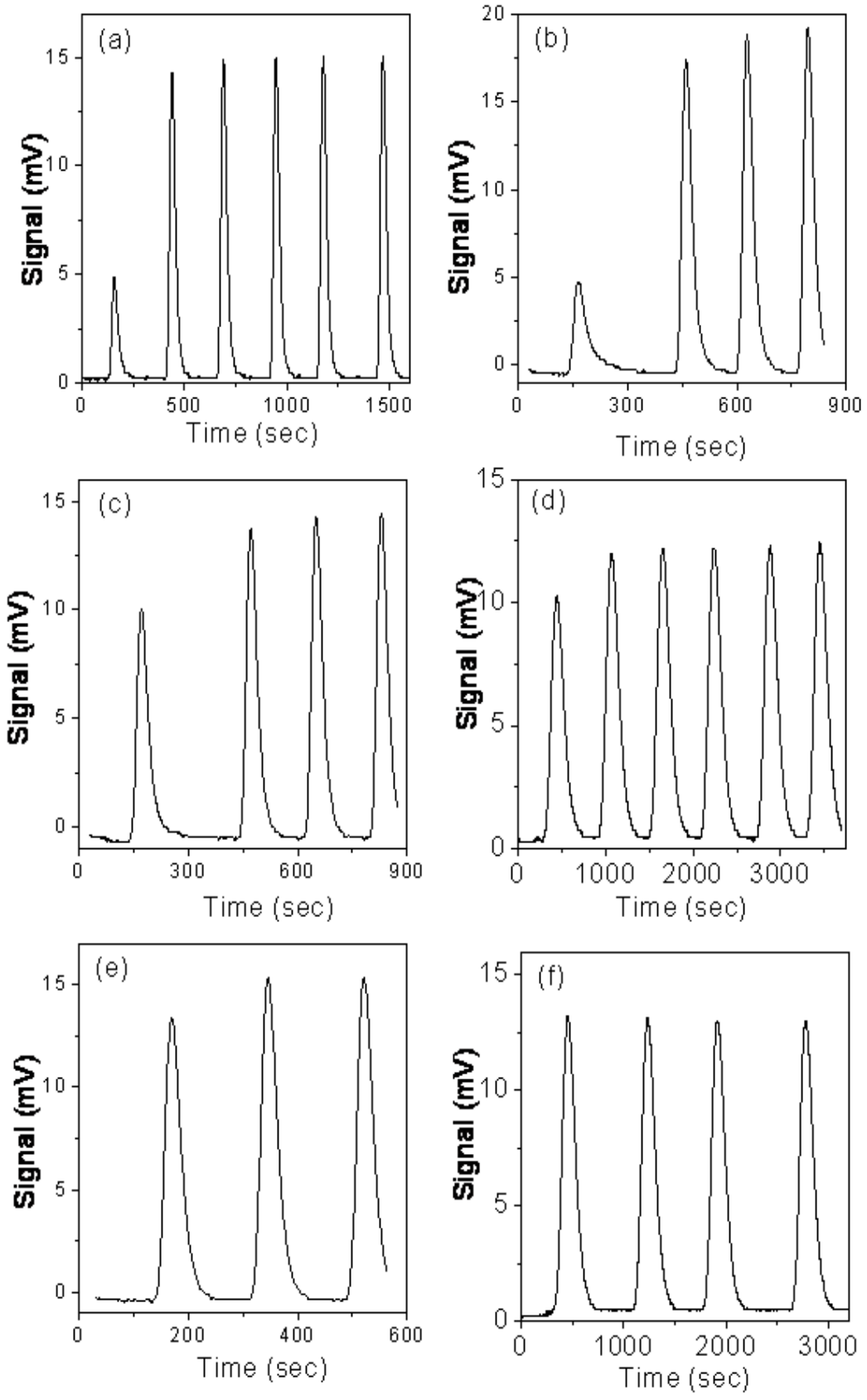

Figure 5.9 CO pulse titration peaks of (a) RuC, (b) RuCu0.3C, (c) RuCu0.5C, (d) RuCu1.0C, (e) RuCu1.5C, (f) CuC.

Table 5.2 The chemisorption results of the catalysts.

Catalysts	H_2/Ru (μmole/g)	CO/Ru (μmole/g)	H/CO
RuC	12.73	29.07	0.88
RuCu0.3C	14.77	25.75	1.15
RuCu0.5C	18.62	20.18	1.85
RuCu1.0C	19.11	18.66	2.04
RuCu1.5C	6.55	17.90	0.37
CuC	0.82	0.18	-

The H_2 and CO chemisorption results, expressed as H_2/Ru and CO/Ru, means the total mole adsorbed H_2/CO per gram Ru. H_2/Ru is hydrogen monolayer uptake volume per gram of ruthenium, STP; CO/Ru is carbon monoxide monolayer uptake volume per gram of ruthenium, STP. * the total mole adsorbed per gram Cu.

As can be seen, the CuC sample adsorbed neither H_2 nor CO. Hence, it can be assumed that under the experimental conditions the chemisorption of H_2 and CO for the bimetallic samples may be totally attributed to Ru or bimetallic Ru-Cu. The CO chemisorption data showed that the CO/Ru ratio falls from 29.07 to 17.90 as the Cu/Ru atom ratio increased from 0 to 1.5, indicating that a decrease of the exposed Ru surface. One possible reason is the growth of the Ru particles. However, the sizes of the metal nanoparticles in all the samples were nearly the same. Thus, the effect of growth of Ru particles can be excluded. Alternatively, the surface of Ru particles may be partially covered by Cu species as it was previously observed (Bond and Yide, 1984; Liu et al., 1991; Alvarez-Rodriguez et al., 2006). This confirmed the assumption that the RuCuC samples consists a Ru core covered by Cu atoms.

Opposite trends were observed for the H_2 chemisorption except for catalyst RuCu1.5C. This observation is agreed with hydrogen spillover from Ru to Cu for Ru-Cu supported catalysts (Lai and Vickerman, 1984; Goodman and Peden, 1985; King et

al., 1986; Hong et al., 1987; Hong et al., 1987; Wu et al., 1990; Narayan and King, 1998). For the close contact of Ru and Cu, hydrogen disssociatively adsorbed on Ru surface and then migrated to the Cu surface. For the RuCu1.5C sample with higher Cu loadings, the addition of Cu blocked the most Ru defect-like sites reducing the amount of the weakly bound hydrogen and subsequent transfer (Bhatia et al., 1992).

5.3 Catalytic properties

The catalytic activities of the catalysts in the hydrogenation of D-glucose were evaluated in the liquid phase at 100 ^{o}C and hydrogen pressure 8MPa. The catalytic activities of the catalysts together with two commercial catalysts were summarized in Figure 5.10. The single-metal Ru catalyst prepared in this work using the template method displayed a much higher catalytic activity than the commercial catalysts while the single-metal Cu catalyst showed a negligible catalytic activity. However, most bimetallic catalysts showed higher catalytic activities than the single-metal catalyst RuC and the commercial catalysts. When the molar ratio of Cu/Ru was 0.5, RuCu0.5C exhibited the best catalytic performance with a catalytic activity of about 0.25 mol/mol·s. These catalytic results indicate that the bimetallic Ru-Cu catalysts indeed catalytically performed better than the single-metal catalysts and the commercial catalysts.

Since the particle size and the pore structure of the single-metal Ru catalysts and the bimetallic RuCuC catalysts were similar due to the template method. The much higher activity of bimetallic RuCuC catalysts compared to the single-metal Ru catalyst may be attributed entirely to the presence of Cu. The Cu single sites must be in close contact with the Ru particles to exert a beneficial effect on the hydrogenation activity since no activity improved is observed for the mixture of RuC and CuC catalysts. The results may be considered as another evidence for the formation of Ru-Cu bimetallic

nanoparticles. At lower Cu/Ru ratio (<1.0), the catalytic activity improved with the increase of Cu/Ru ratio. Additional activity sites for glucose hydrogenation may have been created by Cu addition due to the spillover of H from Ru to Cu, permitting reaction on the Cu. At higher Cu/Ru ratio (>1.0), the complete preferential population of defect-like edge and corner of Ru sites by Cu would subsequently limit the dissociation of hydrogen on the metal surface (King et al., 1986; Narayan et al., 1998; Asedegbega-Nieto et al., 2006; He et al., 2007), which is necessary for glucose hydrogenation.

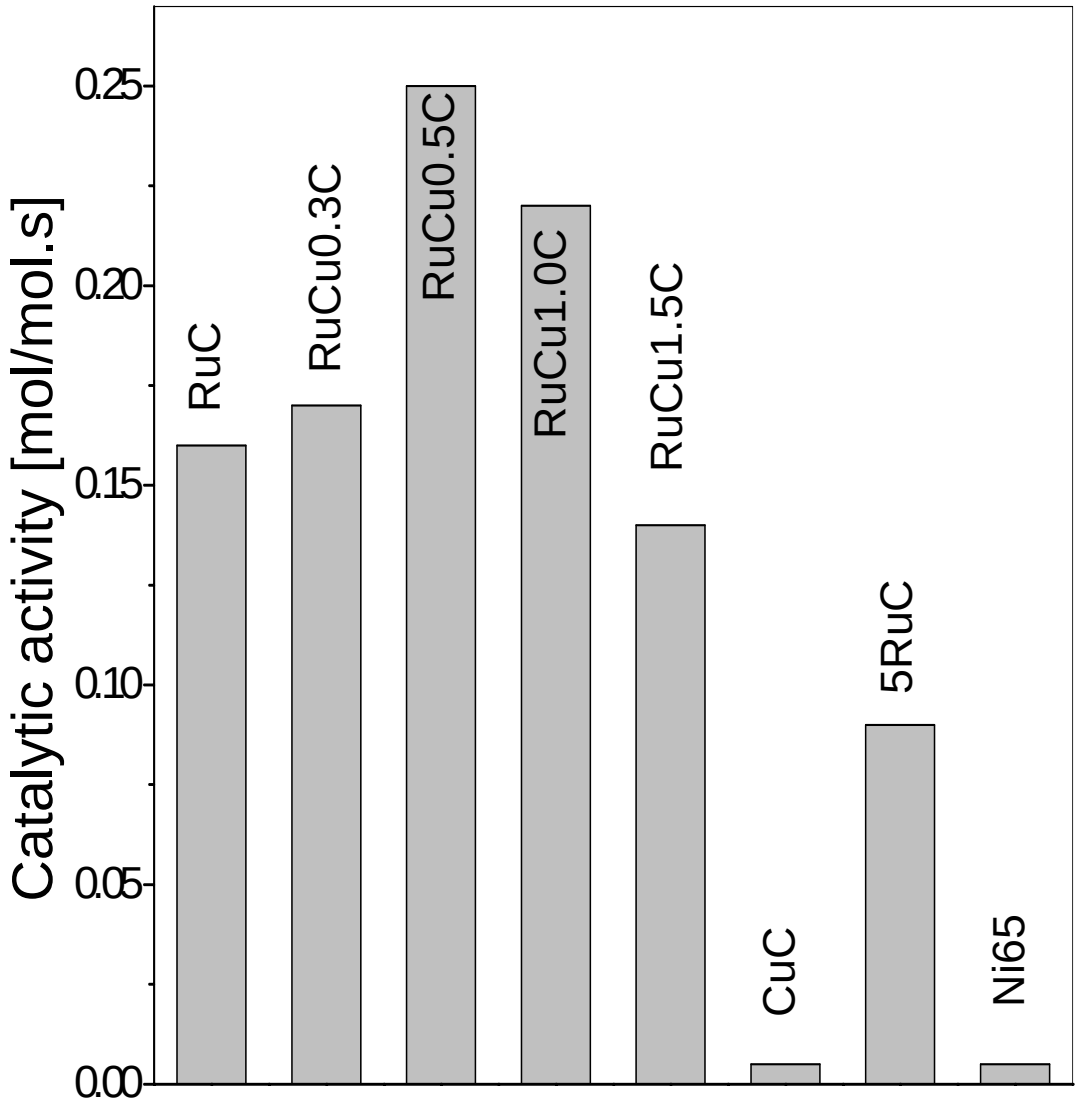

Figure 5.10 Catalytic activities of the catalysts.

5.4 Summary

In Summary, a novel nanostructured bimetallic catalyst with Ru-Cu nanoparticles sandwiched in the pore walls of mesoporous carbon were synthesized via a template route. For the unique property of template method, the addition of Cu did no affect the particle size or the dispersion of Ru. Based on the XRD, H_2 and CO chemisorptions, and X-ray absorption results, we hypothesize that the RuCuC samples have an hcp Ru core, covered by Cu atoms. Overall the bimetallic catalyst showed a higher catalytic activity than single-metal catalysts (RuC and CuC) in hydrogenation of D-glucose. At low Cu/Ru ratios (<1.0), additional activity sites for D-glucose hydrogenation may have been created by Cu addition. Cu could adsorbed the ionized glucose species by coordination of O-1, O-5, and O-6, which was then polarized, and thus more easily attacked by the spillover hydrogen atom from Ru to Cu. At high Cu/Ru ratios (>1.0), the presence of Cu decreased the catalytic activity. This effect may be due to the complete preferential population of defect-like edge and corner of Ru sites by Cu, subsequently limiting the dissociation of hydrogen on the metal surface, which is necessary for D-glucose hydrogenation.

CHAPTER 6

Ruthenium nanoparticles embedded in mesoporous carbon fibers

6.1 Introduction

Mesoporous carbon materials have attracted consideration attention because of their ordered pore structure, high surface areas, large pore volumes, and chemical inertness. One-dimensional (1-D) nanostructures such as carbon nanotubes (CNTs) and nanofibers (CNFs) have been used as attractive catalyst supports, especially for fluid phase reactions (Serp et al., 2003; Lu et al., 2009), for such 1-D morphology facilitates the diffusion of the reactants and products. However, these CNTs and CNFs have a low porosity, random pore structure and small surface area, strictly limiting their application in catalysis. To combine the advantage of these two types of materials together, the preparation of 1-D mesoporous carbon materials is a good alternative. Recently, a number of research groups have reported the synthesis of the porous carbon nanofibers by using porous silica or organic surfactant filled inside channels of porous anodic alumina membrane as a dual template (Chae et al., 2006; Cott et al., 2006; Rodriguez et al., 2006; Steinhart et al., 2007; Zheng et al., 2007; Liang et al., 2009). Figure 6.1 schematically illustrates the synthesis procedure. Disordered powders of amorphous mesoporous carbon nanorods were obtained as replicas of solution-grown mesoporous silica nanorods serving as sacrificial templates (Yu et al., 2002). However, these researchers focused on the synthesis and characterization of these 1-D porous carbon materials, the application of these materials are rarely reported (Cui et al., 2007).

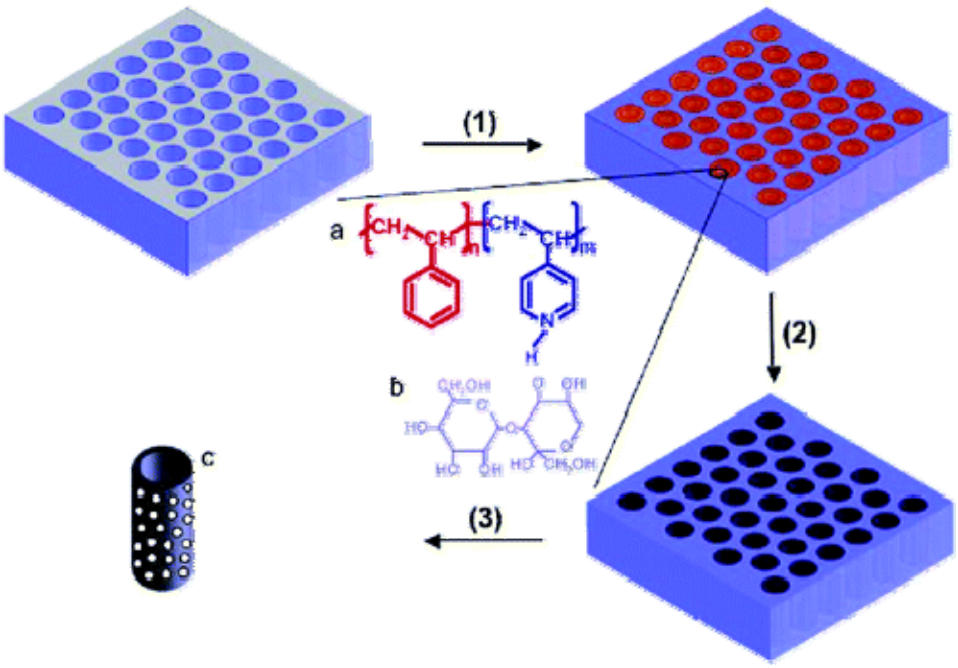

Figure 6.1 Schematic illustration of the synthesis of nanoporous carbon nanotubes by using organic surfactant filled inside channels of porous anodic alumina membrane (AAO) as a dual template (Rodriguez et al., 2006): (1) infiltration of the polymer and carbohydrate DMF solution into the AAO templates; (2) carbonization in argon; (3) removal of AAO templates and formation of individual nanoporous carbon nanotubes.

Recently, doping of heteroatoms into carbon materials has offered new opportunities for tailoring their chemical/physical properties and in turn, their catalytic performance. Nitrogen inclusion in different carbon structures has been reported to improve the catalytic performance in the liquid phase hydrogenation of cinnamaldehyde (Amadou et al., 2008), the gas phase hydrogenation of butyronitrile (Nieto-Márquez et al., 2010), the catalytic oxidation of SO_2 (Raymundo-Piñero et al., 2003), the ammonia decomposition (Garcia-Garcia et al., 2010) and oxygen reduction and methanol oxidation in fuel cells (Choi et al., 2007; Kim et al., 2007; Chetty et al., 2009; Lyth et al., 2009; Kim et al., 2010). The improvement of the catalytic activity is usually ascribed to either electronic or morphological modifications of the active metal phase or the creation of new surface active sites.

In this work, mesoporous carbon microfibers and nitrogen-doped carbon microfiber supported Ru catalysts were prepared by using alumina microfibers as the templates

via chemical vapor deposition method. The catalytic properties of the catalysts were evaluated in the hydrogenation of D-glucose, and compared with that of Ru catalysts supported on carbon nanotubes, carbon fibers, alumina microfibers and activated charcoals. Moreover, the effect of doped nitrogen atoms on catalytic performance was investigated. The synthesis process can be found in section 3.2.3.

6.2 Characterization of Ru nanoparticles catalysts

Nitrogen Adsorption. Figure 6.2 showed the nitrogen isotherms of Ru/AF-H, RuCMF, RuCMFN, Ru/CNT-H, Ru/CF-H, and 5RuC. It can be seen that Ru/AF-H revealed a type-IV isotherm with an H2 hysteresis loop, indicating mesoporous materials with an average pore size of around 3.5 nm. The nitrogen isotherms of RuCMF and RuCMFN were of type IV and exhibited hysteresis loops in the mesopore range. The pore size distribution of RuCMF was a slightly broader than that of RuCMFN. The larger pores of RuCMF may arise from incomplete filling of benzene into the alumina template during the CVD process or merging of smaller pores into large ones during the alumina template etching step. The pore parameters of the samples were summarized in Table 6.1. The RuCMF possesses the average pore size of 3.7 nm, the surface area of 760 m^2/g and the specific pore volume of 1.10 cm^3/g, while the average pore size, surface area and the pore volume of RuCMFN were 3.7 nm, 790 m^2/g and 0.71 cm^3/g, respectively. The surface area and pore size of RuCMF and RuCMFN are comparable, while the pore volume of RuCMF is higher than that of RuCMFN due to the existence of larger pores. The nitrogen sorption isotherms of Ru/CNT-H exhibited very high adsorption above P/P_0=0.8, which was ascribed to outer surface adsorption. The inner diameter of the Ru/CNT-H was about 2~4 nm, as shown in the inset of Figure 6.2d. The nitrogen sorption isotherms of Ru/CF-H and

5RuC exhibited very high adsorption below P/P_0=0.1, suggesting that a large proportion of the pore channels in the carbon fibers and 5RuC are micropores.

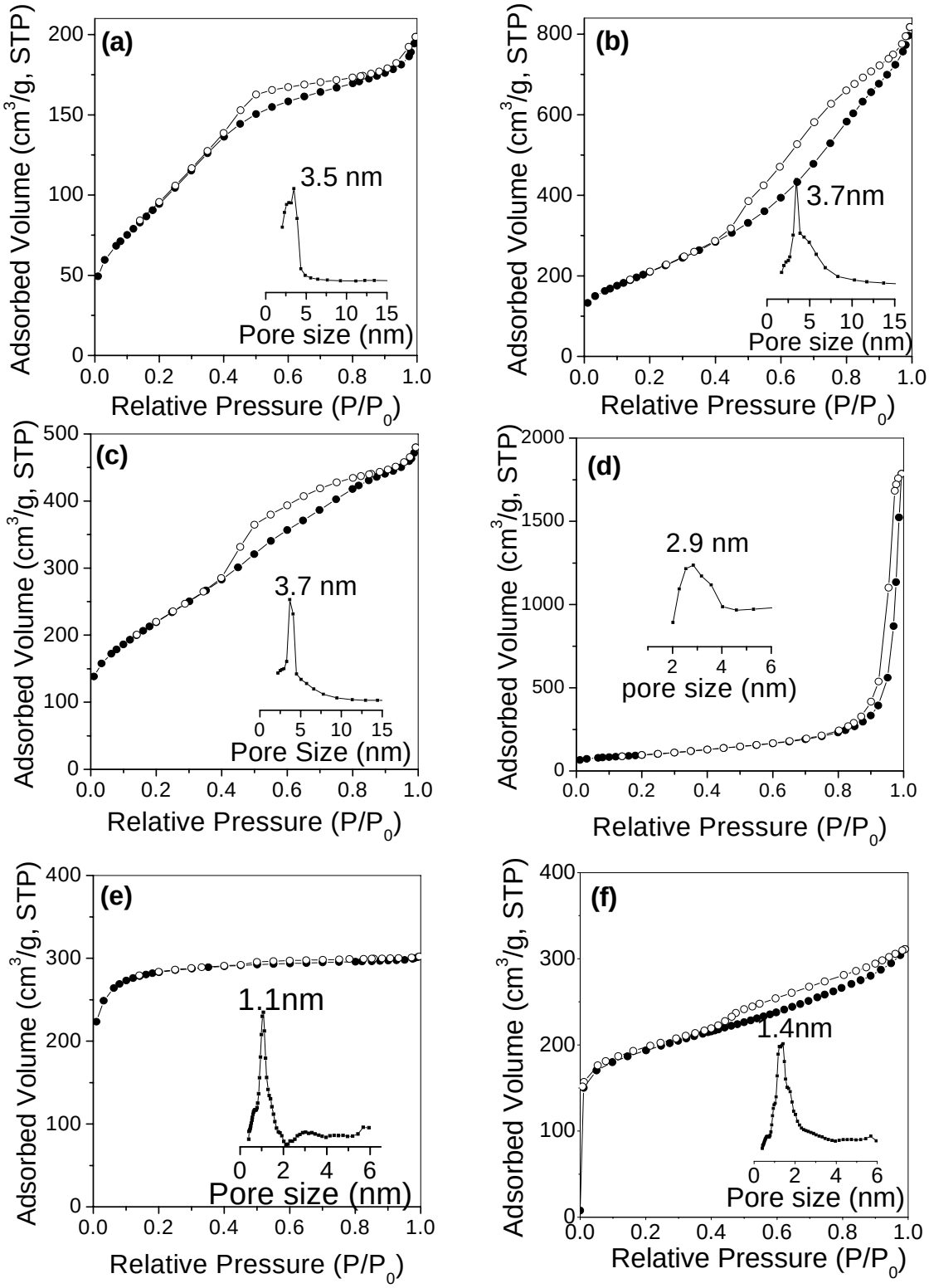

Figure 6.2 N_2 adsorption-desorption isotherms and PSD (the inset) of catalysts: (a) Ru/AF-H, (b) RuCMF, (c) RuCMFN, (d) Ru/CNT-H, (e) Ru/CF-H, (f) 5RuC.

Table 6.1 Physicochemical properties of the catalysts.

Catalysts	Ru content (wt%)	A (m^2/g)	V (cm^3/g)	d (nm)
RuCMF	6.4	760	1.10	3.7
RuCMFN	6.3	790	0.71	3.7
Ru/AF-H	5.2	354	0.29	3.5
Ru/CNT-H	3.2	336	1.46	2.9
Ru/CF-H	4.3	960	0.46	1.1
5RuC	5.0	690	0.48	1.4

XRD Analysis. Figure 6.3 compares the XRD patterns of the catalysts. For sample RuCMF and RuCMFN, the peaks at 38.3, 42.2, 44.0, 58.3, 69.4, and 78.4 degree two theta are respectively due to the diffractions of the (100), (002), (101), (102), (110), and (103) planes of hexagonal close-packed (hcp) Ru metal (ICDD-JCPDS card No. 06-0663). The peak centered at 25 degree two theta corresponds to the (002) diffraction of the graphite structure (Kim et al., 2003). The XRD patterns recorded for RuCMFN do not differ significantly from those of RuCMF, except for a slightly broadening of the C (002) peak and a decrease in the intensity. The low intensity of the C (002) peak suggests a general lack of graphitic ordering in carbon framework of sample RuCMFN by introducing C-N bonding, which shorter than C-C bonding (Xia and Mokaya, 2005; Lim et al., 2009; White et al., 2009). In contrast, no similar peaks were observed on Ru/AF-H, probably due to the small Ru particle size or amorphous phase, which is further confirmed by TEM images shown in Figure 6.5e. The XRD patterns of Ru/CF-H and Ru/CNT-H showed a broad peak located at 44 degree two theta, which overlaps with C (101) and Ru (101) diffractions, indicating the presence of relatively large Ru nanoparticles on Ru/CF-H and Ru/CNT-H, in good agreement with TEM observation (Figure 6.5).

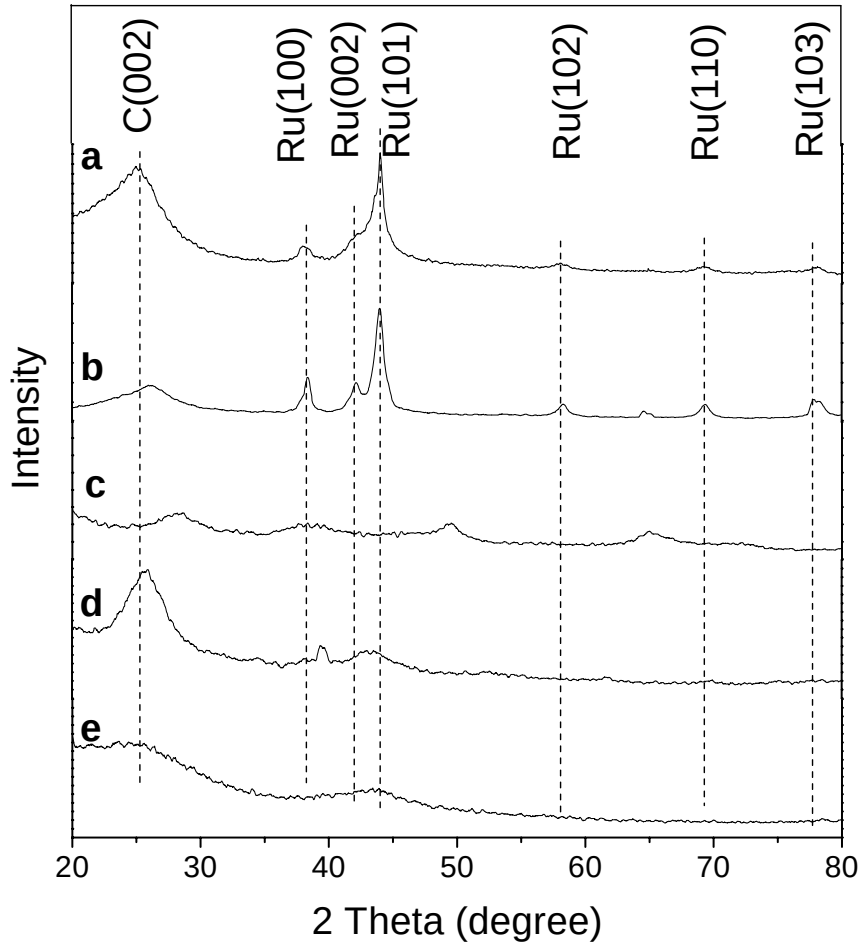

Figure 6.3 XRD patterns of (a) RuCMF, (b) RuCMFN, (c) Ru/AF-H, (d) Ru/CNT-H, and (e) Ru/CF-H.

FESEM Observation. Figure 6.4 showed FESEM images of Ru/AF-H, RuCMF, RuCMFN, Ru/CNT-H, Ru/CF-H, and 5RuC. The template alumina fiber (AF) in Figure 6.4a were made of uniformly sized microfibers with the width of less than 0.5 μm and length of about 5-10 μm. Samples RuCMF and RuCMFN templated from AF (Figure 6.4b, c) preserved morphology similar to that of AF, indicating they were replicated from the hard templates. The multi-walled carbon nanotubes were homogeneous with diameter about 20 nm and length up to several micrometers (Figure 6.4d). The surface roughness was due to the platinum coating not Ru nanoparticles. The carbon microfiber consisted of bundles of fibers with width about 10 μm and

length of about dozens micrometers (Figure 6.4e). The commercial catalyst 5RuC was made of random sized sheets (Figure 6.4f).

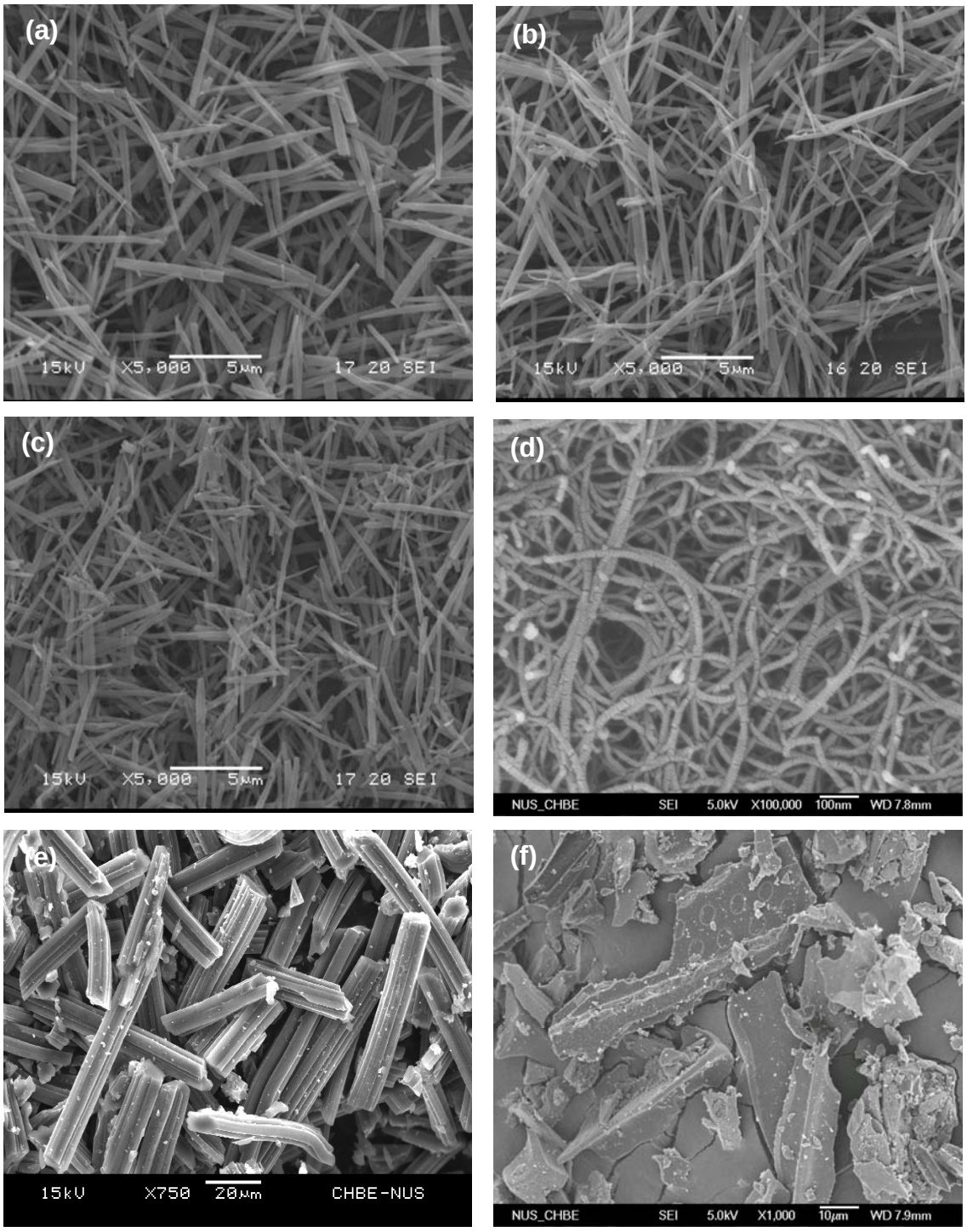

Figure 6.4 FESEM images of catalysts: (a) Ru/AF-H, (b) RuCMF, (c) RuCMFN, (d) Ru/CNT-H, (e) Ru/CF-H, and (f) 5RuC.

TEM Observation. The metallic dispersions and the average metal particle sizes of the Ru catalysts were determined from CO chemisorption and TEM images. The TEM images of RuCMF, RuCMFN, Ru/AF-H, Ru/CF-H, and Ru/CNT-H, were depicted in Figure 6.5. The dark dots seen on the grey carbon background were due to the Ru metal nanoparticles. As shown in Figure 6.5a and 6.5c, the Ru nanoparticles were uniformly dispersed within the carbon framework of catalysts RuCMF and RuCMFN. The Ru nanoparticles had a narrow size distribution that ranges from 3 to 5 nm, comparable to that of the pore size of porous AF. The presence of few large Ru particles was due to the formation of Ru particles on the external surface of the porous hard templates during the impregnation step, which were subsequently buried by the deposition carbon layers on the external surface of the hard template. The introduction of nitrogen into the carbon structure seemed to have almost no influence on the Ru phase dispersion and particle size. Figure 6.5b and 6.5d showed the TEM images of a single Ru nanocrystal with a diameter of around 5 nm taken from catalyst RuCMF and RuCMFN. Aligned crystal lattices with an average spacing of about 0.21 nm were corresponding to the (101) plane of Ru (Hansen et al., 2001). The TEM image of Ru/AF-H (Figure 6.5e) displayed the disordered wormlike mesopore structure of AF. However, no Ru particles could be seen on Ru/AF-H, which is in accordance to the XRD results. Ru nanoparticles were dispersed on the external surface of CF and CNT (highlighted with arrows) in Figure 6.5f and 6.5h. Moderate aggregation of Ru nanoparticles was also observed for Ru/CNF-H catalyst.

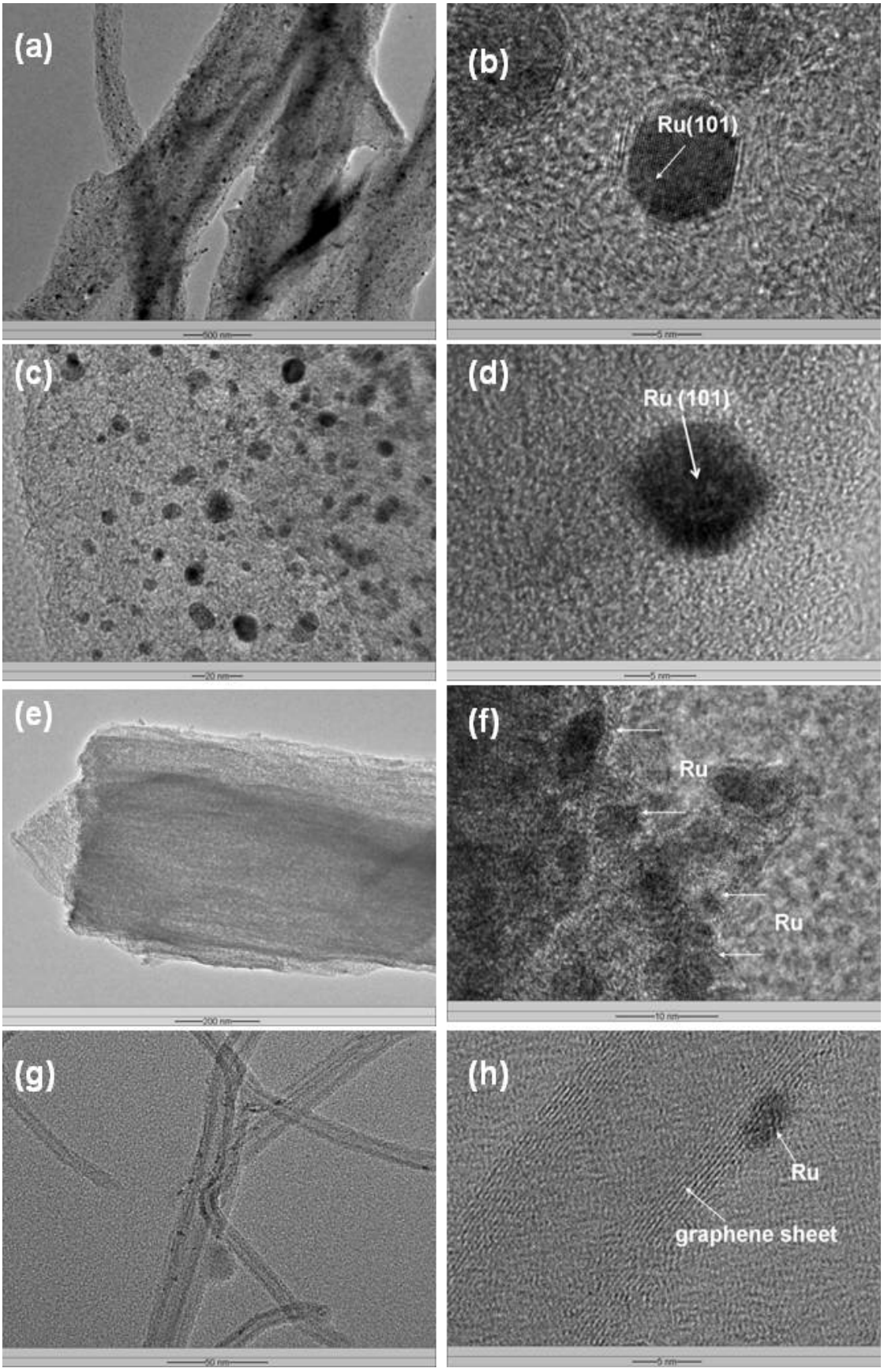

Figure 6.5 TEM images of catalysts: (a, b) RuCMF, (c, d) RuCMFN, (e) Ru/AF-H, (f) Ru/CF-H, (g, h) Ru/CNT-H.

CO Chemisorption. CO uptake was determined by titration method and dispersion values obtained using a stoichiometric ration Ru:CO of 1:1. CO pulse titration peaks of samples were shown in Figure 6.6, and the results obtained were summarized in Table 6.2.

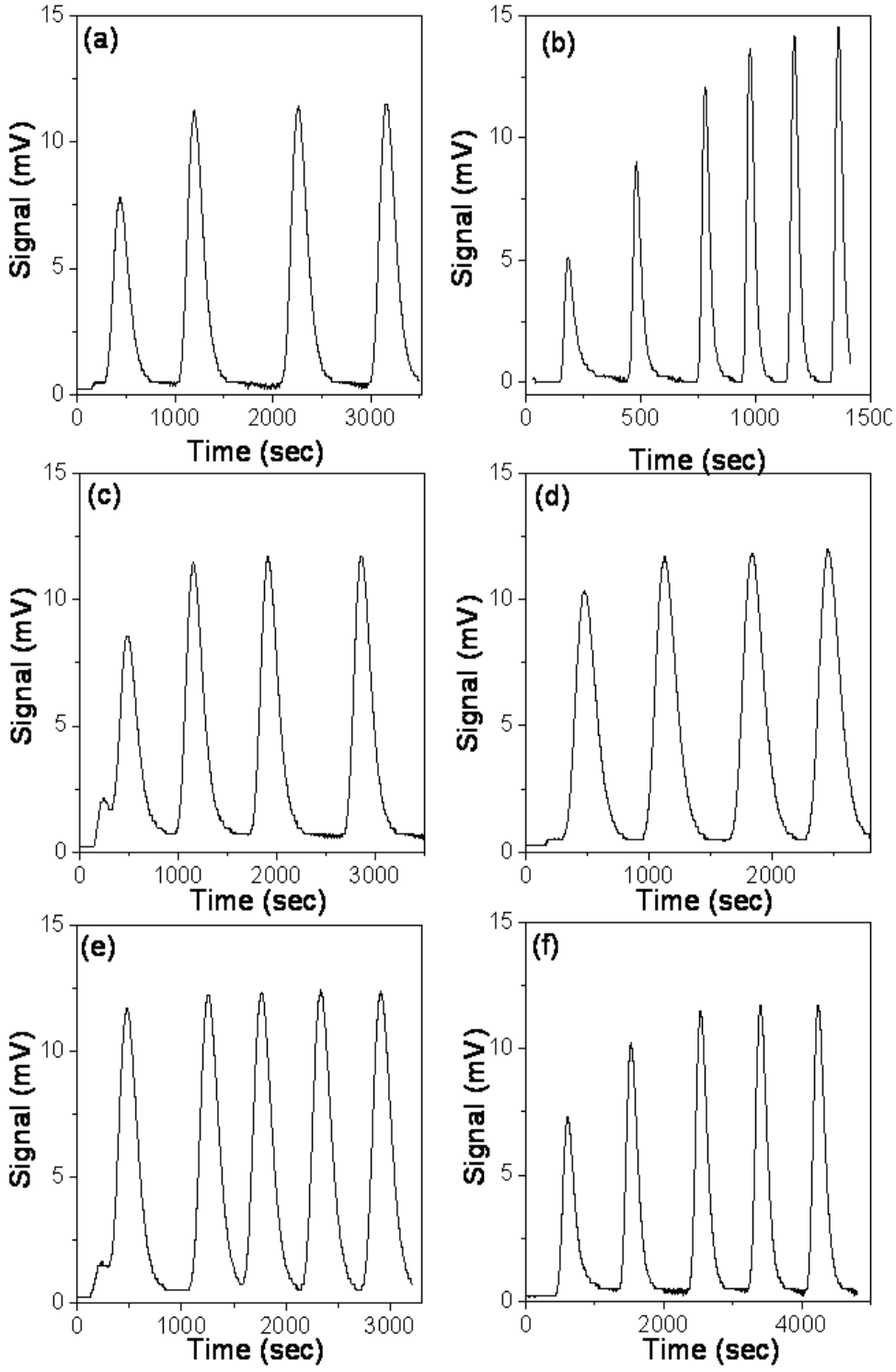

Figure 6.6 CO pulse titration peaks of (a) RuCMF, (b) RuCMFN, (c) Ru/AF-H, (d) Ru/CNT-H, (e) Ru/CF-H, (f) 5RuC.

According to CO chemisorption uptake, the average metallic particle size of RuCMF and RuCMFN were around 3.5 nm, consistent with the TEM observations. Ru/AF-H presented the highest Ru dispersion among the catalysts. This good dispersion could be attributed to the presence of internal abundant pores and the terminal functional group of AF, which facilitated the contact between the $RuCl_3$ precursor solution and the support surface resulting high Ru dispersion and loading. While, as-produced CNT and CF does not possess an high amount of functional groups on their surface and mainly surface defects can be considered as anchoring sites for metals. Therefore, the Ru dispersion and loading were low for these two samples.

Table 6.2 Metallic dispersions and average particle sizes of Ru catalysts calculated from CO chemisorption.

Catalyst	RuCMF	RuCMFN	Ru/AF-H	Ru/CNT-H	Ru/CF-H	5RuC
wt% Ru	6.4	6.3	5.2	3.2	4.3	5
D (%)	12.9	12.8	47	11	12	18.1
d (nm)	3.5	3.5	0.9	4.1	3.7	2.5

XPS Analysis. Figure 6.7a and b showed survey scan XPS spectrum of RuCMF and RuCMFN. No peaks from Ru 3p were observed, implying no Ru nanoparticles on the external surface of catalysts. As expected, sample RuCMF obtained from benzene precursor did not produce any measurable nitrogen-associated signal. The surface of catalyst RuCMF contained carbon and small amount of oxygen. The existence of oxygen may arise from the replication process which involves contact with various oxygen containing reagents (alumina template and aqueous acid). The surface of the catalyst RuCMFN contained carbon, nitrogen and small amount oxygen. The nitrogen content determined from XPS analysis was about 7.5wt%, while the bulk nitrogen content (determined by EDX analysis) was around 7.0wt%. The slightly lower value

of the bulk nitrogen content was due to the inclusion of Ru mass. Therefore, the N was almost uniformly distributed throughout the sample RuCMFN in both the external surface and within the bulk. Figure 6.7c and d showed the XPS spectra of sample RuCMF and RuCMFN for C 1s electronic state. The C 1s spectrum of RuCMF consisted of three components labeled C_1 (284.5eV, 82.8% area), C_2 (285.9eV, 11.3% area), and C_3 (290eV, 5.9% area). Strong C_1 peak indicates that carbon is mostly in the form of graphite (Shalagina et al., 2007). Furthermore, a small broad band C_3 is assigned to the "shake-up" π-π^* satellite, which is common feature in XPS spectra of graphitic carbon (Barr and Yin, 1992). The C_2 peak corresponds to the amorphous carbon (Li et al., 2006). The C_1, C_2, and C_3 peaks were also observed in the C 1s spectrum of RuCMFN. In addition, a new C_* peak appeared at 287.5 eV. This peak corresponds to sp^2 carbon atoms bonded to nitrogen atoms (Ghosh et al., 2010). After deconvolution of the N 1s peak of RuCMFN (Figure 6.7e), the peak could be assigned to the pyridinic nitrogen (398eV, 12.8% area), to quaternary nitrogen (400.6eV, 69.7% area), and to the adsorbed nitrogen, nitrogen oxides or to a π- π^* shake-up satellite peak (402.5 eV, 17.5% area) (Amadou et al., 2008; Nieto-Márquez et al., 2010). Peak of quaternary nitrogen showed the highest proportion among the deconvoluted peaks.

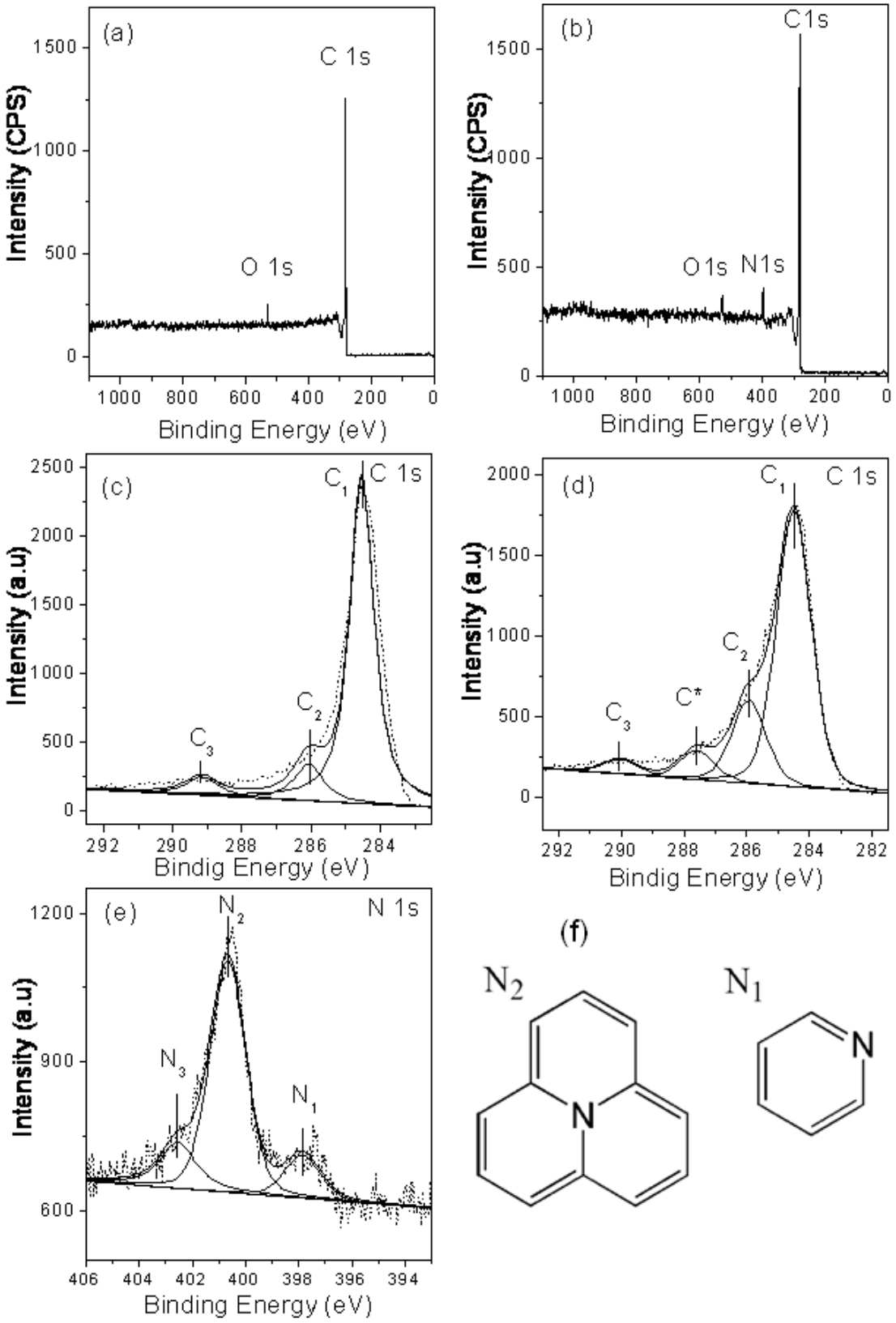

Figure 6.7 The XPS survey spectrum of (a) RuCMF, (b) RuCMFN, the C 1s XPS spectrum of (c) RuCMF, (d) RuCMFN, (e) N 1s XPS spectrum of RuCMFN, and (f) types of nitrogen functionalities.

FTIR Analysis. The surface chemical-bonding state of samples RuCMF and RuCMFN were also characterized by FTIR spectroscopy (Figure 6.8). Catalyst RuCMFN showed three major broad bands centered around 1235, 1587, and 3420 cm^{-1}. The bands at 1235 cm^{-1} and 1587 cm^{-1} are assigned to aromatic C-N stretching bonds and aromatic ring modes, respectively, while the low intensity peaks between 3500 and 3000 cm^{-1} are assigned to N-H stretches (Vinu et al., 2005; Vinu, 2008). All the results from our XPS and FT-IR suggest that the nitrogen was doped in the catalyst RuCMFN.

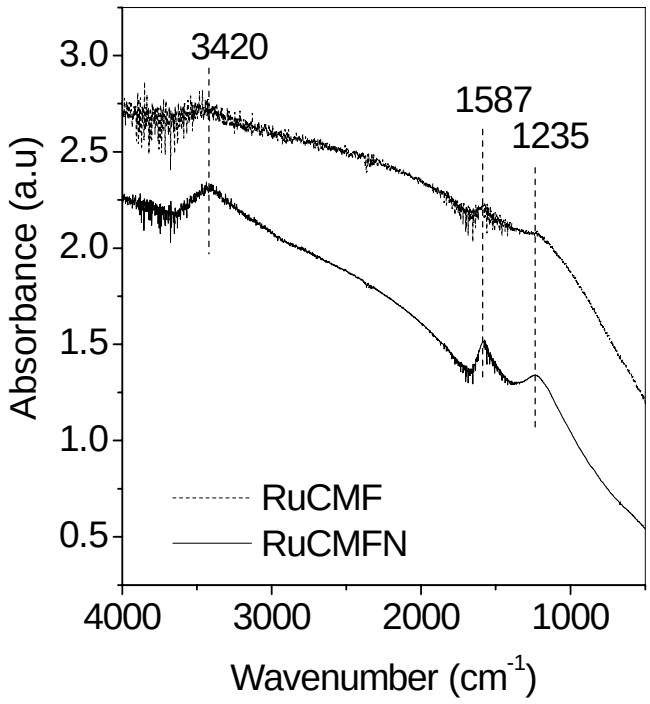

Figure 6.8 FTIR spectra of the RuCMF and RuCMFN.

6.3 Catalytic properties

The catalytic activities of the catalysts together with the commercial catalyst were summarized in Figure 6.9. The activity of these catalysts decreased in the order RuCMFN>RuCMF>5RuC>Ru/AF-H>Ru/CNT-H>Ru/CF-H. Both RuCMFN and RuCMF catalysts showed a remarkably higher catalytic activity than the Ru catalysts prepared using the hydrogen reduction method and commercial catalyst. After the first

reaction run, catalysts RuCMF and RuCMFN were washed with deionized water, dried at 120 ^{o}C in air, and reused without further treatment. No lost in catalytic activity was observed. In addition, long-term storage (1 year) under ambient conditions did not lead to obvious deterioration in catalytic performance. Furthermore, the much lower Ru concentration of RuCMF and RuCMFN in water after 2 h ultrasonication demonstrated their negligible leaching compared with other Ru catalysts. Therefore, the Ru catalysts prepared in this work are highly stable and reusable.

Several factors could account for the observed high catalytic activity and stability for the RuCMF and RuCMFN catalysts, such as 1-D morphology, the unblocked mesopores of the catalysts, and the unique contact between the Ru nanoparticles and carbon support. First, the 1-D morphology and interconnected mesoporous ruthenium/carbon system of RuCMF and RuCMFN allow the easy diffusion of both the reactants and products and highly dispersed Ru nanoparticles offer more catalytically active sites for the reactants. The lower catalytic activity of the commercial catalyst 5RuC comes from the presence of microporosity in the activated carbon, which may cause diffusion limitations (Kusserow et al., 2003). Secondly, template method created a highly intimate contact between the Ru nanoparticles and the carbon support because of the carbon deposition on the Ru surface via CVD. Such intimate contact may also favour hydrogen spillover (Wang and Yang, 2008). Hydrogen can adsorb disssociatively on the exposed Ru surface to form atomic H species, followed by spillover throughout the carbon support. The spillover hydrogen from Ru can make carbon active for hydrogenation of D-glucose, resulting in the observed high catalytic activity. The lower catalytic activities of Ru/AF-H and Ru/CNT-H than that of the commercial one could be attributed to the low specific surface area of the supports and the presence of residual chloride species. The EDX

analysis results confirmed the residence of chloride, and it seems difficult to remove the residual chloride species during low temperature hydrogen reduction (Wu et al., 1992). The small pore size of Ru/CF-H could restrict the diffusion of reactants, resulting lowest catalytic activity among the catalysts.

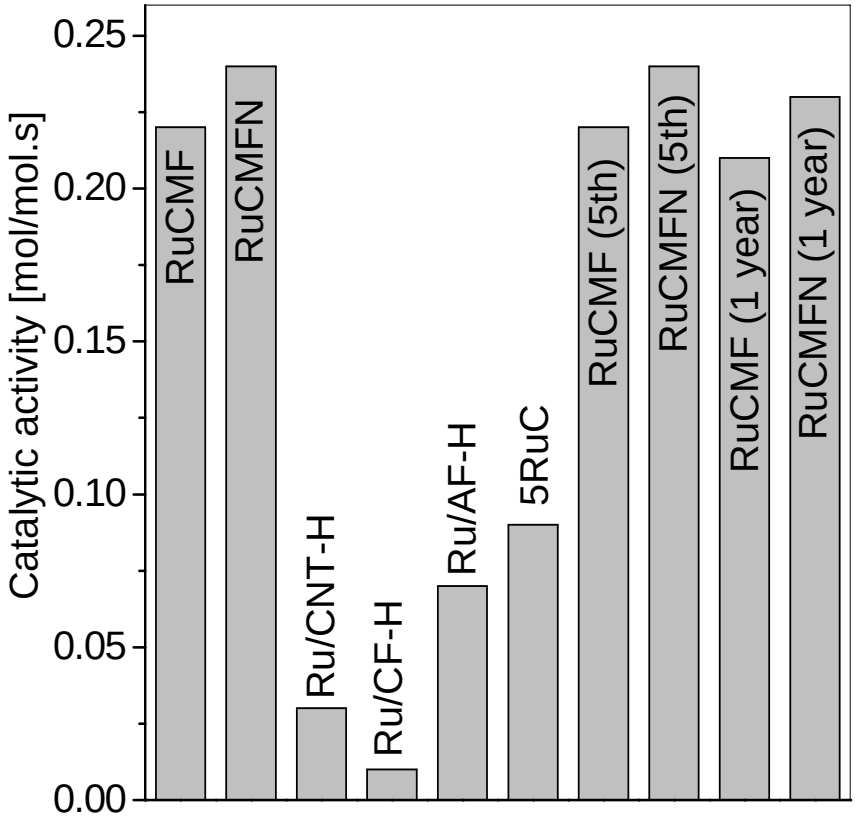

Figure 6.9 Catalytic activities of the catalysts.

Since the Ru nanoparticles size, distribution and the pore structure of the RuCMF and RuCMFN were comparable, the higher catalytic activity for the RuCMFN than that of RuCMF could attribute to the presence of nitrogen (preferentially in the quaternary form). The incorporation of nitrogen could enhance hydrogen adsorption, improve the wettability of carbon supports, and modify electronic properties of Ru. First, H_2 chemisorption results showed that the H_2 monolayer uptake volume of RuCMFN (80.76 μmole/g_{Ru}) was almost twice as that of RuCMF (44.93 μmole/g_{Ru}) (shown in Figure 6.10). Since the effect of any variations in the Ru active site and the

pore structure of carbon supports can be ruled out, the higher hydrogen uptake of RuCMFN could be attributed to the nitrogen incorporation. It was reported that N doping is more favourable for hydrogen adsorption via spillover than that on pure carbons (Wang et al., 2009; Wang and Yang, 2009; Xia et al., 2009; Sadek et al., 2010).

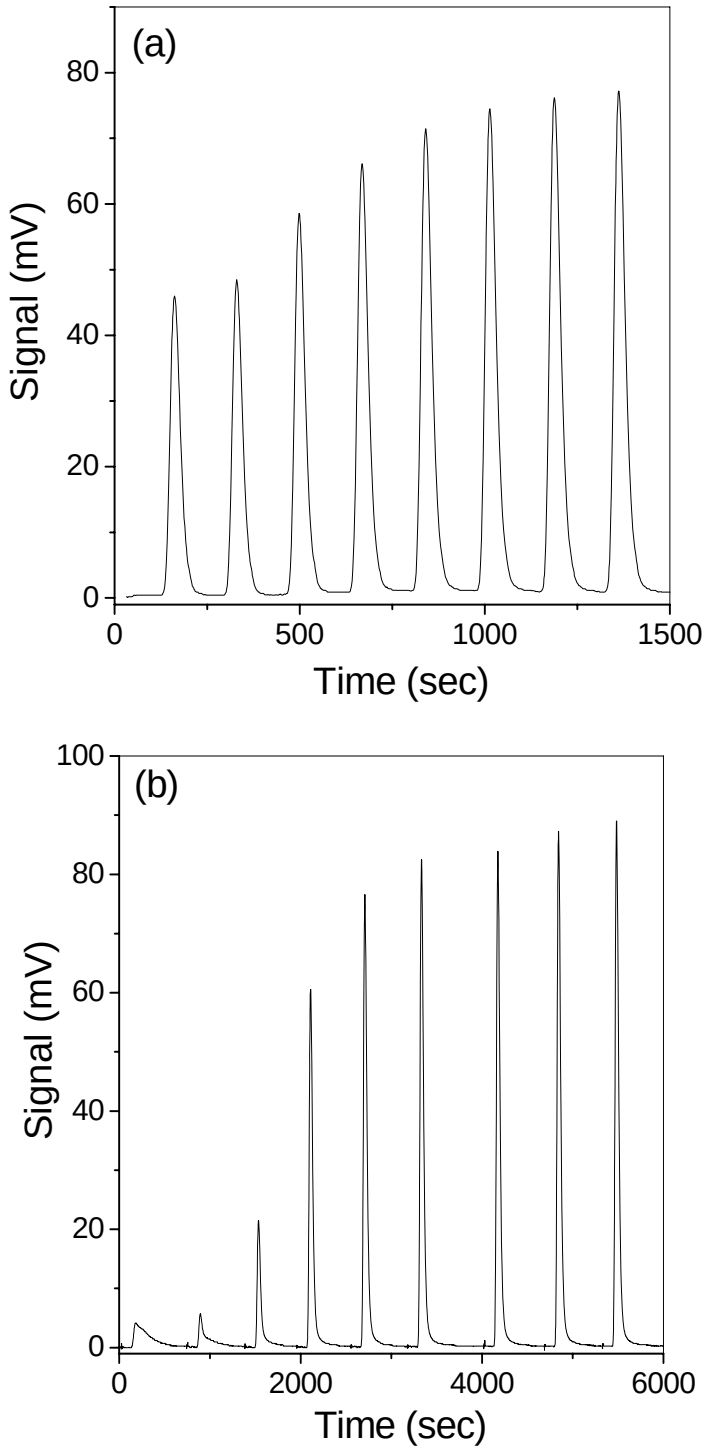

Figure 6.10 H_2 pulse titration peaks for (a) RuCMF and (b) RuCMFN.

Moreover, the presence of N atoms substituted on the carbon surface, especially quaternary nitrogen, improved the carbon wettability (Matsuoka et al., 2004; Hou et al., 2005). This could facilitate the transfer of D-glucose; hence improved the catalytic activity. Therefore, the doped nitrogen atoms could act as a promoter of Ru nanoparticles increasing their activities in the D-glucose hydrogenation.

6.4 Summary

In summary, 1-D mesoporous carbon microfiber supported Ru catalysts were prepared by using alumina microfibers as the templates via CVD method. The obtained catalysts possessed a mesoporous structure with a surface area above 650 m^2/g, average pore size of 3.7 nm, length of 5-10 μm, and width of about 0.5 μm. Small Ru nanoparticles with a narrow size distribution (3-5 nm) were homogeneously dispersed in the interconnected mesoporous carbon matrix. Compared with Ru deposited on multi-walled carbon nanotubes, carbon fibers, alumina microfibers, and the activated charcoals, the mesoporous carbon microfiber supported Ru catalysts displayed remarkably higher catalytic activity and better stability in the hydrogenation of D-glucose. The excellent catalytic performances of the catalysts are attributed to their unique 1-D morphology, the unblocked mesoporous structure, and the hydrogen spillover effect enhanced by the unique surface contact between the Ru nanoparticles and the carbon supports. In addition, the incorporation of nitrogen significantly improved the catalytic performance due to the enhanced hydrogen adsorption and better wettability.

Table 6.3 the main characteristic of RuCMF and RuCMFN.

Catalysts	wt% Ru	A (m^2/g)	V (cm^3/g)	d (nm)	D (%)	d (Ru, nm)
RuCMF	6.4	760	1.10	3.7	12.9	3.5
RuCMFN	6.3	790	0.71	3.7	12.8	3.5

CHAPTER 7

Kinetics of the catalytic hydrogenation of D-glucose over bimetallic Ru-Cu carbon catalyst

7.1 Introduction

A common method to obtain the information about reaction mechanism is to study the kinetics of the reaction. Hydrogenation kinetics of D-glucose has been studied over Ru/C (Crezee et al., 2003), Ru/Al_2O_3 (Bizhanov and Drozdova, 1982), silica-alumina supported Ni catalysts (Dechamp et al., 1995) and Raney Ni catalyst (Brahme and Doraiswamy, 1976). Usually a Langmuir-Hinshelwood mechanism is a good approximation for the kinetics. In aqueous solution D-glucose cyclize to produce six-membered rings (pyranoses), which are much more stable than their open chain counterparts. Depending on the position of the OH group at the C_1 atom, there are two stereochemical species (anomers) for a pyranose. The anomers are termed α- and β-pyranose when the OH group at C_1 is below or above the ring plane of the Haworth formula, respectively (Ma et al., 1998) (Figure 7.1). These forms will have different adsorption constants and their own characteristic rates of hydrogenation. These factors will determine which form is preferentially adsorbed and hydrogenated. Molecular models indicate that the adsorption of the β-pyranose form will more favorable through the coordination of O-1, O-5, and O-6 (Makkee et al., 1985). By adsorption the anomeric carbon becomes more susceptible to attack by hydrides (Castoldi et al., 2007).

Here we present experimental D-glucose hydrogenation over RuCu0.5C catalyst in a batch three-phase reactor and kinetic modeling based on Langmuir-Hinshelwood-Hougen-Watson (LHHW) type kinetics.

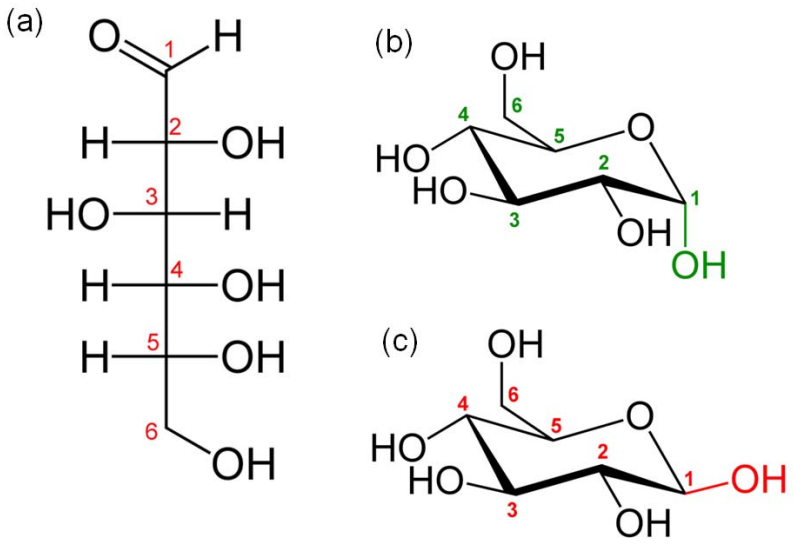

Figure 7.1 (a) the Fischer projection of the chain form of D-glucose, (b) α-D-glucopyranose, and (c) β-D-glucopyranose. (From http://en.wikipedia.org/wiki/Glucose).

7.2 Kinetics of the hydrogenation of D-glucose

The D-glucose hydrogenation experiments were carried out batchwise in a Parr Reactor (Parr 4560) operating at 4-10 MPa and between 90 and 120 ^{o}C. The effect of stirring rate was studied in the beginning of the work, in order to eliminate the mass transfer limitation. The affection on initial reaction rate by changing the stirrer speed from 300 rpm to 1500 rpm was shown in Figure 7.2a. The stirring speed was fixed at 1000 rpm for the experiments to ensure that the gas-liquid mass transfer does not affect the reaction rate. Aqueous solutions contained about 20-50 wt% glucose initially. The liquid volume was 30 ml and the amount of catalyst RuCu0.5C was 0.05 g. The average catalyst particle length is 15μm. The initial rate r_0 was obtained by recording the drop of H_2 pressure with time, which was then transferred into the hydrogen uptake rate per square meter of Ru (mol·min^{-1}·m^{-2}) according to the ideal gas equation and the active surface area (calculated by H_2 chemisorption). The influence of the catalyst loading was evaluated by varying the catalyst-to-glucose ratio in D-glucose hydrogenation experiments at 100 ^{o}C and 8MPa. The initial reaction rate showed a

linear dependency on the catalyst load between 0.03 and 0.1 g, i.e. the normalized activity was independent of the catalyst loading, indicating that in the range of operating variables the systems is not controlled by gas-liqiuid mass transport (Figure 7.2b). Nevertheless, a further increase of the catalyst loading did not give a full benefit.

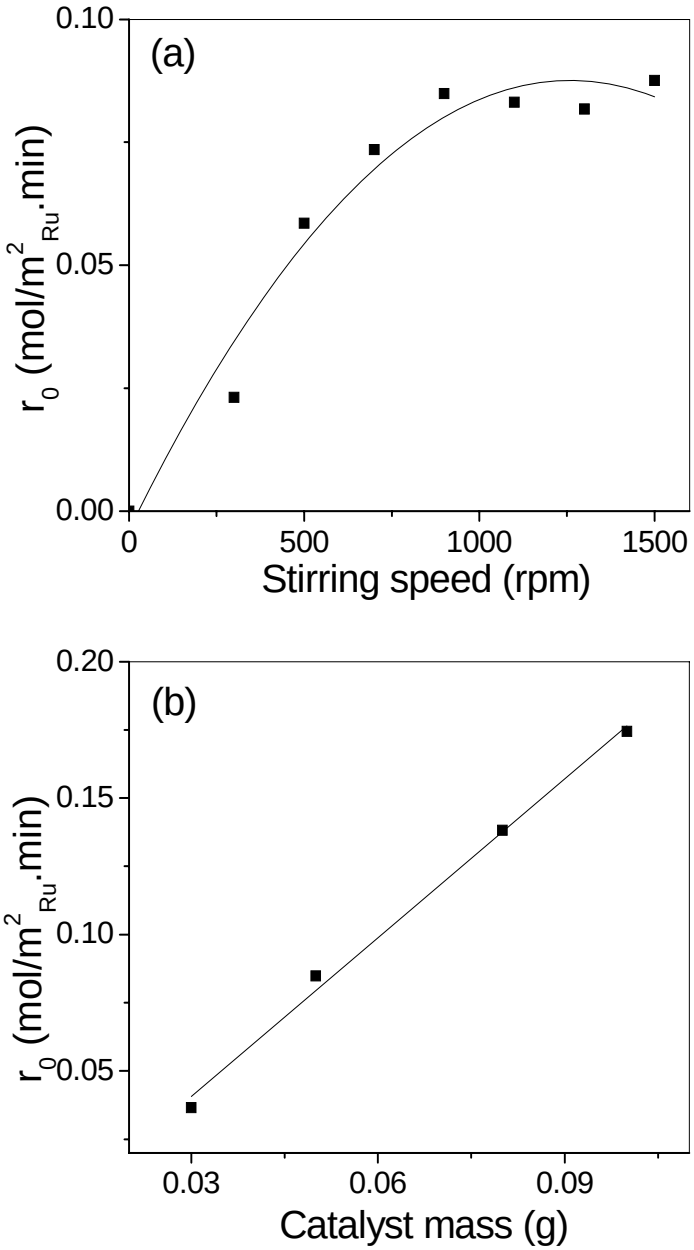

Figure 7.2 (a) Effect of the stirring speed on the initial reaction rate at 100 ^{o}C and 8MPa, (b) The influence of catalyst loading on the initial reaction rate at 100 ^{o}C and 8MPa.

From the experiments carried out at the temperature range at 90-120 ^{o}C and at pressure 4-10 MPa, it was found that the apparent activation energy for D-glucose

hydrogenation over RuCu0.5C was 49.7-66.4 kJ/mol (Figure 7.3). The estimated activation energies were much larger than the activation energy of diffusion in liquids (12-21 kJ/mol) (Dechamp et al., 1995), thus indicating that the experiments were performed under kinetics control.

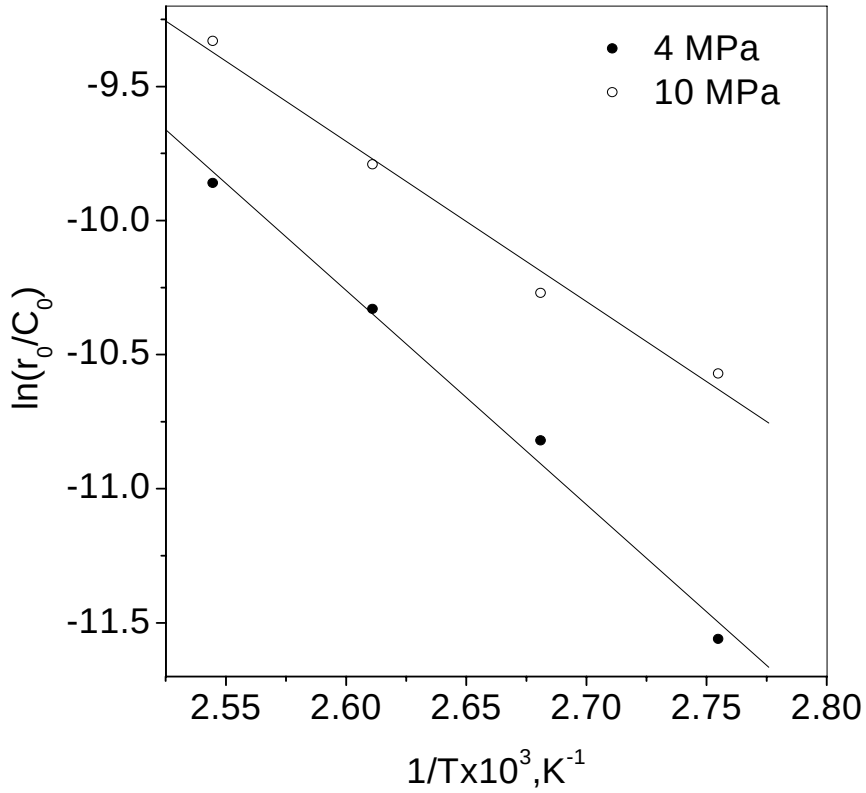

Figure 7.3 Arrhenius plots of the initial glucose (40wt% in water) hydrogenation rates carried out at 4 MPa (E_a=66.4 kJ/mol) and 10 MPa (E_a=49.7 kJ/mol) and at the temperature range 90-120 ^{o}C.

The dependency of initial reaction rate on initial D-glucose concentration at 100 ^{o}C was plotted in Figure 7.4a. This figure would well agree with a classical Langmuir-Hinshelwood model, in which the products and the solvent are not involved in the rate expression:

$$r_0 = \frac{kK_G C_{G0}}{1 + K_G C_{G0}} \tag{7.1}$$

At low D-glucose concentration (< 40 wt%), apparent first order kinetics was observed. At high D-glucose concentration (≥ 40 wt%), saturation of the catalyst surface occurred and zero order was observed.

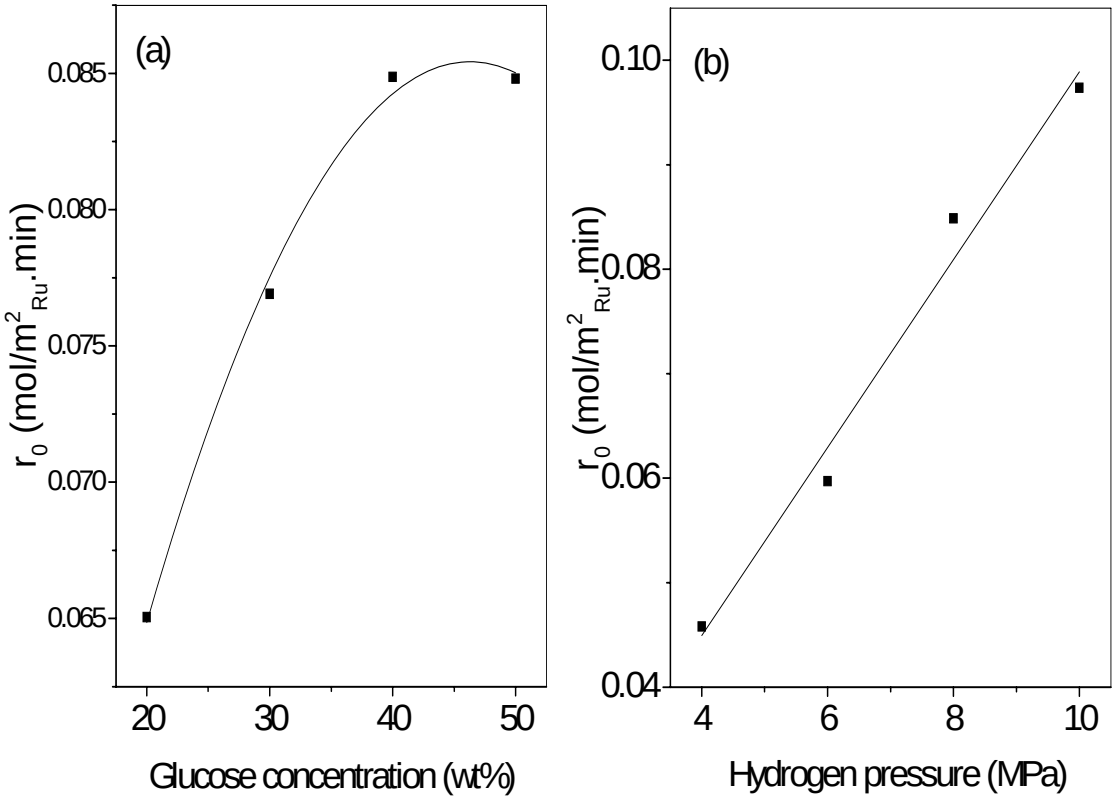

Figure 7.4 (a) D-glucose concentration dependency of the initial hydrogenation rate at 100 ^{o}C, 0.05g catalyst, 8 MPa; (b) initial D-glucose hydrogenation rate as a function of hydrogen pressure at 100 ^{o}C, C_{G0}=40wt%, 0.05 g catalyst.

An increased hydrogen pressure had a positive effect on the initial reaction rate, showing first order behavior at 100 ^{o}C (Figure 7.4b). The kinetic behavior in Figure 7.4b could be understood by considering the difference in the adsorption strength between D-glucose and hydrogen on RuCu0.5C catalysts. As the D-glucose molecule was strongly adsorbed, it reached to saturated adsorption rapidly. Thus, the change in the D-glucose concentration in the liquid phase did not change its adsorption amount on the catalyst and thus, did not affect the rate of the surface hydrogenation. The adsorption of hydrogen on RuCu0.5C was relatively weak and could not reach

saturated adsorption under the present reaction conditions. Therefore, the initial rate exhibited first-order with respect to hydrogen pressure.

7.3 Modeling results of kinetics and mechanism

Based on preliminary kinetics analysis, some simplifications can be made: i) during reaction no catalyst deactivation occurred; ii) the reaction is 100% selective to D-sorbitol; iii) there is negligible adsorption of solvent and D-sorbitol; iv) the adsorption and desorption steps are assumed to be rapid, whereas the hydrogenation steps on the surface are presumed to be rate controlling; v) the hydrogenation steps are regarded as irreversible; vi) hydrogen adsorption was assumed to be dissociative, but hydrogen atoms were supposed to be added pairwise to the organic species.

As a summary, the complete set of plausible surface steps is presented below:

$H_2 + 2^* \leftrightarrow 2\,(H^*)$

$G + {}^* \leftrightarrow G^*$

$G^* + 2\,(H^*) \rightarrow S + 3^*$

It has previously been proposed that sugar hydrogenation follow a competitive adsorption model, where adsorbed atomic hydrogen is added pairwise to adsorbed organics. However, because of the larger size of difference between sugar molecules and hydrogen, another non-competitive adsorption model was assumed, where hydrogen and D-glucose adsorbed at different sites (Mikkola et al., 1999; Crezee et al., 2003; Kuusisto et al., 2008). As a result, two models based on Langmuir-Hinshelwood-Hougen-Watson (LHHW) were used. Model 1: non-competitive adsorption of dissociatively chemisorbed hydrogen and D-glucose at different sites, see Eq. (7.2); Model 2: competitive adsorption of dissociatively chemisorbed hydrogen and D-glucose, see Eq. (7.3).

$$r = \frac{k_r K_G C_G K_H P_{H_2}}{1 + K_G C_G} \tag{7.2}$$

$$r = \frac{k_r K_G C_G K_H P_{H_2}}{\left(1 + K_G C_G\right)^3} \tag{7.3}$$

The temperature dependencies of k_r, K_G and K_H are:

$$k_r = k_0 \exp\left(\frac{-E_a}{RT}\right) \tag{7.4}$$

$$K_G = \exp\left(\frac{-\Delta H_G}{RT} + \frac{\Delta S_G}{R}\right) \tag{7.5}$$

$$K_H = \exp\left(\frac{-\Delta H_H}{RT} + \frac{\Delta S_H}{R}\right) \tag{7.6}$$

Since k_r and K_H only appear as a product in the rate expressions, it was expressed as $k_r K_H$.

$$k_r K_H = k_0 \exp\left(\frac{\Delta S_H}{R}\right) \exp\left(\frac{-\left(E_a + \Delta H_H\right)}{RT}\right) \tag{7.7}$$

The experiments performed at 100 ^{o}C were used to obtain the parameters $k_r K_H$ and K_G at this temperature. The fit of the experimental data to the kinetic model was carried out by Matlab software by fminsearch method (generally referred to as unconstrained nonlinear optimization). The results of parameter estimation are summarized in Table 7.1. Figure 7.5 illustrates that the Model 2 nicely described the behavior of the system.

Table 7.1 Comparison of the fitted parameters for D-glucose hydrogenation over RuCu0.5C catalyst.

	Model 1	Model 2
$k_r K_H$ (mol/(min·m$^2_{Ru}$·MPa))	0.0137	0.0722
K_G (l/mol)	1.1398	0.1427
Sum of squares of residuals (SSR)	5.7665×10^{-4}	4.8929×10^{-4}

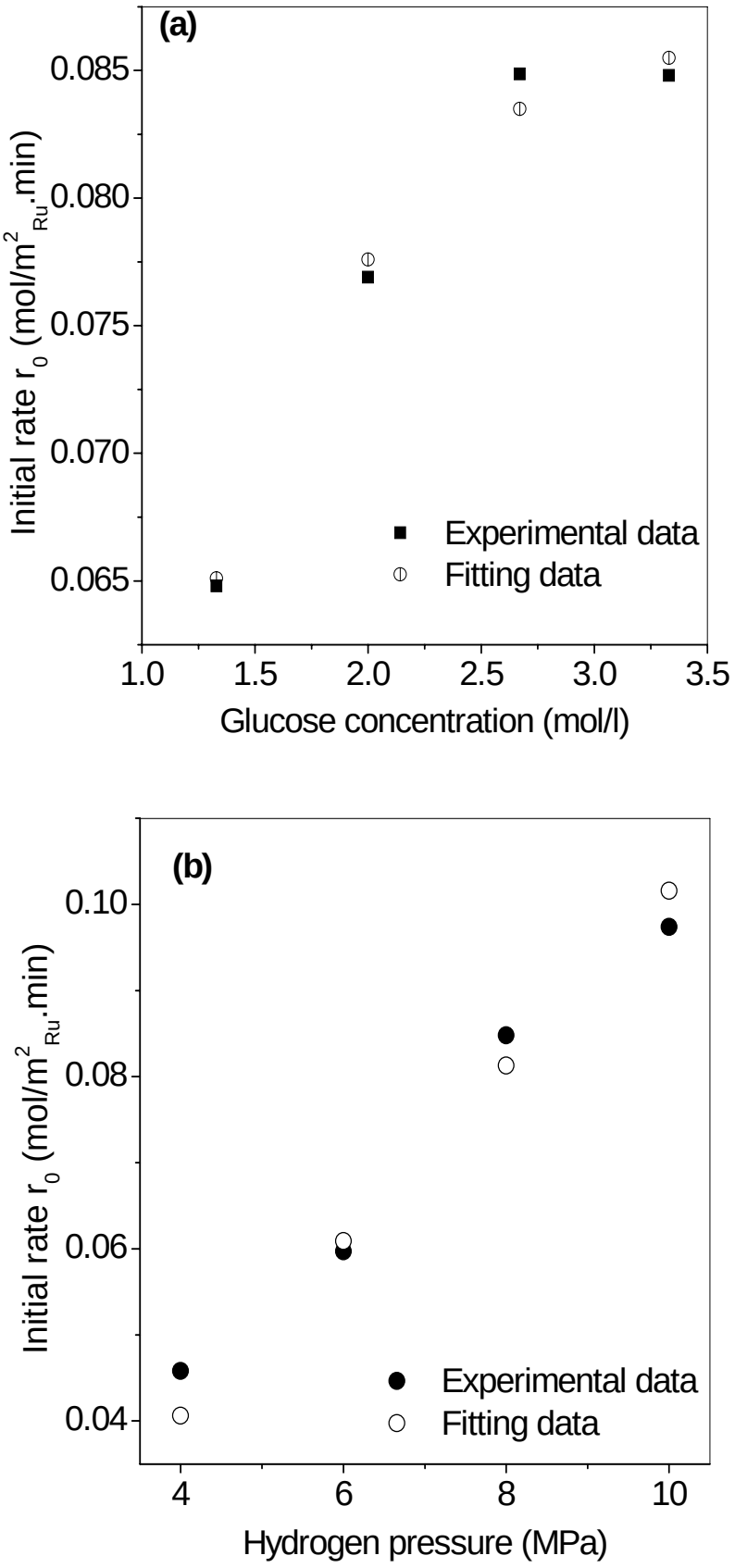

Figure 7.5 Fit of kinetic model 2 to experimental data for hydrogenation of D-glucose over RuCu0.5C.

Therefore, based on the literature review (Crezee et al., 2003) and the kinetic data, we proposed that the hydrogenation of D-glucose over RuCuC involves the formation of an ionized glucose species adsorbed on the Ru or Cu surface by coordination of O-1, O-2, and O-5, which was then polarized, and attacked by a hydride-like species from the Ru surface or the spillover hydrogen atom from Ru to Cu (see Figure 7.6). The adsorptions of dissociatively chemisorbed hydrogen and D-glucose are competitive.

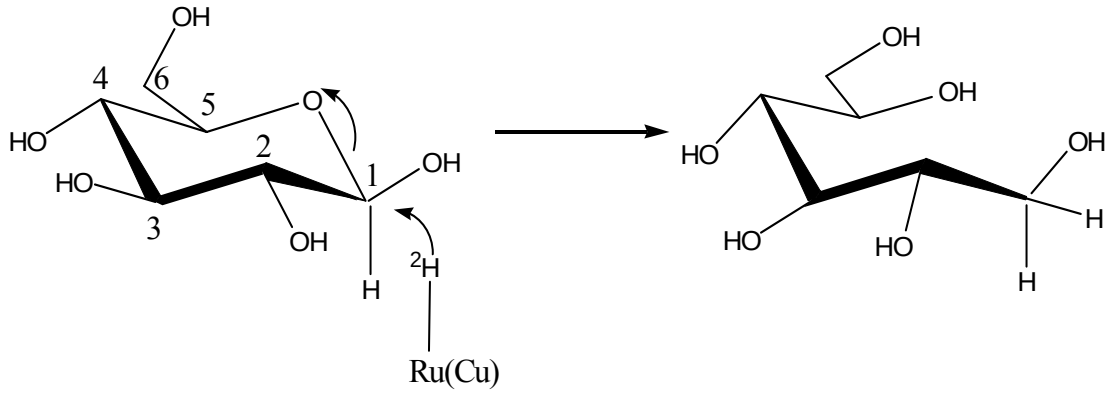

Figure 7.6 Schematic representation of the reaction mechanism between adsorbed β-D-glucopyranose and hydrogen.

7.4 Summary

The kinetics of D-glucose hydrogenation to D-sorbitol over RuCuC catalyst in aqueous solutions was studied in batch-wise Parr reactor operating at 90-120 ^{o}C and 4.0-10.0 MPa hydrogen pressure. The D-glucose concentration was varied between 20 and 50wt%. The kinetics experiments were carried out in the absence of mass transport limitations. In the operating regime the reaction rate showed a first order dependency with respect to hydrogen, and a shift in the order of D-glucose. At low D-glucose concentrations (up to 40wt%) the reaction showed a first order dependency, while at higher concentrations this changed to zero order behavior. The kinetic data were modeled using two rate models based on LHHW kinetic assuming that the surface

reaction is rate-determining. Model 1 involves non-competitive adsorption of hydrogen and D-glucose; Model 2 is based on competitive adsorption dissociatively chemisorbed hydrogen and D-glucose. The parameter estimation was performed for 100 ^{o}C, and the results indicated that the Model 2 fits the experimental data better. It is proposed that the hydrogenation of D-glucose involves the formation of an ionized β-pyranose species adsorbed on the Ru or Cu surface by coordination of O-1, O-5, and O-6, which is susceptible to attack by hydrogen at the anomeric carbon.

CHAPTER 8

CONCLUSIONS AND RECOMMENDATIONS

8.1 Conclusions

Ruthenium nanoparticles embedded in the pore walls of template carbon (RuC) were prepared by using H-form zeolite Y and mesoporous silica SBA-15 as template. Compared with other catalysts, the RuC catalyst displayed a higher catalytic activity and stability in hydrogenation of D-glucose because of the enhanced contact between the Ru nanoparticles and carbon matrix. Such a unique contact between Ru nanoparticles and carbon support may stimulate the hybridization of pz orbital of graphene (π-bonded states) and the d orbital of Ru, resulting in less oxidation of Ru metal particles and hydrogen spillover. Also it was found that the mesoporous pore structure was better than the microporous pore structure. This may account for the small pore size inhibit the mass transfer of the reactant and the product. This synthesis provides a feasible solution to prevent the metal particles leaching, and to control the particle sizes.

Bimetallic Ru-Cu nanoparticles embedded in the pore walls of mesoporous carbon were prepared. The presence of bimetallic entities was supported by the characterization data of both Ru L_{III} edge and Cu K-edge X-ray absorption. For the unique property of template method, the addition of Cu did no affect the particle size or the dispersion of Ru. Overall the bimetallic catalyst showed a higher catalytic activity than single-metal catalysts (RuC and CuC) in hydrogenation of D-glucose. At low Cu/Ru ratios (<1.0), additional activity sites for D-glucose hydrogenation may have been created by Cu addition. At high Cu/Ru ratios (>1.0), the presence of Cu decreased the catalytic activity. This effect may be due to the complete preferential

population of defect-like edge and corner of Ru sites by Cu, subsequently limiting the dissociation of hydrogen on the metal surface, which is necessary for D-glucose hydrogenation.

Alumina microfibers were used as templates to prepare Ru nanoparticles embedded in mesoporous carbon fibers. Small Ru nanoparticles with a narrow size distribution (3-5nm) were homogeneously dispersed in the interconnected mesoporous carbon matrix. Compared with other Ru nanoparticles supported on other carbon materials (e.g., multi-walled carbon nanotubes, carbon fibers, alumina microfibers, and the activated charcoals), the Ru catalysts prepared using the template method displayed higher catalytic activity and a better stability, again attributed to the features of unblocked mesopores, hydrogen spillover, and unique surface contact between the Ru nanoparticles and the carbon supports catalysts. In addition, the incorporation of nitrogen played a beneficial role in catalytic activity. This improvement was attributed to the enhanced hydrogen adsorption of catalyst, improved carbon wettability, and promoter effect of nitrogen.

The kinetics of D-glucose hydrogenation to D-sorbitol over RuCuC catalyst in aqueous solutions was studied in batch-wise Parr reactor operating at 90-120 ^{o}C and 4.0-10.0 MPa hydrogen pressure. The kinetics experiments were carried out in the absence of mass transport limitations. In the operating regime the reaction rate showed a first order dependency with respect to hydrogen, and a shift in the order of D-glucose. At low D-glucose concentrations (up to 40wt%) the reaction showed a first order dependency, while at higher concentrations this changed to zero order behavior. The kinetic data were modeled using two rate models based on LHHW kinetic assuming that the surface reaction is rate-determining. Model 1 involves non-competitive adsorption of hydrogen and D-glucose; Model 2 is based on competitive adsorption of

dissociatively chemisorbed hydrogen and D-glucose. The parameter estimation was performed for 100 ^{o}C, and the results indicated that the Model 2 fits the experimental data better. It is proposed that the hydrogenation of D-glucose involves the formation of an ionized β-pyranose species adsorbed on the Ru or Cu surface by coordination of O-1, O-5, and O-6, which is susceptible to attack by hydrogen at the anomeric carbon. The adsorption of D-glucose and dissociative hydrogen is competitive.

8.2 Recommendations

It appears that the template synthesis method can improve the control of the metal particle size and composition. This control is effective in studying the effect of the particle size and the pore structure on the catalytic activity. Although the template method is a time-consuming and high-cost procedure, this method has provided a better basic understanding of the carbon support material.

There are several interesting directions for future work in the areas of research described in this thesis. One possible avenue of future work is the extension of the Ru/C catalyst system to the partial hydrogenation of entities, such as aliphatic nitro groups, nitriles, carbonxylic acids and easters, because heterogeneous catalyzed selective hydrogenations are effective reactions for the preparation of a number of synthetically useful compounds.

Another direction of the extension of this work is the use of organic compounds as templates in contrast to the hard templates since the removal using toxic HF solution could be saved. Two groups (Gao et al., 2008; Wan et al., 2009) have demonstrated the possibility of this concept, but detailed study still will be needed. This simple and effective approach may promote the applications in many fields.

REFERENCES

Acosta, D., N. Ramirez, E. Erdmann, H. Destefanis, E. Gonzo. Transition Metals as Dopants on Nickel Borides: Their Catalytic Activity Effect on Hydrogenation Reactions. Catal. Today, *133*, pp.49-55. 2008.

Adkins, H., Connor, R. The Catalytic Hydrogenation of Organic Compounds over Copper Chromite. J. Am. Chem. Soc., *53*, pp. 1091-1095. 1931.

Aidan M. Doyle, S. K. S. S. D. J. H.-J. F. Hydrogenation on Metal Surfaces: Why are Nanoparticles More Active than Single Crystals? Angew. Chem. Int. Ed., *4*2, pp.5240-5243. 2003.

Albertazzi, S., R. Ganzerla, C. Gobbi, M. Lenarda, M. Mandreoli, E. Salatelli, P. Savini, L. Storaro, A. Vaccari. Hydrogenation of Naphthalene on Noble-Metal-Containing Mesoporous MCM-41 Aluminosilicates. J. Mol. Catal. A-Chem, *200*, pp.261-270. 2003.

Alvarez-Rodriguez, J., A. Guerrero-Ruiz, I. Rodriguez-Ramos, A. Arcoya-Martin. Surface and Structural Effects in the Hydrogenation of Citral over RuCu/KL Catalysts. Microporous Mesoporous Mat., *97*, pp.122-131. 2006.

Alvarez-Rodriguez, J., A. Guerrero-Ruiz, I. Rodriguez-Ramos, A. Arcoya. Changes in the Selective Hydrogenation of Citral Induced by Copper Addition to Ru/KL Catalysts. Microporous Mesoporous Mat., *110*, pp.186-196. 2008.

Amadou, J., K. Chizari, M. Houlle, I. Janowska, O. Ersen, D. Begin, C. Pham-Huu. N-doped Carbon Nanotubes for Liquid-phase C=C Bond Hydrogenation. Catal. Today, *138*, pp.62-68. 2008.

An-Hui Lu, Wen-Cui Li, Zhenshan Hou, F. Schuth. Molecular Level Dispersed Pd Clusters in the Carbon Walls of Ordered Mesoporous Carbons as a Highly Selective Alcohol Oxidation Catalyst. Chem. Commun., *10*, pp.1038-1040. 2007.

Arena, B. J. Deactivation of Ruthenium Catalysts in Continuous Glucose Hydrogenation. Appl. Catal. A: Gen., *87*, pp.219-229. 1992.

Asedegbega-Nieto, E., B. Bachiller-Baeza, A. Guerrero-Ruiz, I. Rodriguez-Ramos. Modification of Catalytic Properties over Carbon Supported Ru-Cu and Ni-Cu Bimetallics II. Paracetamol Hydrogenation and N-hexane Conversion. Appl. Catal. A: Gen., *303*, pp.88-95. 2006a.

Asedegbega-Nieto, E., B. Bachiller-Baeza, A. Guerrero-Ruiz, I. Rodriguez-Ramos. Modification of Catalytic Properties over Carbon Supported Ru-Cu and Ni-Cu Bimetallics - I. Functional Selectivities in Citral and Cinnamaldehyde Hydrogenation. Appl. Catal. A: Gen., *300*, pp.120-129. 2006b.

Auer, E., A. Freund, J. Pietsch, T. Tacke. Carbons as Supports for Iindustrial Precious Metal Catalysts. Appl. Catal. A: Gen., *173*, pp.259-271. 1998.

Augustine, R. L. Heterogeneous Catalysis for the Synthetic Chemist. pp. 134-137, Marcel Dekker, Inc. 1996.

Augustine, R. L. Selective Heterogeneously Catalyzed Hydrogenations. Catal. Today, *37*, pp.419-440. 1997.

Bachiller-Baeza, B., I. Rodriguez-Ramos, A. Guerrero-Ruiz. Influence of Mg and Ce Addition to Ruthenium Based Catalysts Used in the Selective Hydrogenation of Alpha,Beta-unsaturated Aldehydes. Appl. Catal. A: Gen., *205*, pp.227-237. 2001.

Bachiller-Baeza, B., A. Guerrero-Ruiz, I. Rodriguez-Ramos. Ruthenium-Supported Catalysts for the Stereoselective Hydrogenation of Paracetamol to 4-trans-acetamidocyclohexanol: Effect of Support, Metal Precursor, and Solvent. J. Catal., *229*, pp.439-445. 2005.

Bai, P., Su, F. B. Wu, P. P. Wang, L. K. Lee, F. Y. Lv, L. Yan, Z. F. Zhao, X. S. Copolymer-Controlled Homogeneous Precipitation for the Synthesis of Porous Microfibers of Alumina. Langmuir, *23*, pp.4599-4605. 2007.

Baijun, L., L. Lianhai, W. Bingchun, C. Tianxi, I. Katsuyoshi. Liquid Phase Selective Hydrogenation of Furfural on Raney Nickel Modified by Iimpregnation of Salts of Heteropolyacids. Appl. Catal. A: Gen., *171*, pp.117-122. 1998.

Barata-Rodrigues, P. M., T. J. Mays, G. D. Moggridge. Structured Carbon Adsorbents from Clay, Zeolite and Mesoporous Aluminosilicate Templates. Carbon, *41*, pp.2231-2246. 2003.

Barbe, G., A. B. Charette. Highly Chemoselective Metal-Free Reduction of Tertiary Amides. J. Am. Chem. Soc., *130*, pp.18-19. 2007.

Barr, T. L., M. P. Yin. Concerted X-ray Photoelectron-Spectroscopy Study of the Character of Select Carbonaceous Materials. J. Vac. Sci. Technol. A-Vac. Surf. Films, *10*, pp.2788-2795. 1992.

Berkessel, A., T. J. S. Schubert, T. N. Muller. Hydrogenation without a Transition-Metal Catalyst: On the Mechanism of the Base-Catalyzed Hydrogenation of Ketones. J. Am. Chem. Soc., *124*, pp.8693-8698. 2002.

Besson, M., P. Gallezot. Deactivation of Metal Catalysts in Lliquid Phase Organic Reactions. Catal. Today, *81*, pp.547-559. 2003.

Besson, M., P. Gallezot, A. Perrard, C. Pinel. Active Carbons as Catalysts for Liquid Phase Reactions. Catal. Today, *102*, pp.160-165. 2005.

Bhatia, S., X. Wu, D. K. Sanders, B. C. Gerstein, M. Pruski, T. S. King. Ethene Hydrogenation over Silica-Supported Ru and Ru-Cu Bimetallic Catalysts - the Role of Defects and Special Sites. Catal. Today, *12*, pp.165-175. 1992.

Bhattacharjee, S., D. M. Dotzauer, M. L. Bruening. Selectivity as a Function of Nanoparticle Size in the Catalytic Hydrogenation of Unsaturated Alcohols. J. Am. Chem. Soc., *131*, pp.3601-3610. 2009.

Bizhanov, F. B., R. B. Drozdova. Studies of the Kinetics and Mechanism of Glucose Hydrogenation over Ruthenium Catalysts. React. Kinetics. Catal. Lett., *21*, pp.35-39. 1982.

Blaser, H. U., C. Malan, B. Pugin, F. Spindler, H. Steiner, M. Studer. Selective Hydrogenation for Fine Chemicals: Recent Trends and New Developments. Adv. Synth. Catal., *345*, pp.103-151. 2003.

Bond, G.C., Webb, G., Wells, P.B., Winterbottom, J.M. Patterns of Behavior in Catalysis by Metals. J. Catal., 1, pp. 74-84. 1962.

Bond, G. C., X. Yide. Silica-Supported Ruthenium-Copper Catalysts: Structural Studies and Activities for N-butane Hydrogenolysis. J. Mol. Catal., *25*, pp.141-150. 1984.

Boronat, M., P. Concepcion, A. Corma, S. Gonzalez, F. Illas, P. Serna. A Molecular Mechanism for the Chemoselective Hydrogenation of Substituted Nitroaromatics with Nanoparticles of Gold on TiO2 Catalysts: A Cooperative Effect between Gold and the Support. J. Am. Chem. Soc., *129*, pp.16230-16237. 2007.

Boualleg, M., J. M. Basset, J. P. Candy, P. Delichere, K. Pelzer, L. Veyre, C. Thieuleux. Regularly Distributed and Fully Accessible Pt Nanoparticles in Silica Pore Channels via the Controlled Growth of a Mesostructured Matrix around Pt Colloids. Chem. Mater., *21*, pp.775-779. 2009.

Boutros, M., F. Launay, A. Nowicki, T. Onfroy, V. Herledan-Semmer, A. Roucoux, A. Gedeon. Reduced forms of Rh(III) containing MCM-41 silicas as hydrogenation catalysts for arene derivatives. J. Mol. Catal. A-Chem, *259*, pp.91-98. 2006.

Brahme, P. H., L. K. Doraiswamy. Modelling of a Slurry Reaction. Hydrogenation of Glucose on Raney Nickel. Ind. Eng. Chem. Proc. Des. Develop., *15*, pp.130-137. 1976.

Broadbent, H. S., Slaugh, L. H., Jarvis, N. L., Rhenium Sulfides as Liquid-Phase Hydrgoeantion Catalysts. A Comparison with Molybdenum Sulfide and Cobalt Polysulfide. J. Am. Chem. Soc., *76*, pp. 1519-1523. 1954.

Bromley, S. T., G. Sankar, C. R. A. Catlow, T. Maschmeyer, B. F. G. Johnson, J. M. Thomas. New Insights into the Structure of Supported Bimetallic Nanocluster Catalysts Prepared from Carbonylated Precursors: a Combined Density

Functional Theory and EXAFS Study. Chem. Phys. Lett., *340*, pp.524-530. 2001.

Busygin, I., J. Warna, E. Toukoniitty, D. Y. Murzin, R. Leino. Hydrogenation of 1-phenyl-1,2-propanedione over Pt Catalysts Modified by Cinchona Alkaloid O-ethers and the Kinetic Resolution of the 1-hydroxyketones Generated. J. Catal., *254*, pp.339-348. 2008.

Cake, W. E. The Catalytic Hydrogenation of Dextro Glucose Preliminary Notice. J. Am. Chem. Soc., *44*, pp. 859-861. 1922.

Campo, B., G. Santori, C. Petit, M. Volpe. Liquid Phase Hydrogenation of Crotonaldehyde over Au/CeO2 Catalysts. Appl. Catal. A: Gen., *359*, pp.79-83. 2009.

Castillejos, E., P. J. Debouttiere, L. Roiban, A. Solhy, V. Martinez, Y. Kihn, O. Ersen, K. Philippot, B. Chaudret, P. Serp. An Efficient Strategy to Drive Nanoparticles into Carbon Nanotubes and the Remarkable Effect of Confinement on Their Catalytic Performance. Angew. Chem. Int. Ed., *48*, pp.2529-2533. 2009.

Castoldi, M. C., L. D. T. Camaraa, R. S. Monteiro, A. M. Constantino, L. Camacho, J. W. D. Carneiro, D. G. Aranda. Experimental and Theoretical Studies on Glucose Hydrogenation to Produce Sorbitol. React. Kinetics. Catal. Lett., *91*, pp.341-352. 2007.

Centomo, P., M. Zecca, S. Lora, G. Vitulli, A. M. Caporusso, M. L. Tropeano, C. Milone, S. Galvagno, B. Corain. Novel Pt Catalysts Supported on Functional Resins for the Chemoselective Hydrogenation of Citral to the [alpha],[beta]-Unsaturated Alcohols Geraniol and Nerol. J. Catal., *229*, pp.283-297. 2005.

Chae, W.-S., M.-J. An, S.-W. Lee, M.-S. Son, K.-H. Yoo, Y.-R. Kim. Templated Carbon Nanofiber with Mesoporosity and Semiconductivity. J. Phys. Chem. B, *110*, pp.6447-6450. 2006.

Chai, G. S., S. B. Yoon, J. S. Yu, J. H. Choi, Y. E. Sung. Ordered Porous Carbons with Tunable Pore Sizes as Catalyst Supports in Direct Methanol Fuel Cell. J. Phys. Chem. B, *108*, pp.7074-7079. 2004.

Chatterjee, M., Y. Ikushima, Y. Hakuta, H. Kawanami. In Situ Synthesis of Gold Nanoparticles Inside the Pores of MCM-48 in Supercritical Carbon Dioxide and its Catalytic Application. Adv. Synth. Catal., *348*, pp.1580-1590. 2006.

Chen, B., J. G. Goodwin. Isotopic Transient Kinetic Analysis of Ethane Hydrogenolysis on Cu Modified Ru/SiO2. J. Catal., *158*, pp.228-235. 1996.

Chen, L. F., P. J. Guo, M. H. Qiao, S. R. Yan, H. X. Li, W. Shen, H. L. Xu, K. N. Fan. CU/SiO2 Catalysts Prepared by the Ammonia-Evaporation Method: Texture, Structure, and Catalytic Performance in Hydrogenation of Dimethyl Oxalate to Ethylene Glycol. J. Catal., *257*, pp.172-180. 2008.

Chen, Y. Chemical Preparation and Characterization of Metal-Metalloid Ultrafine Amorphous Alloy Particles. Catal. Today, *44*, pp.3-16. 1998.

Chen, Y. Y., C. A. Wang, H. Y. Liu, J. S. Qiu, X. H. Bao. Ag/SiO2: A Novel Catalyst with High Activity and Selectivity for Hydrogenation of Chloronitrobenzenes. Chem. Commun., *21*, 5298-5300. 2005.

Chetty, R., S. Kundu, W. Xia, M. Bron, W. Schuhmann, V. Chirila, W. Brandl, T. Reinecke, M. Muhler. PtRu Nanoparticles Supported on Nitrogen-Doped Multiwalled Carbon Nanotubes as Catalyst for Methanol Electrooxidation. Electrochim. Acta, *54*, pp.4208-4215. 2009.

Choi, B., H. Yoon, I. S. Park, J. Jang, Y. E. Sung. Highly Dispersed Pt Nanoparticles on Nitrogen-Doped Magnetic Carbon Nanoparticles and Their Enhanced Activity for Methanol Oxidation. Carbon, *45*, pp.2496-2501. 2007.

Choi, W. C., S. I. Woo, M. K. Jeon, J. M. Sohn, M. R. Kim, H. J. Jeon. Platinum Nanoclusters Studded in the Microporous Nanowalls of Ordered Mesoporous Carbon. Adv. Mater., *17*, pp.446-451. 2005.

Claus, P., A. Bruckner, C. Mohr, H. Hofmeister. Supported Gold Nanoparticles from Quantum Dot to Mesoscopic Size Scale: Effect of Electronic and Structural Properties on Catalytic Hydrogenation of Conjugated Functional Groups. J. Am. Chem. Soc., *122*, pp.11430-11439. 2000.

Claus, P., H. Hofmeister. Electron Microscopy and Catalytic Study of Silver Catalysts: Structure Sensitivity of the Hydrogenation of Crotonaldehyde. J. Phys. Chem. B, *103*, pp.2766-2775. 1999.

Coloma, F., A. Sepúlveda-Escribano, J. L. G. Fierro, F. Rodríguez-Reinoso. Gas Phase Gydrogenation of Crotonaldehyde over Pt/Activated Carbon Catalysts. Influence of the Oxygen Surface Groups on the Support. Appl. Catal. A: Gen., *150*, pp.165-183. 1997.

Conner, W. C., J. L. Falconer. Spillover in Heterogeneous Catalysis. Chem. Rev., *95*, pp.759-788. 1995.

Coq, B., F. Figueras. Structure-Activity Relationships in Catalysis by Metals: Some Aspects of Particle Size, Bimetallic and Supports Effects. Coord. Chem. Rev., *180*, pp.1753-1783. 1998.

Corma, A., P. Serna. Chemoselective Hydrogenation of Nitro Compounds with Supported Gold Catalysts. Science, *313*, pp.332-334. 2006.

Cott, D. J., N. Petkov, M. A. Morris, B. Platschek, T. Bein, J. D. Holmes. Preparation of Oriented Mesoporous Carbon Nano-Filaments within the Pores of Anodic Alumina Membranes. J. Am. Chem. Soc., *128*, pp.3920-3921. 2006.

Crezee, E., B. W. Hoffer, R. J. Berger, M. Makkee, F. Kapteijn, J. A. Moulijn. Three-Phase Hydrogenation of D-glucose over a Carbon Supported Ruthenium Catalyst-Mass Transfer and Kinetics. Appl. Catal. A: Gen., *251*, pp.1-17. 2003.

Crosman, A., W. F. Hoelderich. Enantioselective Hydrogenation over Immobilized Rhodium Diphosphine Complexes on Aluminated SBA-15. J. Catal., *232*, pp.43-50. 2005.

Crosman, A., W. F. Hoelderich. Enantioselective Hydrogenation over Immobilized Rhodium Diphosphine Complexes on Mesostructured Naterials. Catal. Today, *121*, pp.130-139. 2007.

Cui, G. L., L. J. Zhi, A. Thomas, U. Kolb, I. Lieberwirth, K. Mullen. One-Dimensional Porous Carbon/Platinum Composites for Nanoscale Electrodes. Angew. Chem. Int. Ed., *46*, pp.3464-3467. 2007.

Czerw, R., M. Terrones, J. C. Charlier, X. Blase, B. Foley, R. Kamalakaran, N. Grobert, H. Terrones, D. Tekleab, P. M. Ajayan, W. Blau, M. Ruhle, D. L. Carroll. Identification of Electron Donor States in N-doped Carbon Nanotubes. Nano Letters, *1*, pp.457-460. 2001.

Davda, R. R., J. A. Dumesic. Renewable Hydrogen by Aqueous-Phase Reforming of Glucose. Chem. Commun., *1*, 36-37. 2004.

De Jong, K. P., J. W. Geus. Carbon nanofibers: Catalytic Synthesis and Applications. Catal. Rev. –Sci. Eng., *42*, pp.481-510. 2000.

Dechamp, N., A. Gamez, A. Perrard, P. Gallezot. Kinetics of Glucose Hydrogenation in a Trickle-Bed Reactor. Catal. Today, *24*, pp.29-34. 1995.

Deng, J.-F., H. Li, W. Wang. Progress in Design of New Amorphous Alloy Catalysts. Catal. Today, *51*, pp.113-125. 1999.

Dodgson, I. Trends and Opportunities with Modern Hydrogenation Catalysts. 3rd International Symposium on Heterogeneous Catalysis and Fine Chemicals, 1993, Poitiers, France, pp. 124-127.

Dominguez-Dominguez, S., A. Berenguer-Murcia, A. Linares-Solano, D. Cazorla-Amoros. Inorganic Materials as Supports for Palladium Nanoparticles: Application in the Semi-Hydrogenation of Phenylacetylene. J. Catal., *257*, pp.87-95. 2008.

Dominguez, F., J. Sanchez, G. Arteaga, E. Choren. Gallia as Support of Pt in Benzene Hydrogenation Reaction. J. Mol. Catal. A-Chem, *228*, pp.319-324. 2005.

Drelinkiewicz, A., M. Hasik, M. Kloc. Liquid-Phase Hydrogenation of 2-Ethylanthraquinone over Pd/Polyaniline Catalysts. J. Catal., *186*, pp.123-133. 1999.

Dwars, T., G. Oehme. Complex-Catalyzed Hydrogenation Reactions in Aqueous Media. Adv. Synth. Catal., *344*, pp.239-260. 2002.

Echeverri, D. A., J. M. Marin, G. M. Restrepo, L. A. Rios. Characterization and Carbonylic Hydrogenation of Methyl Oleate over Ru-Sn/Al_2O_3: Effects of Metal Precursor and Chlorine Removal. Appl. Catal. A: Gen., *366*, pp.342-347. 2009.

Eisenbeis, C., R. Guettel, U. Kunz, T. Turek. Monolith Loop Reactor for Hydrogenation of Glucose. Catal. Today, pp. S342-S346. 2009.

Fajardie, F., J. F. Tempere, G. DjegaMariadassou, G. Blanchard. Benzene Hydrogenation as a Tool for the Determination of the Percentage of Metal Exposed on Low Loaded Ceria Supported Rhodium Catalysts. J. Catal., *163*, pp.77-86. 1996.

Fedor, W. S. Sorbitol. Ind. Eng. Chem., *52*, pp.282-286. 1960.

Ferrando, R., J. Jellinek, R. L. Johnston. Nanoalloys: From Theory to Applications of Alloy Clusters and Nanoparticles. Chem. Rev., *108*, pp.845-910. 2008.

Figueiredo, F. C. A., E. Jordao, R. Landers, W. A. Carvalho. Acidity Control of Ruthenium Pillared Clay and its Application as a Catalyst in Hydrogenation Reactions. Appl. Catal. A: Gen., *371*, pp.131-141. 2009.

Fouilloux, P. The Nature of Raney-Nickel, Its Adsorbed Hydrogen and Its Catalytic Activity for Hydrogenation Reactions - Review. Appl. Catal., *8*, pp.1-42. 1983.

Gallezot, P., P. J. Cerino, B. Blanc, G. Fleche, P. Fuertes. Glucose Hydrogenation on Promoted Raney-Nickel Catalysts. J. Catal., *146*, pp.93-102. 1994.

Gallezot, P., N. Nicolaus, G. Fleche, P. Fuertes, A. Perrard. Glucose Hydrogenation on Ruthenium Catalysts in a Trickle-Bed Reactor. J. Catal., *180*, pp.51-55. 1998.

Gao, P., Wang, A., Wang, X., and Zhang, T. Synthesis of Highly Ordered Ir-Containing Mesoporous Carbon Materials by Organic-Organic Self-Assembly. Chem. Mater., *20*, pp.1881-1888. 2008

Garcia-Garcia, F. R., J. Alvarez-Rodriguez, I. Rodriguez-Ramos, A. Guerrero-Ruiz. The Use of Carbon Nanotubes with and without Nitrogen Doping as Support for Ruthenium Catalysts in the Ammonia Decomposition Reaction. Carbon, *48*, pp.267-276. 2010.

Gaspar, A. B., G. R. dos Santos, R. D. Costa, M. A. P. da Silva. Hydrogenation of Synthetic PYGAS - Effects of Zirconia on Pd/Al2O3. Catal. Today, *133*, pp.400-405. 2008.

Gebauer-Henke, E., J. Grams, E. Szubiakiewicz, J. Farbotko, R. Touroude, J. Rynkowski. Pt/Ga_2O_3 Catalysts of Selective Hydrogenation of Crotonaldehyde. J. Catal., *250*, pp.195-208. 2007.

Ghosh, K., M. Kumar, T. Maruyama, Y. Ando. Tailoring the Field Emission Property of Nitrogen-Doped Carbon Nanotubes by Controlling the Graphitic/Pyridinic Substitution. Carbon, *48*, pp.191-200. 2010.

Gomez, S., J. A. Peters, T. Maschmeyer. The Reductive Amination of Aldehydes and Ketones and the Hydrogenation of Nitriles: Mechanistic Aspects and Selectivity Control. Adv. Synth. Catal., *344*, pp.1037-1057. 2002.

Goodman, D. W., C. H. F. Peden. Hydrogen Spillover from Ruthenium to Copper in Cu/Ru Catalysts: A Potential Source of Error in Active Metal Titration. J. Catal., *95*, pp.321-324. 1985.

Gorgulho, H. F., F. Goncalves, M. F. R. Pereira, J. L. Figueiredo. Synthesis and Characterization of Nitrogen-Doped Carbon Xerogels. Carbon, *47*, pp.2032-2039. 2009.

Guczi, L. Bimetallic Nano-Particles: Featuring Structure and Reactivity. Catal. Today, *101*, pp.53-64. 2005.

Guo, H. B., H. X. Li, J. Zhu, W. H. Ye, M. H. Qiao, W. L. Dai. Liquid Phase Glucose Hydrogenation to D-glucitol over an Ultrafine Ru-B Amorphous Alloy Catalyst. J. Mol. Catal. A-Chem, *200*, pp.213-221. 2003.

Haller, G. L., D. E. Resasco, H. P. D.D. Eley, B. W. Paul. Metal-Support Interaction: Group VIII Metals and Reducible Oxides. Adv. Catal., *36*, pp.173-235. 1989.

Halpern, J. in Asymmetric Synthesis. pp. 41-69, London: Academic Press. 1985.

Hansen, T. W., J. B. Wagner, P. L. Hansen, S. Dahl, H. Topsoe, C. J. H. Jacobsen. Atomic-Resolution in Situ Transmission Electron Microscopy of a Promoter of a Heterogeneous Catalyst. Science, *294*, pp.1508-1510. 2001.

Highfield, J., T. Liu, Y. S. Loo, B. Grushko, A. Borgna. Skeletal Ru/Cu Catalysts Prepared from Crystalline and Quasicrystalline Ternary Alloy Precursors: Characterization by X-ray Absorption Spectroscopy and CO Oxidation. Phys. Chem. Chem. Phys., *11*, pp.1196-1208. 2009.

Hoffer, B. W., E. Crezee, F. Devred, P. R. M. Mooijman, W. G. Sloof, P. J. Kooyman, A. D. van Langeveld, F. Kapteijn, J. A. Moulijn. The Role of the Active Phase of Raney-type Ni Catalysts in the Selective Hydrogenation of D-glucose to D-sorbitol. Appl. Catal. A: Gen., *253*, pp.437-452. 2003a.

Hoffer, B. W., E. Crezee, P. R. M. Mooijman, A. D. van Lagneveld, F. Kapteijn, J. A. Moulijn. Carbon Supported Ru Catalysts as Promising Alternative for Raney-type Ni in the Selective Hydrogenation of D-glucose. Catal. Today, *79*, pp.35-41. 2003b.

Holmes, S. M., P. Foran, P. L. Roberts, J. M. Newton. Encapsulation of Metal Particles within the Wall Structure of Mesoporous Carbons. Chem. Commun., *12*, 1912-1913. 2005.

Hong, A. J., A. J. Rouco, D. E. Resasco, G. L. Haller. Effect of Silica Support on Ru-Cu Cluster Morphology as Determined by Catalytic Activity. J. Phys. Chem., *91*, pp.2665-2671. 1987.

Hong, A. J., A. J. Rouco, D. E. Resasco, G. L. Haller. Effect of Silica Support on Ruthenium-Copper Cluster Morphology as Determined by Catalytic Activity. J. Phys. Chem., *91*, pp.2665-2671. 1987.

Hou, P. X., H. Orikasa, T. Yamazaki, K. Matsuoka, A. Tomita, N. Setoyama, Y. Fukushima, T. Kyotani. Synthesis of Nitrogen-Containing Microporous Carbon with a Highly Ordered Structure and Effect of Nitrogen Doping on H_2O Adsorption. Chem. Mater., *17*, pp.5187-5193. 2005a.

Hou, P. X., T. Yamazaki, H. Orikasa, T. Kyotani. An Easy Method for the Synthesis of Ordered Microporous Carbons by the Template Technique. Carbon, *43*, pp.2624-2627. 2005b.

Hoxha, F., N. van Vegten, A. Urakawa, F. Krurneich, T. Mallat, A. Baiker. Remarkable Particle Size effect in Rh-Catalyzed Enantioselective Hydrogenations. J. Catal., *261*, pp.224-231. 2009.

Hu, A., G. T. Yee, W. Lin. Magnetically Recoverable Chiral Catalysts Immobilized on Magnetite Nanoparticles for Asymmetric Hydrogenation of Aromatic Ketones. J. Am. Chem. Soc., *127*, pp.12486-12487. 2005.

Huang, J., T. Jiang, H. X. Gao, B. X. Han, Z. M. Liu, W. Z. Wu, Y. H. Chang, G. Y. Zhao. Pd Nanoparticles Immobilized on Molecular Sieves by Ionic Liquids: Heterogeneous Catalysts for Solvent-Free Hydrogenation. Angew. Chem. Int. Ed., *43*, pp.1397-1399. 2004.

Huang, S. F., K. Terakura, T. Ozaki, T. Ikeda, M. Boero, M. Oshima, J. Ozaki, S. Miyata. First-principles Calculation of the Electronic Properties of Graphene Clusters Doped with Nitrogen and Boron: Analysis of Catalytic Activity for the Oxygen Reduction Reaction. Phys. Rev. B, *80*, pp. 2009.

Huber, G. W., R. D. Cortright, J. A. Dumesic. Renewable Alkanes by Aqueous-Phase Reforming of Biomass-Derived Oxygenates13. Angew. Chem. Int. Ed., *43*, pp.1549-1551. 2004.

Huber, G. W., J. W. Shabaker, J. A. Dumesic. Raney Ni-Sn Catalyst for H_2 Production from Biomass-Derived Hydrocarbons. Science, *300*, pp.2075-2077. 2003.

Ismagilov, Z. R., A. E. Shalagina, O. Y. Podyacheva, A. V. Ischenko, L. S. Kibis, A. I. Boronin, Y. A. Chesalov, D. I. Kochubey, A. I. Romanenko, O. B. Anikeeva, T. I. Buryakov, E. N. Tkachev. Structure and Electrical Conductivity of Nitrogen-Doped Carbon Nanofibers. Carbon, *47*, pp.1922-1929. 2009.

Jen, P. H., Y. H. Hsu, S. D. Lin. The Activity and Stability of Pd/C Catalysts in Benzene Hydrogenation. Catal. Today, *123*, pp.133-141. 2007.

Jiang, Y. J., Q. M. Gao. Heterogeneous Hydrogenation Catalyses over Recyclable Pd(0) Nanoparticle Catalysts Stabilized by PAMAM-SBA-15 Organic-Inorganic Hybrid Composites. J. Am. Chem. Soc., *128*, pp.716-717. 2006.

Joo, S. H., S. J. Choi, I. Oh, J. Kwak, Z. Liu, O. Terasaki, R. Ryoo. Ordered Nanoporous Arrays of Carbon Supporting High Dispersions of Platinum Nanoparticles. Nature, *412*, pp.169-172. 2001.

Jun, S., S. H. Joo, R. Ryoo, M. Kruk, M. Jaroniec, Z. Liu, T. Ohsuna, O. Terasaki. Synthesis of New, Nanoporous Carbon with Hexagonally Ordered Mesostructure. J. Am. Chem. Soc., *122*, pp.10712-10713. 2000.

Kacer, P., L. Cerveny. Structure Effects in Hydrogenation Reactions on Noble Metal Catalysts. Appl. Catal. A: Gen., *229*, pp.193-216. 2002.

Kantam, M. L., B. P. C. Rao, B. M. Choudary, B. Sreedhar. Selective Transfer Hydrogenation of Carbonyl Compounds by Ruthenium Nanoclusters Supported on Alkali-Exchanged Zeolite Beta. Adv. Synth. Catal., *348*, pp.1970-1976. 2006.

Kijenski, J., P. Winiarek, T. Paryjczak, A. Lewicki, A. Mikolajska. Platinum Deposited on Monolayer Supports in Selective Hydrogenation of Furfural to Furfuryl alcohol. Appl. Catal. A: Gen., *233*, pp.171-182. 2002.

Kim, D. B., D.-H. Lim, H.-J. Chun, H.-H. Kwon, H.-I. Lee. Nitrogen-Containing Graphitized Carbon Support for Methanol Oxidation Pt Catalyst. Carbon, *48*, pp.673-679. 2010.

Kim, M., S. Hwang, J.-S. Yu. Novel Ordered Nanoporous Graphitic C3N4 as a Support for Pt-Ru Anode Catalyst in Direct Methanol Fuel Cell. J. Mater. Chem., *17*, pp.1656-1659. 2007.

Kim, T.-W., I.-S. Park, R. Ryoo. A Synthetic Route to Ordered Mesoporous Carbon Materials with Graphitic Pore Walls13. Angew. Chem. Int. Ed., *42*, pp.4375-4379. 2003.

King, T. S., X. Wu, B. C. Gerstein. Direct Evidence for Spillover of Hydrogen from Ruthenium to Copper in Supported Cu-Ru/SiO_2 Catalysts - a Study by NMR of Chemisorbed Hydrogen. J. Am. Chem. Soc., *108*, pp.6056-6058. 1986.

Kiraly, Z., B. Veisz, A. Mastalir, G. Kofarago. Preparation of Ultrafine Palladium Particles on Cationic and Anionic Clays, Mediated by Oppositely Charged Surfactants: Catalytic Probes in Hydrogenations. Langmuir, *17*, pp.5381-5387. 2001.

Kluson, P., L. Cerveny. Selective Hydrogenation over Ruthenium Catalysts. Appl. Catal. A: Gen., *128*, pp.13-31. 1995.

Knox, J. H., B. Kaur, G. R. Millward. Structure and Performance of Porous Graphitic Carbon in Liquid Chromatography. J. Chromatogr. A, *352*, pp.3-25. 1986.

Kolaric, S., V. Sunjic. Comparative Study of Homogeneous Hydrogenation of D-glucose and D-mannose Catalyzed by Water soluble [Ru(tri(m-sulfophenyl)phosphine)] Complex. J. Mol. Catal. A-Chem, *110*, pp.189-193. 1996.

Koo-amornpattana, W., J. M. Winterbottom. Pt and Pt-alloy Catalysts and Their Properties for the Liquid-phase Hydrogenation of Cinnamaldehyde. Catal. Today, *66*, pp.277-287. 2001.

Koopman, P. G. J., A. P. G. Kieboom, H. V. Bekkum. Preparation and High Temperature Activation of Ruthenium on Carbon Hydrogenation Catalysts. Carbon, *17*, pp.399-402. 1979.

Kralik, M., A. Biffis. Catalysis by Metal Nanoparticles Supported on Functional Organic Polymers. J. Mol. Catal. A-Chem, *177*, pp.113-138. 2001.

Kumar, N., P. Mäki-Arvela, J. Hajek, T. Salmi, D. Y. Murzin, T. Heikkilä, E. Laine, P. Laukkanen, J. Väyrynen. Physico-chemical and Catalytic Properties of Ru-MCM-41 Mesoporous Molecular Sieve Catalyst: Influence of Ru Modification Methods. Microporous Mesoporous Mat., *69*, pp.173-179. 2004.

Kun, I., G. Szöllösi, M. Bartók. Crotonaldehyde Hydrogenation over Clay-Supported Platinum Catalysts. J. Mol. Catal. A-Chem, *169*, pp.235-246. 2001.

Kusserow, B., S. Schimpf, P. Claus. Hydrogenation of Glucose to Sorbitol over Nickel and Ruthenium Catalysts. Adv. Synth. Catal., *345*, pp.289-299. 2003.

Kuusisto, J., J. P. Mikkola, M. Sparv, J. Warna, H. Karhu, T. Salmi. Kinetics of the Catalytic Hydrogenation of D-lactose on a Carbon Supported Ruthenium Catalyst. Chem. Eng. J., *139*, pp.69-77. 2008.

Kyotani, T., T. Nagai, S. Inoue, A. Tomita. Formation of New Type of Porous Carbon by Carbonization in Zeolite Nanochannels. Chem. Mater., *9*, pp.609-615. 1997.

Kyotani, T., Z. X. Ma, A. Tomita. Template Synthesis of Novel Porous Carbons Using Various Types of Zeolites. Carbon, *41*, pp.1451-1459. 2003.

Lai, S. Y., J. C. Vickerman. Carbon Monoxide Hydrogenation over Silica-Supported Ruthenium-Copper Bimetallic Catalysts. J. Catal., *90*, pp.337-350. 1984.

Lang, H. F., R. A. May, B. L. Iversen, B. D. Chandler. Dendrimer-encapsulated Nanoparticle Precursors to Supported Platinum Catalysts. J. Am. Chem. Soc., *125*, pp.14832-14836. 2003.

Lashdaf, M., A. O. I. Krause, M. Lindblad, M. Tiitta, T. Venäläinen. Behaviour of Palladium and Ruthenium Catalysts on Alumina and Silica Prepared by Gas and Liquid Phase Deposition in Cinnamaldehyde Hydrogenation. Appl. Catal. A: Gen., *241*, pp.65-75. 2003.

Lee, J.-S., S. H. Joo, R. Ryoo. Synthesis of Mesoporous Silicas of Controlled Pore Wall Thickness and Their Replication to Ordered Nanoporous Carbons with Various Pore Diameters. J. Am. Chem. Soc., *124*, pp.1156-1157. 2002.

Lee, J., S. Yoon, T. Hyeon, S. M. Oh, K. B. Kim. Synthesis of a New Mesoporous Carbon and its Application to Electrochemical Double-Layer Capacitors. Chem. Commun., *15*, 2177-2178. 1999.

Lee, J., J. Kim, T. Hyeon. Recent Progress in the Synthesis of Porous Carbon Materials. Adv. Mater., *18*, pp.2073-2094. 2006.

Lee, S. S., B. K. Park, S. H. Byeon, F. Chang, H. Kim. Mesoporous Silica-Supported Pd Nanoparticles; Highly Selective Catalyst for Hydrogenation of Olefins in Supercritical Carbon Dioxide. Chem. Mater., *18*, pp.5631-5633. 2006.

Lei, Z. B., Y. G. Zhang, H. Wang, Y. X. Ke, J. M. Li, F. Q. Li, J. Y. Xing. Fabrication of Well-ordered Macroporous Active Carbon with a Microporous Framework. J. Mater. Chem., *11*, pp.1975-1977. 2001.

Lenarda, M., R. Ganzerla, L. Storaro, R. Frattini, S. Enzo, R. Zanoni. X-ray Diffraction and X-ray Photoelectron Spectroscopy Study of the Ru-Cu/SiO_2 System Prepared by Low Temperature Reduction: Occurrence of a Metastable Amorphous or Nanocrystalline Phase. J. Mater. Res., *11*, pp.325-331. 1996.

Lenz, J., B. C. Campo, M. Alvarez, M. A. Volpe. Liquid Phase Hydrogenation of Alpha,Beta-unsaturated Aldehydes over Gold Supported on Iron Oxides. J. Catal., *267*, pp.50-56. 2009.

Li, B., Z. Xu. A Nonmetal Catalyst for Molecular Hydrogen Activation with Comparable Catalytic Hydrogenation Capability to Noble Metal Catalyst. J. Am. Chem. Soc., *131*, pp.16380-16382. 2009.

Li, F. B., Q. L. Qian, F. Yan, G. Q. Yuan. Nitrogen-doped Porous Carbon Microspherules as Supports for Preparing Monodisperse Nickel Nanoparticles. Carbon, *44*, pp.128-132. 2006.

Li, H., D. S. Chu, J. Liu, M. H. Qiao, W. L. Dai, H. X. Li. A Novel Ruthenium-Phosphorus Amorphous Alloy Catalyst for Maltose Hydrogenation to Maltitol. Adv. Synth. Catal., *350*, pp.829-836. 2008.

Li, H., P. Yang, D. Chu, H. Li. Selective Maltose Hydrogenation to Maltitol on a Ternary Co-P-B Amorphous Catalyst and the Synergistic Effects of Alloying B and P. Appl. Catal. A: Gen., *325*, pp.34-40. 2007.

Li, H. X., H. Li, M. H. Wang. Glucose Hydrogenation over Promoted Co-B Amorphous Alloy Catalysts. Appl. Catal. A: Gen., *207*, pp.129-137. 2001.

Li, H. X., W. J. Wang, J. F. Deng. Glucose Hydrogenation to Sorbitol over a Skeletal Ni-P Amorphous Alloy Catalyst (Raney Ni-P). J. Catal., *191*, pp.257-260. 2000.

Li, J., M. H. Qiao, J. F. Deng. Amorphous Ni-B/gamma-Al_2O_3 Catalyst Prepared in a Modified Drying Approach and its Excellent Activity in Benzene Hydrogenation. J. Mol. Catal. A-Chem, *169*, pp.295-301. 2001.

Li, J., Y. M. Zhang, D. F. Han, Q. Gao, C. Li. Asymmetric Transfer Hydrogenation Using Recoverable Ruthenium Catalyst Iimmobilized into Magnetic Mesoporous Silica. J. Mol. Catal. A-Chem, *298*, pp.31-35. 2009.

Liang, C., Z. Li, S. Dai. Mesoporous Carbon Materials: Synthesis and Modification. Angew. Chem. Int. Ed., *47*, pp.3696-3717. 2008.

Liang, Y. Y., X. L. Feng, L. J. Zhi, U. Kolb, K. Mullen. A Simple Approach towards One-dimensional Mesoporous Carbon with Superior Electrochemical Capacitive Activity. Chem. Commun., *9*, 809-811. 2009.

Liberková, K., R. Touroude. Performance of Pt/SnO_2 Catalyst in the Gas Phase Hydrogenation of Crotonaldehyde. J. Mol. Catal. A-Chem, *180*, pp.221-230. 2002a.

Liberková, K., R. Touroude, D. Y. Murzin. Analysis of Deactivation and Selectivity Pattern in Catalytic Hydrogenation of a Molecule with Different Functional Groups: Crotonaldehyde Hydrogenation on Pt/SnO_2. Chem. Eng. Sci., *57*, pp.2519-2529. 2002b.

Lim, S., S. H. Yoon, I. Mochida, D. H. Jung. Direct Synthesis and Structural Analysis of Nitrogen-Doped Carbon Nanofibers. Langmuir, *25*, pp.8268-8273. 2009.

Liu, B., L. Lu, T. Cai, K. Iwatani. Selective Hydrogenation of Cinnamaldehyde over Raney Cobalt Catalysts Modified with Salts of Heteropolyacids. Appl. Catal. A: Gen., *180*, pp.105-111. 1999.

Liu, J. Tian, X. N. Zhao, X. S. Hydrogenation of Glucose over Ru Nanoparticles Embedded in Templated Porous Carbon. Aust. J. Chem., *62*, pp.1020-1026. 2009.

Liu, R. B., B. Tesche, H. Knozinger. Characterization of Rucu/SiO_2 Catalysts by Infrared-Spectroscopy of Adsorbed Carbon-Monoxide. J. Catal., *129*, pp.402-413. 1991.

Liu, S. H., R. F. Lu, S. J. Huang, A. Y. Lo, C. Shu-Hua, S. B. Liu. Controlled Synthesis of Highly Dispersed Platinum Nanoparticles in Ordered Mesoporous Carbon. Chem. Commun., *15*, 3435-3437. 2006.

Lindlar, H., Dubuis, R. Palladium Catalyst for Partial Reduction of Acetylenes. Org. Synth. Coll., 5, pp. 880-884. 1973.

Lu, A.-H., W. Schmidt, N. Matoussevitch, H. Bönnemann, B. Spliethoff, B. Tesche, E. Bill, W. Kiefer, F. Schüth. Nanoengineering of a Magnetically Separable Hydrogenation Catalyst. Angew. Chem. Int. Ed., *43*, pp.4303-4306. 2004a.

Lu, A. H., A. Kiefer, W. Schmidt, F. Schuth. Synthesis of Polyacrylonitrile-based Ordered Mesoporous Carbon with Tunable Pore Structures. Chem. Mater., *16*, pp.100-103. 2004b.

Lu, A.-H., F. Schüth. Nanocasting: A Versatile Strategy for Creating Nanostructured Porous Materials. Adv. Mater., *18*, pp.1793-1805. 2006.

Lu, X. F., C. Wang, Y. Wei. One-Dimensional Composite Nanomaterials: Synthesis by Electrospinning and Their Applications. Small, *5*, pp.2349-2370. 2009.

Lynch, J. Physico-Chemical Analysis of Industrial Catalysts. pp. 219-236, Paris: Editions Technip. 2003.

Lyth, S. M., Y. Nabae, S. Moriya, S. Kuroki, M. Kakimoto, J. Ozaki, S. Miyata. Carbon Nitride as a Nonprecious Catalyst for Electrochemical Oxygen Reduction. J. Phys. Chem. C, *113*, pp.20148-20151. 2009.

Ma, B., H. F. Schaefer, N. L. Allinger. Theoretical Studies of the Potential Energy Surfaces and Compositions of the d-Aldo- and d-Ketohexoses. J. Am. Chem. Soc., *120*, pp.3411-3422. 1998.

Ma, Z. X., T. Kyotani, A. Tomita. Preparation of a High Surface Area Microporous Carbon Having the Structural Regularity of Y Zeolite. Chem. Commun., *14*, 2365-2366. 2000.

Ma, Z. X., T. Kyotani, Z. Liu, O. Terasaki, A. Tomita. Very High Surface Area Microporous Carbon with a Three-Dimensional Nano-Array Structure: Synthesis and its Molecular Structure. Chem. Mater., *13*, pp.4413. 2001.

Ma, Z. X., T. Kyotani, A. Tomita. Synthesis Methods for Preparing Microporous Carbons with a Structural Regularity of Zeolite Y. Carbon, *40*, pp.2367-2374. 2002.

Machnikowski, J., B. Grzyb, J. V. Weber, E. Frackowiak, J. N. Rouzaud, F. Béguin. Structural and Electrochemical Characterisation of Nitrogen Enriched Carbons Produced by the Co-pyrolysis of Coal-tar Pitch with Polyacrylonitrile. Electrochim. Acta, *49*, pp.423-432. 2004.

Mäki-Arvela, P., L. P. Tiainen, M. Lindblad, K. Demirkan, N. Kumar, R. Sjöholm, T. Ollonqvist, J. Väyrynen, T. Salmi, D. Y. Murzin. Liquid-phase Hydrogenation of Citral for Production of Citronellol: Catalyst Selection. Appl. Catal. A: Gen., *241*, pp.271-288. 2003.

Maki-Arvela, P., J. Hajek, T. Salmi, D. Y. Murzin. Chemoselective Hydrogenation of Carbonyl Compounds over Heterogeneous Catalysts. Appl. Catal. A: Gen., *292*, pp.1-49. 2005.

Makkee, M., A. P. G. Kieboom, H. Vanbekkum. Hydrogenation of D-Fructose and D-Fructose D-Glucose Mixtures. Carbohydr. Res., *138*, pp.225-236. 1985.

Manyar, H. G., D. Weber, H. Daly, J. M. Thompson, D. W. Rooney, L. F. Gladden, E. H. Stitt, J. J. Delgado, S. Bernal, C. Hardacre. Deactivation and Regeneration of Ruthenium on Silica in the Liquid-phase Hydrogenation of Butan-2-one. J. Catal., *265*, pp.80-88. 2009.

Marchi, A. J., D. A. Gordo, A. F. Trasarti, C. R. Apesteguia. Liquid Phase Hydrogenation of Cinnamaldehyde on Cu-based Catalysts. Appl. Catal. A: Gen., *249*, pp.53-67. 2003.

Maris, E. P., W. C. Ketchie, V. Oleshko, R. J. Davis. Metal Particle Growth During Glucose Hydrogenation over Ru/SiO_2 Evaluated by X-ray Absorption Spectroscopy and Electron Microscopy. J. Phys. Chem. B, *110*, pp.7869-7876. 2006.

Masalska, A. Ni-loaded Catalyst Containing ZSM-5 Zeolite for Toluene Hydrogenation. Appl. Catal. A: Gen., *294*, pp.260-272. 2005.

Mastalir, A., B. Rac, Z. Kiraly, A. Molnar. In Situ Generation of Pd Nanoparticles in MCM-41 and Catalytic Applications in Liquid-phase Alkyne Hydrogenations. J. Mol. Catal. A-Chem, *264*, pp.170-178. 2007.

Matsuoka, T., H. Hatori, M. Kodama, J. Yamashita, N. Miyajima. Capillary Condensation of Water in the Mesopores of Nitrogen-enriched Carbon Aerogels. Carbon, *42*, pp.2346-2349. 2004.

Matsuoka, K., Y. Yamagishi, T. Yamazaki, N. Setoyama, A. Tomita, T. Kyotani. Extremely High Microporosity and Sharp Pore Size Distribution of a Large Surface area Carbon Prepared in the Nanochannels of Zeolite Y. Carbon, *43*, pp.876-879. 2005.

Meng, Q., H. Li, H. X. Li. Self-assembly of Mesoporous Ruthenium-boron Amorphous Alloy Catalysts with Enhanced Activity in Maltose Hydrogenation to Maltitol. J. Phys. Chem. C, *112*, pp.11448-11453. 2008.

Meyers, C. J., S. D. Shah, S. C. Patel, R. M. Sneeringer, C. A. Bessel, N. R. Dollahon, R. A. Leising, E. S. Takeuchi. Templated Synthesis of Carbon Materials from Zeolites (Y, beta, and ZSM-5) and a Montmorillonite Clay (K10): Physical and Electrochemical Characterization. J. Phys. Chem. B, *105*, pp.2143-2152. 2001.

Miao, S. D., Z. M. Liu, B. X. Han, J. Huang, Z. Y. Sun, J. L. Zhang, T. Jiang. Ru Nanoparticles Immobilized on Montmorillonite by Ionic Liquids: A Highly Efficient Heterogeneous Catalyst for the Hydrogenation of Benzene. Angew. Chem. Int. Ed., *45*, pp.266-269. 2006.

Mikkola, J.-P., T. Salmi, R. Sjöholm. Modelling of Kinetics and Mass Transfer in the Hydrogenation of Xylose over Raney Nickel Catalyst. J. Chem. Technol. Biotechnol., *74*, pp.655-662. 1999.

Molnar, A., A. Sarkany, M. Varga. Hydrogenation of Carbon-carbon Multiple Bonds: Chemo-, Regio- and Stereo-selectivity. J. Mol. Catal. A-Chem, *173*, pp.185-221. 2001.

Narayan, R. L., T. S. King. Hydrogen Adsorption States on Silica-supported Ru-Ag and Ru-Cu Bimetallic Catalysts Iinvestigated via Microcalorimetry. Thermochim. Acta, *312*, pp.105-114. 1998.

Nieto-Márquez, A., D. Toledano, P. Sánchez, A. Romero, J. L. Valverde. Impact of Nitrogen Doping of Carbon Nanospheres on the Nickel-catalyzed Hydrogenation of Butyronitrile. J. Catal., *269*, pp.242-251. 2010.

Nishimura, S. Handbook of Heterogeneous Catalytic Hydrogenation for Organic Synthesis. pp. 52-63, New York: John Wiley & Songs, INC. 2001.

Pan, X. L., Z. L. Fan, W. Chen, Y. J. Ding, H. Y. Luo, X. H. Bao. Enhanced Ethanol Production inside Carbon-nanotube Reactors Containing Catalytic Particles. Nat. Mater., *6*, pp.507-511. 2007.

Panella, B., A. Vargas, A. Baiker. Magnetically Separable Pt Catalyst for Asymmetric Hydrogenation. J. Catal., *261*, pp.88-93. 2009.

Papp, A., A. Molnar, A. Mastalir. Catalytic Investigation of Pd Particles Supported on MCM-41 for the Selective Hydrogenations of Terminal and Internal Alkynes. Appl. Catal. A: Gen., *289*, pp.256-266. 2005.

Patterson, H. B. W. Hydrogenation of Fat and Oils. pp. 132-230, London and New York: Applied Science Publishers. 1983.

Penny A. Chaloner, M. A. E., Ferenc Joo, Luis A. Oro. Homogeneous Hydrogenation. London: Kluwer Academic. 1994.

Perrard, A., P. Gallezot, J.-P. Joly, R. Durand, C. Baljou, B. Coq, P. Trens. Highly Efficient Metal Catalysts Ssupported on Activated Carbon Cloths: A Catalytic Application for the Hydrogenation of D-glucose to D-sorbitol. Appl. Catal. A: Gen., *331*, pp.100-104. 2007.

Pham-Huu, C., N. Keller, G. Ehret, L. J. Charbonniere, R. Ziessel, M. J. Ledoux. Carbon Nanofiber Supported Palladium Catalyst for Lliquid-phase Reactions - An Active and Selective Catalyst for Hydrogenation of Cinnamaldehyde into Hydrocinnamaldehyde. J. Mol. Catal. A-Chem, *170*, pp.155-163. 2001.

Pinna, F., F. Menegazzo, M. Signoretto, P. Canton, G. Fagherazzi, N. Pernicone. Consecutive Hydrogenation of Benzaldehyde over Pd Catalysts: Influence of Supports and Sulfur Poisoning. Appl. Catal. A: Gen., *219*, pp.195-200. 2001.

Planeix, J. M., N. Coustel, B. Coq, V. Brotons, P. S. Kumbhar, R. Dutartre, P. Geneste, P. Bernier, P. M. Ajayan. Application of Carbon Nanotubes as Supports in Heterogeneous Catalysis. J. Am. Chem. Soc., *116*, pp.7935-7936. 1994.

Ponec, V. On the Role of Promoters in Hydrogenations on Metals; α,β-Unsaturated Aldehydes and Ketones. Appl. Catal. A: Gen., *149*, pp.27-48. 1997.

Ramos-Fernandez, E. V., A. F. P. Ferreira, A. Sepulveda-Escribano, F. Kapteijn, F. Rodriguez-Reinoso. Enhancing the Catalytic Performance of Pt/ZnO in the

Selective Hydrogenation of Cinnamaldehyde by Cr Addition to the Support. J. Catal., *258*, pp.52-60. 2008.

Raymundo-Piñero, E., D. Cazorla-Amorós, A. Linares-Solano. The Role of Different Nitrogen Functional Groups on the Removal of SO_2 from Flue Gases by N-doped Activated Carbon Powders and Fibres. Carbon, *41*, pp.1925-1932. 2003.

Recchia, S., C. Dossi, N. Poli, A. Fusi, L. Sordelli, R. Psaro. Outstanding Performances of Magnesia-Supported Platinum-Tin Catalysts for Citral Selective Hydrogenation. J. Catal., *184*, pp.1-4. 1999.

Reyes, P., M. C. Aguirre, J. L. G. Fierro, G. Santori, O. Ferretti. Hydrogenation of Crotonaldehyde on Rh-Sn/SiO_2 Catalysts Prepared by Reaction of Tetrabutyltin on Prereduced Rh/SiO_2 Precursors. J. Mol. Catal. A-Chem, *184*, pp.431-441. 2002.

Rioux, R. M., H. Song, J. D. Hoefelmeyer, P. Yang, G. A. Somorjai. High-surface-area Catalyst Design: Synthesis, Characterization, and Reaction Studies of Platinum Nanoparticles in Mesoporous SBA-15 Silica. J. Phys. Chem. B, *109*, pp.2192-2202. 2005.

Rocha, A. S., E. L. Moreno, G. P. M. da Silva, J. L. Zotin, A. C. Faro. Tetralin Hydrogenation on Dealuminated Y Zeolite-supported Bimetallic Pd-Ir Catalysts. Catal. Today, *133*, pp.394-399. 2008.

Rodríguez-Reinoso, F. The Role of Carbon Materials in Heterogeneous Catalysis. Carbon, *36*, pp.159-175. 1998.

Rodriguez, A. T., M. Chen, Z. Chen, C. J. Brinker, H. Fan. Nanoporous Carbon Nanotubes Synthesized through Confined Hydrogen-Bonding Self-Assembly. J. Am. Chem. Soc., *128*, pp.9276-9277. 2006.

Rodriguez, N. M., M.-S. Kim, R. T. K. Baker. Carbon Nanofibers: A Unique Catalyst Support Medium. J. Phys. Chem., *98*, pp.13108-13111. 1994.

Rossi, L. M., F. P. Silva, L. L. R. Vono, P. K. Kiyohara, E. L. Duarte, R. Itri, R. Landers, G. Machado. Superparamagnetic Nanoparticle-supported Palladium: a Highly Stable Magnetically Recoverable and Reusable Catalyst for Hydrogenation Reactions. Green Chem., *9*, pp.379-385. 2007.

Rouco, A. J., G. L. Haller, J. A. Oliver, C. Kemball. A Comparative Investigation of Silica-supported Ru-Cu and Ru-Ag Catalysts. J. Catal., *84*, pp.297-307. 1983.

Rueping, M., A. P. Antonchick, T. Theissmann. A Highly Enantioselective Brosted Acid Catalyzed Cascade Reaction: Organocatalytic Transfer Hydrogenation of Quinolines and their Application in the Synthesis of Alkaloids13. Angew. Chem. Int. Ed., *45*, pp.3683-3686. 2006.

Rylander, P. Catalytic Hydrogenation in Organic Syntheses. pp. 5-6, New York: Academic Press. 1979.

Ryoo, R., S. H. Joo, S. Jun. Synthesis of Highly Ordered Carbon Molecular Sieves via Template-mediated Structural Transformation. J. Phys. Chem. B, *103*, pp.7743-7746. 1999.

Ryoo, R., S. H. Joo, M. Kruk, M. Jaroniec. Ordered Mesoporous Carbons. Adv. Mater., *13*, pp.677-681. 2001.

Saadi, A., Z. Rassoul, M. M. Bettahar. Gas Phase Hydrogenation of Benzaldehyde over Supported Copper Catalysts. J. Mol. Catal. A-Chem, *164*, pp.205-216. 2000.

Sabatier, P.; Senderens, J.-B. New Methane Synthesis. Ann. Chim. Phys. 1905, 4, pp.319-323.

Sadek, A. Z., C. Zhang, Z. Hu, J. G. Partridge, D. G. McCulloch, W. Wlodarski, K. Kalantar-zadeh. Uniformly Dispersed Pt-Ni Nanoparticles on Nitrogen-Doped Carbon Nanotubes for Hydrogen Sensing. J. Phys. Chem. C, *114*, pp.238-242. 2010.

Santori, G. F., M. L. Casella, O. A. Ferretti. Hydrogenation of Carbonyl Compounds Using Tin-modified Platinum-based Catalysts Prepared via Surface Organometallic Chemistry on Metals (SOMC/M). J. Mol. Catal. A-Chem, *186*, pp.223-239. 2002.

Scharringer, P., T. E. Muller, J. A. Lercher. Investigations into the Mechanism of the Liquid-phase Hydrogenation of Nitriles over Raney-Co Catalysts. J. Catal., *253*, pp.167-179. 2008.

Schimpf, S., C. Louis, P. Claus. Ni/SiO_2 Catalysts Prepared with Ethylenediamine Nickel Precursors: Influence of the Pretreatment on the Catalytic Properties in Glucose Hydrogenation. Appl. Catal. A: Gen., *318*, pp.45-53. 2007.

Schoenmakerstolk, M. C., J. W. Verwijs, J. J. F. Scholten. The Catalytic-Hydrogenation of Benzene over Supported Metal-Catalysts. 3. Gas-phase Hydrogenation of Benzene over Silica-supported Ru-Cu Catalysts. Appl. Catal., *30*, pp.339-352. 1987.

Serp, P., M. Corrias, P. Kalck. Carbon Nanotubes and Nanofibers in Catalysis. Appl. Catal. A: Gen., *253*, pp.337-358. 2003.

Shalagina, A. E., Z. R. Ismagilov, O. Y. Podyacheva, R. I. Kvon, V. A. Ushakov. Synthesis of Nitrogen-containing Carbon Nanofibers by Catalytic Decomposition of Ethylene/ammonia Mixture. Carbon, *45*, pp.1808-1820. 2007.

Sharma, G., Mei, Y., Lu, Y., Ballauff, M., Irrgang, T., Proch S., Kempe, R. Spherical Polyelectrolyte Brushes as Carriers for Platinum Nanoparticles in Heterogeneous Hydrogenation Reactions. J. Catal., *246*, pp.10-14.2007.

Shastri, A. G., J. Schwank, S. Galvagno. The Microstructure of Bimetallic Ru-Cu/SiO_2 Catalysts-a Chemisorption and Analytical Electron-microscopy Study. J. Catal., *100*, pp.446-457. 1986.

Shephard, D. S., T. Maschmeyer, G. Sankar, J. M. Thomas, D. Ozkaya, B. F. G. Johnson, R. Raja, R. D. Oldroyd, R. G. Bell. Preparation, Characterisation and Performance of Encapsulated Copper-ruthenium Bimetallic Catalysts Derived from Molecular Cluster cCarbonyl Precursors. Chem.-Eur. J., *4*, pp.1214-1224. 1998.

Silva, A. M., O. A. A. Santos, M. J. Mendes, E. Jordao, M. A. Fraga. Hydrogenation of Citral over Ruthenium-tin Catalysts. Appl. Catal. A: Gen., *241*, pp.155-165. 2003.

Sinfelt, J. H. Supported "bimetallic cluster" Catalysts. J. Catal., *29*, pp.308-315. 1973.

Sinfelt, J. H., G. H. Via, F. W. Lytle. Structure of Bimetallic Clusters-extented X-ray Absorption Fine-structure (EXAFS) Studieds of Ru-Cu Clusters. J. Chem. Phys., *72*, pp.4832-4844. 1980.

Singh, U. K., M. A. Vannice. Kinetics of Liquid-phase Hydrogenation Reactions over Supported Metal Catalysts - a Review. Appl. Catal. A: Gen., *213*, pp.1-24. 2001.

Smale, M. W., T. S. King. Ethane Hydrogenolysis over Well-defined Ru-Cu/SiO_2 Catalysts. J. Catal., *119*, pp.441-450. 1989.

Smale, M. W., T. S. King. Kinetics of Ethane Hydrogenolysis over Silica-supported Ruthenium-groupd IB Metal-catalysts. J. Catal., *125*, pp.335-352. 1990.

Song, H., R. M. Rioux, J. D. Hoefelmeyer, R. Komor, K. Niesz, M. Grass, P. Yang, G. A. Somorjai. Hydrothermal Growth of Mesoporous SBA-15 Silica in the Presence of PVP-Stabilized Pt Nanoparticles: Synthesis, Characterization, and Catalytic Properties. J. Am. Chem. Soc., *128*, pp.3027-3037. 2006.

Sordelli, L., R. Psaro, G. Vlaic, A. Cepparo, S. Recchia, C. Dossi, A. Fusi, R. Zanoni. EXAFS Studies of Supported Rh-Sn Catalysts for Citral Hydrogenation. J. Catal., *182*, pp.186-198. 1999.

Sprock, M., X. Wu, T. S. King. N-Butane Hydrogenolysis over Silica-supported Ru-Cu Catalysts. J. Catal., *138*, pp.617-629. 1992.

Srinivas, S. T., P. K. Rao. Direct Observation of Hydrogen Spillover on Carbon-Supported Platinum and Its Influence on the Hydrogenation of Benzene. J. Catal., *148*, pp.470-477. 1994.

Steinhart, M., C. Liang, G. W. Lynn, U. Gösele, S. Dai. Direct Synthesis of Mesoporous Carbon Microwires and Nanowires. Chem. Mater., *19*, pp.2383-2385. 2007.

Strohl, J. K., T. S. King. Monte Carlo Simulations of Supported Bimetallic Catalysts. J. Catal., *116*, pp.540-555. 1989.

Su, F. and Zhao, X. S. Synthesis and Characterization of Microporous Carbons Templated by Ammonium-form Zeolite Y. Carbon, *42*, pp.2821-2831. 2004.

Su, F., Lv, L., Zhao, X. S. Synthesis of Nanostructured Porous Carbon. Int. J. Nanosci., *4*, pp.261-268. 2005.

Su, F. and Zhao, X. S. Template Synthesis of Microporous Carbon for Direct Methanol Fuel Cell Application. Carbon, *43*, pp.2368-2373. 2005.

Su, F., Lee, F. Y., Lv, L., Liu, J., Tian, X. N., Zhao, X. S. Sandwiched Ruthenium/Carbon Nanostructures for Highly Active Heterogeneous Hydrogenation. Adv. Funct. Mater., *17*, pp.1926-1931. 2007a.

Su, F., Lv, L., Lee, F. Y., Liu, T., Cooper, A. I., and Zhao, X. S. Thermally Reduced Ruthenium Nanoparticles as a Highly Active Heterogeneous Catalyst for Hydrogention of Monoaromatics. J. Am. Chem. Soc., 129, pp. 14213-14223. 2007b.

Sulman, E., Y. Bodrova, V. Matveeva, N. Semagina, L. Cerveny, V. Kurtc, L. Bronstein, O. Platonova, P. Valetsky. Hydrogenation of Dehydrolinalool with Novel Catalyst Derived from Pd Colloids Stabilized in Micelle Cores of Polystyrene-poly-4-vinylpyridine Block Copolymers. Appl. Catal. A: Gen., *176*, pp.75-81. 1999.

Sun, Z. Y., Z. M. Liu, B. X. Han, Y. Wang, J. M. Du, Z. L. Xie, G. J. Han. Fabrication of Ruthenium-Carbon Nanotube Nanocomposites in Supercritical Water. Adv. Mater., *17*, pp.928. 2005.

Szöllösi, G., B. Török, L. Baranyi, M. Bartók. Chemoselective Hydrogenation of Cinnamaldehyde to Cinnamyl Alcohol over Pt/K-10 Catalyst. J. Catal., *179*, pp.619-623. 1998.

Toebes, M. L., F. F. Prinsloo, J. H. Bitter, A. J. van Dillen, K. P. de Jong. Influence of Oxygen-Containing Surface Groups on the Activity and Selectivity of Carbon Nanofiber-Supported Ruthenium Catalysts in the Hydrogenation of Cinnamaldehyde. J. Catal., *214*, pp.78-87. 2003.

Tosheva, L., J. Parmentier, V. Valtchev, C. Vix-Guterl, J. Patarin. Carbon Spheres Prepared from Zeolite Beta Beads. Carbon, *43*, pp.2474-2480. 2005.

Van Gorp, K., E. Boerman, C. V. Cavenaghi, P. H. Berben. Catalytic Hydrogenation of Fine Chemicals: Sorbitol Production. Catal. Today, *52*, pp.349-361. 1999.

Villani, K., C. E. A. Kirschhock, D. Liang, G. Van Tendeloo, J. A. Martens. Catalytic Carbon Oxidation over Ruthenium-Based Catalysts. Angew. Chem. Int. Ed., *45*, pp.3106-3109. 2006.

Vinu, A., K. Ariga, T. Mori, T. Nakanishi, S. Hishita, D. Golberg, Y. Bando. Preparation and Characterization of Well-Ordered Hexagonal Mesoporous Carbon Nitride. Adv. Mater., *17*, pp.1648-1652. 2005.

Vinu, A. Two-Dimensional Hexagonally-Ordered Mesoporous Carbon Nitrides with Tunable Pore Diameter, Surface Area and Nitrogen Content. Adv. Funct. Mater., *18*, pp.816-827. 2008.

Vu, H., F. Goncalves, R. Philippe, E. Lamouroux, M. Corrias, Y. Kihn, D. Plee, P. Kalck, P. Serp. Bimetallic Catalysis on Carbon Nanotubes for the Selective Hydrogenation of Cinnamaldehyde. J. Catal., *240*, pp.18-22. 2006.

Wan, Y., Wang, H., Zhao, Q., Klingstedt, M., Terasaki, O., and Zhao, D. Ordered Mesoporous Pd/Silica-Carbon as a Highly Active Heterogeneous Catalyst for Coupling Reaction of Chlorobenzene in Aqueous Media. J. Am. Chem. Soc., *131*, pp. 4541-4550. 2009.

Wang, L., R. T. Yang. Hydrogen Storage Properties of Carbons Doped with Ruthenium, Platinum, and Nickel Nanoparticles. J. Phys. Chem. C, *112*, pp.12486-12494. 2008.

Wang, L. F., F. H. Yang, R. T. Yang. Hydrogen Storage Properties of B- and N-Doped Microporous Carbon. Aiche J., *55*, pp.1823-1833. 2009a.

Wang, L. F., R. T. Yang. Hydrogen Storage Properties of N-Doped Microporous Carbon. J. Phys. Chem. C, *113*, pp.21883-21888. 2009b.

White, R. J., M. Antonietti, M. M. Titirici. Naturally Inspired Nitrogen Doped Porous Carbon. J. Mater. Chem., *19*, pp.8645-8650. 2009.

Wisniak, J., M. Hershkowitz, S. Stein. Hydrogenation of Xylose over Platinum Group Catalysts. Product R&D, *13*, pp.232-236. 1974.

Wisnlak, J., R. Simon. Hydrogenation of Glucose, Fructose, and Their Mixtures. Ind. Eng. Chem. Prod. Res. Develop., *18*, pp.50-57. 1979.

Wu, X., B. C. Gerstein, T. S. King. Characterization of Silica-Supported Cu Monometallic and Ru-Cu Bimetallic Catalysts by Hydrogen Chemisorption and NMR of Adsorbed Hydrogen. J. Catal., *121*, pp.271-293. 1990.

Wu, X., B. C. Gerstein, T. S. King. The Effect of Chlorine on Hydrogen Chemisorption by Silica-Supported Ru Catalysts: A Proton NMR Study. J. Catal., *135*, pp.68-80. 1992.

Xia, Y. D., R. Mokaya. Synthesis of Ordered Mesoporous Carbon and Nitrogen-Doped Carbon Materials with Graphitic Pore Walls via a Simple Chemical Vapor Deposition Method. Adv. Mater., *16*, pp.1553. 2004.

Xia, Y. D., R. Mokaya. Generalized and Facile Synthesis Approach to N-Doped Highly Graphitic Mesoporous Carbon Materials. Chem. Mater., *17*, pp.1553-1560. 2005.

Xia, Y. D., G. S. Walker, D. M. Grant, R. Mokaya. Hydrogen Storage in High Surface Area Carbons: Experimental Demonstration of the Effects of Nitrogen Doping. J. Am. Chem. Soc., *131*, pp.16493-16499. 2009.

Yang, C.-M., M. El-Merraoui, H. Seki, K. Kaneko. Characterization of Nitrogen-Alloyed Activated Carbon Fiber. Langmuir, *17*, pp.675-680. 2001.

Yang, P. F., Z. X. Jiang, P. L. Ying, C. Li. Effect of Surface Composition on the Catalytic Performance of Molybdenum Phosphide Catalysts in the Hydrogenation of Acetonitrile. J. Catal., *253*, pp.66-73. 2008.

Yu, C., J. Fan, B. Tian, D. Zhao, G. D. Stucky. High-Yield Synthesis of Periodic Mesoporous Silica Rods and Their Replication to Mesoporous Carbon Rods. Adv. Mater., *14*, pp.1742-1745. 2002.

Yu, J. S., S. Kang, S. B. Yoon, G. Chai. Fabrication of Ordered Uniform Porous Carbon Networks and Their Application to a Catalyst Supporter. J. Am. Chem. Soc., *124*, pp.9382-9383. 2002.

Yu, W., H. Liu, M. Liu, Q. Tao. Selective hydrogenation of α,β-Unsaturated Aldehyde to α,β-Unsaturated Alcohol over Polymer-stabilized Platinum Colloid and the Promotion Effect of Metal Cations. J. Mol. Catal. A-Chem., *138*, pp.273-286. 1999.

Yuan, Q., A. X. Yin, C. Luo, L. D. Sun, Y. W. Zhang, W. T. Duan, H. C. Liu, C. H. Yan. Facile Synthesis for Ordered Mesoporous Gamma-Aluminas with high Thermal Stability. J. Am. Chem. Soc., *130*, pp.3465-3472. 2008.

Zakhidov, A. A., R. H. Baughman, Z. Iqbal, C. X. Cui, I. Khayrullin, S. O. Dantas, I. Marti, V. G. Ralchenko. Carbon Structures with Three-Dimensional Periodicity at Optical Wavelengths. Science, *282*, pp.897-901. 1998.

Zhao, D., J. Feng, Q. Huo, N. Melosh, G. H. Fredrickson, B. F. Chmelka, G. D. Stucky. Triblock Copolymer Syntheses of Mesoporous Silica with Periodic 50 to 300 Angstrom Pores. Science, *279*, pp.548-552. 1998.

Zhao, X. S., Su, F., Yan, Q., Guo, W., Bao, X.Y., Lv, L., and Zhou, Z. Templating Methods for Preparation of Porous Structures. J. Mater. Chem., *16*, pp. 637-648. 2006a.

Zhao, X.S., Bao, X. Y., Guo, W., and Lee, F. Y. Immobilizing Catalysts on Porous Materials. Mater. Today, *9*, pp. 32-39. 2006b.

Zheng, M., J. Cao, X. Ke, G. Ji, Y. Chen, K. Shen, J. Tao. One-step Synthesis of New Mesoporous Carbon Nanofibers through an Easy Template Method. Carbon, *45*, pp.1111-1113. 2007.

APPENDIX

List of publications coming from this thesis work

Papers published (or accepted) in international referred journal and book

(1) Liu, J., Zhao, X.S. Glucose Hydrogenation over Ru Nanoparticles Embedded in Template Porous Carbon. *Studies in Surface Science and Catalysis*, 2008, 174, 1315-1318.

(2) Liu, J., Tian, X.N., and Zhao, X. S. Hydrogenation of Glucose over Ru Nanoparticles Embedded in Templated Porous Carbon. *Australian Journal of Chemistry*, 2009, *62*, 1020-1026.

(3) Su, F., Lee F. Y., Lv, L., Liu, J., Tian, X.N., and Zhao, X.S. Sandwiched Ruthenium/Carbon Nanostructures for Highly Active Heterogeneous Hydrogenation. *Advanced Functional Materials*, 2007, 17, 1926-1931.

(4) Su, F., Zhou, Z., Guo, W., Liu, J., Tian X.N., and Zhao, X.S. Template Approaches to Synthesis of Porous Carbon. in *Chemistry and Physics of Carbon*, Vol. 30, pp. 63-128, Ed: L. R. Radovic, CRC Press, 2008.

(5) Liu, J., Zhao, X.S. Ru Nanoparticles Embedded in Templated Carbon Pore Walls as a Highly Active Catalyst for Glucose Hydrogenation. Accepted by *14th International Congress on Catalysis*. 2008, Seoul, Korea.

(6) Zhao, X.S., Su, F., and Liu, J. Metal Nanoparticles Embedded in Porous Carbon as a New Catalyst System (keynote). Accepted by *XIX International Materials Research Congress*, 2010, Cancún, Mexico.

(7) Liu, J., Zhao, X.S. Ruthenium Nanoparticles Embedded in Carbon Microfibers as a Catalyst for Glucose Hydrogenation. Accepted by *The 6th Tokyo Conference on Advanced Catalytic Science and Technology & 5th Asia-Pacific Congress on Catalysis (TOCAT6/APCAT5*), 2010, Sapporo, Japan.

Papers submitted to international referred journal

(8) Liu, J., Zhang, L.L., Liu, T. and Zhao, X.S. Bimetallic Ruthenium-Copper Nanoparticles embedded in Porous Carbon for Hydrogenation of D-glucose. To be submit to *ACS catalysis*, 2010.

(9) Liu, J., Bai, P. and Zhao, X.S. Template Approach to the Synthesis of Mesoporous Carbon Microfiber Supported Ruthenium Catalyst for the Hydrogenation of D-glucose. To be submit to *Physical Chemistry Chemical Physics*, 2010.